Title

How excess electrons are solvated in water and electrolyte solutions: mixed quantum/classical and ab initio studies

Author

Park, Sanghyun Jonathan

Publication Date

2022

Peer reviewed|Thesis/dissertation

UNIVERSITY OF CALIFORNIA

Los Angeles

How excess electrons are solvated in water and electrolyte solutions: mixed quantum/classical and ab initio studies

A dissertation submitted in partial
satisfaction of the requirements for the degree
Doctor of Philosophy in Chemistry

by

Sanghyun Jonathan Park

2022

ABSTRACT OF THE DISSERTATION

How excess electrons are solvated in water and electrolyte solutions:
mixed quantum/classical and ab initio studies

by

Sanghyun Jonathan Park
Doctor of Philosophy in Chemistry
University of California, Los Angeles, 2022
Professor Benjamin Joel Schwartz, Chair

When an excess electron is solvated by water molecules, it forms a well-known species named the hydrated electron. Although hydrated electrons serve as intermediates in many important reactions, such as radiation, oxidation, and electron transfer reactions, their hydration structure is unknown. This is important because the reactivity of the hydrated electron is strongly coupled with its solvation structure, making it impossible to accurately model chemical reactions involving this species because the structure is unknown. For the past decade, there has been an upsurge of interest in simulating hydrated electron structures with ab initio methods, specifically with density functional theory (DFT). All DFT-generated hydrated electron structures, regardless of the functional of choice, produced a distinct cavity region where no waters enter and a highly structured first hydration shell. Although several groups have claimed that such DFT-generated structures are 'correct', there has been no attempt to rigorously test their accuracy by making direct comparisons to experiments. Thus, the first focus of this thesis lies in evaluating two different DFT-based hydrated electron models that are widely accepted in the literature: a 0 K minimalist model that replaces explicit waters with a polarizable continuum and a fully-periodic molecular dynamics model. This thesis provides proof that DFT calculations make predictions that fail when directly compared with the experiment, a clear indication that the DFT-generated hydration structures cannot be correct. The second focus of this thesis explores how hydrated electrons behave in presence of ions. Experimentally, the hydrated electron's absorption spectrum is known

to blue-shift in electrolyte solutions, but a molecular explanation for this shift is unknown. To understand hydrated electron/electrolyte interactions, both the mixed quantum/classical (MQC) and DFT hydrated electron models were paired with a single Na^+ to examine their detailed pairing interactions. For MQC models, the predicted Na^+-induced blue-shift turns out to be highly sensitive to the simulation parameters of both the electron and the cation. The electron model that has the weakest hydration shell and the smallest cavity produce the blue-shift that is in best agreement with experiment. Most importantly, the DFT electron, with its strongly structured hydration shell, predicts a spectral red-shift upon ion-pairing, another clear proof that DFT-based simulations predict an incorrect hydration structure. In summary, this thesis shows clearly that DFT is not capable of correctly capturing the essence of this simple, yet complex, system.

The dissertation of Sanghyun Jonathan Park is approved.

Anastassia N. Alexandrova

Daniel Neuhauser

Justin Ryan Caram

Benjamin Joel Schwartz. Committee Chair

University of California, Los Angeles

2022

This work is devoted to my mom, Dr. Mi-Hui Cho.

I am following in her footsteps toward a dedicated scholar.

Contents

List of Figures

List of Tables

ACKNOWLEDGEMENTS

Graduate school has been a truly wonderful journey for me. But without people who supported me, I would not be in the position where I'm right now. First, I want to thank my PI, Ben Schwartz, for supporting my work and providing me with superb advice. As graduation gets closer, the more that I realize that I'm heavily influenced by him, clear proof that my interactions with him were a major driving force for me to proceed. I also want to thank Wil Narvaez for collaborating with the grueling work of implementing new features in the hydrated electron code. Next, I want to thank Andy Vong, Ken Mei, and Quynh Duong for their lasting friendship and support. I also would like to thank the entire Schwartz group for their support, especially Will Borrelli for collaborating with future projects. Lastly, but importantly, I want to thank my family, father, mother, and younger sister, for their emotional and financial support. Although the physical distance was far away, it was their support that made everything possible. Below are the particular acknowledgments for my published works, which are included as reprints in this thesis.

Chapter 2 is reprinted with permission from Sanghyun J Park and Benjamin J. Schwartz "Evaluating Simple Ab Initio Models of the Hydrated Electron: The Role of Dynamical Fluctuations" *J. Phys. Chem. B* **2020**, *124*, 9592–603. Copyright 2020 American Chemical Society.

Chapter 3 is reprinted with permission from Sanghyun J Park and Benjamin J. Schwartz "Understanding the Temperature Dependence and Finite Size Effects in Ab Initio MD Simulations of the Hydrated Electron" *J. Chem. Theory Comput.* **2022**, *18*, 4973–82. Copyright 2022 American Chemical Society. Ben Schwartz is the PI.

Chapter 4 is reprinted with permission from Sanghyun J Park, Wilberth A. Narvaez and Benjamin J. Schwartz "How Water-Ion Interactions Control the Formation of Hydrated Electron:Sodium Cation Contact Pairs" *J. Phys. Chem. B* **2021**, *125*, 13027–13040. Copyright 2021 American Chemical Society. For this paper, Wilberth is the coauthor who helped in the development of the simulation code.

This work was supported by the National Science Foundation under Grant No. CHE-1856050 and the U.S. Department of Energy Condensed Phase and Interfacial Molecular Science program under Grant No. DOE-CPIMS-0000228903.

VITA

The author earned a Bachelor of Science in Chemistry from Yonsei university in South Korea. During his undergraduate years, he worked with Myeong Hee Moon on analytical chemistry, using Flow Field-Flow Fractionation to separate and analyze biomolecules. Upon entering UCLA, he transitioned from an experimentalist to a theorist and began working with Ben Schwartz. His research focuses on performing computer simulations on condensed phase systems that require quantum description, most notably the hydrated electron, with various calculation methodologies. He published 3 first-authored papers in reputable journals, such as the Journal of Physical Chemistry and the Journal of Chemical Theory and Computation. He also participated in multiple collaborations that produced 4 papers in reputable journals. Currently, there is one first-author paper that is under review and one more that is being written.

Chapter 1

Introduction

1.1 Introduction to Hydrated Electrons

Solvated electrons are formed when an excess electron is injected into liquid. Their existence has been long recognized due to their distinctive blue color, such as that occurring when alkali metals are dissolved in a liquid ammonia solution.[1, 2] When an excess electron is solvated in water, it is referred to as a hydrated electron. The existence of hydrated electrons were verified by the first work to measure their absorption spectrum back in 1962.[3] Later, hydrated electron formation was further supported by resonance Raman experiments, which indicated that the excess electron is solvated by waters without creating new species.[4] Although the hydrated electron is arguably the simplest quantum mechanical system, it serves as reactive intermediates in many important chemical reactions, such as radiation, ionization, and photoexcitation reactions.[5–7] It is also well known that the excess electrons induce damage to DNA nucleobases,[8] and can serve as a superreductant for chemical reactions.[9] Due to its importance, the hydrated electron has gained immense attention from many researchers.

The most interesting aspect of this system is that its properties are completely dependent on its solvation structure. The hydrated electron system can be effectively viewed as a particle in a quasi-spherical box with an s-like ground state and 3 p-like excited states. Its absorption spectrum is dominated by excitations from the ground state to three p-like excited states. The shape of the experimental absorption spectrum can be cleanly fit to a Gauss-Lorentzian form.[10]

Past simulation work has attempted to reproduce the absorption spectrum with some success, but the blue-tail was never fully reproduced in any simulations.[11–15] Additionally, photoelectron spectroscopy experiments have identified how strongly the electron is bound by liquid water, which is also known as the vertical detachment energy (VDE).[16–19] The generally accepted range for the hydrated electron's VDE is between 3.5 and 3.7 eV.[16–19] In addition, more complex experiments, such as time-resolved photoelectron spectroscopy[20–22] and pump-probe transient absorption spectroscopy[23–26] experiments have examined the hydrated electron's formation and relaxation dynamics.

One interesting feature of electron transfer reactions involving hydrated electrons is that they do not follow Marcus theory.[27] In Marcus theory, it is assumed that the free energy surface of the electron transfer reaction is harmonic, and the activation energy is directly correlated with the reaction free energy.[28] However, experiments on hydrated electron reactions have found that even when the free energy can differ by orders of magnitude, the activation energy hardly varies.[29–31] This strongly implies that the solvent reorganization free energy for hydrated electrons has non-harmonic features, that is, hydrated electrons' structural fluctuations are non-Gaussian.[27] Given that the reactivity of the hydrated electron is directly linked with its structure, without knowing its exact structure, it is impossible to correctly model chemical reactions involving hydrated electrons.

In an attempt to understand the hydrated electron's structure, many past works relied on computer simulations. To date, however, the exact structure of the hydrated electron is still unknown, as not a single simulation model is able to reproduce experiments correctly. Most past simulation work has relied on mixed quantum/classical dynamics, where only the excess electron is treated quantum mechanically via electron–water pseudopotentials.[11, 32, 33] Full quantum treatment was out of reach until recently, as it is computationally too expensive to run dynamics for tens of ps with hundreds of waters treated with ab intio methods. Even with DFT-based simulations on the hydrated electron, understanding its structure is still an open question since DFT-generated structures have not been rigorously tested and compared with experiments.[34–36] Therefore, one of the main thrusts of this thesis is to put DFT-based hydrated electron structure predictions to a meticulous test by calculating properties that are directly connected with experiments. To determine which experimental properties are the most sensitive to the hydration structure, in the next two sections, we will discuss what previous simulation work on hydrated electrons has achieved

and failed.

1.2 Mixed Quantum/Classical Simulations on Hydrated Electrons

Historically, the lack of computational power restricted from running all-electron ab initio dynamics simulations on the hydrated electron system for a long time. Thus, the majority of past simulation works have utilized mixed quantum/classical molecular dynamics, which is significantly cheaper than ab initio methods. The basic idea of MQC calculations is to reduce the dimensionality of quantum calculations by treating only the excess electron quantum mechanically. All the other interactions, including water–water interactions, are treated classically, usually with well-established water models such as the SPC/flex model.[37] The quantum interactions are represented with pseudopotentials that are derived from Hartree-Fock (HF) calculations using the Phillips-Kleinman formalism.[38] Specifically for hydrated electrons, the lowest unoccupied molecular orbital of water is used to describe how would an excess electron interact with a water molecule.

The first MQC-based hydrated electron simulation was performed by Schnitker and Rossky using a newly developed electron–water pseudopotential, called the SR model.[32] The SR model's structure showed a distinct quasi-spherical cavity region where no water molecules can intrude and a weakly defined hydration shell. Later, an error was discovered in this model[39] and was replaced with an independently-developed model without the error by Turi and Borgis, also known as the TB model.[11] The TB hydrated electron, interestingly, showed a structure that is almost identical to that of the SR model. The TB model was able to capture some experimental properties correctly, including the VDE, absorption spectrum, and molar solvation volume, which represents the volume change induced by electron solvation.

About a decade ago, a new electron–water pseudopotential was developed by Larsen, Glover, and Schwartz that used a more rigorous analytical functional form when fitting the pseudopotential.[33] The main goal of this process was to better capture intrinsic details of the pseudopotential and to incorporate an attractive region behind water's oxygen atom, a feature that was not properly included in previously developed pseudopotentials. Surprisingly, LGS generated hydrated electron structures that turned out to be strikingly different to the traditional cavity picture. As the system is propagated, the cavity region collapses and is replaced with a region with enhanced water density.

This is due to the attractive electron–water interactions allowing waters to move closer towards the electron's center-of-mass, resembling more of an inverse plum pudding or a non-cavity structure.[40] After the advent of this model, there was a series of debates on the true structure of the hydrated electron. Many works compared different MQC models to check whether the cavity or the non-cavity picture matches better with experiments. In particular, experimental properties such as the absorption spectrum,[12, 33, 40] resonance Raman spectrum,[15, 41] time-resolved photoelectron spectrum,[42] and temperature-dependence[15, 43] were investigated.

For the steady-state absorption spectrum, both the TB and LGS models are able to relatively accurately match the experiment, which means that both models accurately predict the size of the excess electron.[11, 33] The relationship between the size of the electron and its absorption spectrum is derived in a work by Bartels using moment analysis, which shows that the spectrum peak is inversely correlated with the square of the radius of gyration.[44] The TB model, however, can better account for VDE and molar solvation volume,[45, 46] whereas the LGS model can better predict temperature dependence,[15, 43] excited state dynamics,[42] and the behavior at the air/water interface.[45] LGS suffers from an overly attractive electron–water potential and thus overestimates the VDE. LGS also shows a negative molar solvation volume, which is the main reason why non-cavity structures are not generally accepted in the community.[45, 46] In spite of its weakness, the LGS model is able to correctly represent entropic effects due to its fluxional electronic structure, which is an area where the TB model fails.[15] Due to its rigid and repulsive nature, any experimental properties that require fluctuations are not properly represented in the TB model.

One good example of this is the temperature dependent red-shift of the absorption spectrum.[47, 48] The TB electron does not show any changes in its absorption spectrum or its structure, a reflection of its repulsiveness and rigidity.[15] On the other hand, the LGS model is able to qualitatively reproduce the red-shift but overestimates the magnitude by a factor of two.[15] Thus, fluctuations and entropic effects are crucial to capture the temperature dependent properties, that is, the overall structure must fluctuate to show any spectral shift. A strongly repulsive model like TB does not show any structural changes at different temperatures and thus fails to show any spectral shift, an indication that this model is generating rigid and inaccurate structures.[43] Additionally, the LGS electron is overly attractive and fluxional, which leads to its erroneous positive molar solvation

volume, proof that this model is also not generating the correct structure.[45, 46] Overall, it seems that the correct hydrated electron structure should incorporate features from both models.

Given that both the TB and LGS models are derived from the same HF calculations, why do they produce such a dramatically different structures? It turns out that the analytical fit used to describe the electron–water pseudopotential is the culprit. The analytical fit for the TB model is coarser than that of the LGS model and washes away important details.[33] A good example of this is the attractive region at the back of the water's oxygen atom, which is not described in the TB electron–water potential. Thus, the MQC-based hydrated electron structure is extremely sensitive to the way the quantum mechanical potential is fit to an analytical form. Furthermore, recent work by Glover et al. showed that correcting the ad hoc polarization term in the TB pseudopotential by using CCSD(T) calculations as a reference weakened the cavity region. Overall, the hydrated electron's structure can be notably changed just by simply tweaking some parameters in the pseudopotential, an indication that MQC method is just too sensitive to the parameters used in the calculations. This is the reason why many simulations have started to utilize ab initio methods to simulate hydrated electrons, mainly with DFT, which will be discussed in the next section.

1.3 Ab Initio Simulations of Hydrated Electrons

In the past decade, ab intio simulations have became a popular method to simulate the hydrated electron. Due to computational limitations, earlier work focused more on static 0 K calculations, either by performing single point ab initio calculations on MQC configurations or on geometry-optimized configurations.[49–51] One well-known DFT-based 0 K minimalist model was developed by Kumar et al., which has only 4 explicit water molecules plus a polarizable continuum model (PCM).[52] Upon geometry optimization, the four waters were arranged tetrahedrally with each water coordinating one of its H atoms with the electron, and the electron occupied a modestly large cavity region.

With the minimalist model, Kumar et al. computed experimental properties, including the VDE, vibration modes, EPR g-factor, and thermodynamic properties.[53] Despite being a relatively small and simple model, it seemed to demonstrate good accuracy for all the properties they

calculated. Thus, they concluded that their model correctly captured the essence of the hydrated electron, and that its distinct structure (cavity region with 4 tetrahedrally arranged waters) must be correct. However, we believe that the minimalist model does not correctly capture the room temperature dynamics of the hydrated electron. Since the model is based on a single 0 K structure, it is impossible to incorporate entropic effects or thermal fluctuations, which are crucial to correctly explain many experimental properties. Furthermore, in order for the minimalist model to make sense, its tetrahedral configuration must be the average of a fluctuating structure at room temperature, which is yet to be verified.

Having explored non-dynamical models, we now move on to dynamic simulations on the hydrated electron. The first ab initio-based dynamics simulation was performed by Uhlig et al., who performed QM/MM dynamics with 32 QM waters that are described by DFT.[54] With their model, they generated an average structure that has features of both the TB and LGS models. Their DFT-based hydrated electron showed a distinct cavity region, although the cavity size was smaller than that of the TB model, and a large electron–water overlap, which is due to the electron mixing with the water LUMOs. The electron turns out to be diffuse, as more than 30% of it sits beyond the first solvation shell, a feature reminiscent of the LGS model.[40] Most interestingly, this model showed a distinctively structured hydration shell that closely resembles Cl^- ions, which was never observed in MQC models. They also calculated the VDE and radius of gyration which did not show good accuracy. Unfortunately, due to the high computational cost of ab initio calculations, they were not able to generate additional data that could be directly compared with the experiments. Thus, despite there being some success in identifying DFT-generated structures, the accuracy of such calculations has not been fully verified.

Later, work by Ambrosio et al. utilized a fully periodic ab initio molecular dynamics (AIMD) with DFT to simulate the hydrated electron.[35] Due to the high computational cost, they only incorporated 64 waters in a periodic box, which is susceptible to finite size effects due to the small size. The resulting hydrated electron solvation structure turned out to be very similar to that from the previous QM/MM work with same structural features. Surprisingly, Ambrosio et al. also claimed that the VDE and absorption spectrum were predicted with good accuracy. However, while performing these calculations, they made several assumptions and corrections that they did not fully disclose. In their VDE calculation, to account for finite size effects and for unknown zero of

energy in the periodic calculation, they added corrections to their calculated value. Unfortunately, the correction values they used are not given in their work, so it is not possible to verify their validity. For the absorption spectrum calculations, rather than using TD-DFT, they simply binned the energy differences between the SOMO and higher-lying Kohn-Sham orbitals, a procedure that is known to be inaccurate. Thus, even though it appears their calculations accurately reproduce experiment, based on these uncontrolled assumptions, is hard to conclude that the DFT is producing correct hydrated electron structures.

Another past work to note is from Wilhelm et al., who claimed to have performed MP2-based fully periodic AIMD calculations on the hydrated electron system.[36] Due to the extremely high computational cost to run MP2-based dynamics, their box contained only 47 waters and a total of only 3 ps of dynamics were run. These authors only reported a couple of snapshots that showed cavity-like features and bandgap values that are clearly blue-shifted from experiment. Their main conclusion, based on just the few reported snapshots was that the hydrated electron occupies a cavity. However, after examining the detailed procedures of their simulation, it turns out that five out of every six time steps were propagated with DFT. Thus the configurations generated in this work were mainly DFT-based structures that are only slightly perturbed by MP2. We performed additional structural analysis on this hybrid DFT/MP2 model using the published repository and showed that the structures were not different from previous DFT simulations.[55, 56] Overall, to date, there is no proof that the hydration structures generated via DFT are correct.

Currently, however, DFT-generated hydrated electron structures are considered to be state-of-the-art in the community, even though there is very little direct comparison to experiments. In this thesis, we put DFT-based hydrated electron models to a rigorous test, allowing us to directly understand their accuracy. First, in chapter 2, we put Kumar et al.'s DFT-based minimalist model to a test by using it as a basis to run room temperature AIMD simulations and examine how the model behaves when thermal fluctuations are added. We show that PCM is not capable of restraining the excess electron at room temperature and thus cannot replace explicit water molecules, a clear indication that thermal fluctuations are crucial to correctly model a room temperature fluctuating object like the hydrated electron.

Next, in chapter 3, we employ fully periodic DFT-based AIMD simulations to explore finite size effects and temperature-dependent spectral shifts. Since all previous AIMD simulations on

hydrated electrons utilized a box size that is very small holding only tens of waters,[35, 36] we explore how finite size effects are manifested in small box sizes and determine how large we should go to remove these artifacts. From the past work by Larsen et al, even a system box containing 200 waters was still not large enough to fully remove finite size effects in MQC calculations.[33] Additionally, we also run dynamics on three different temperature points to examine whether the DFT-based model can reproduce the temperature dependent spectral shift,[47, 48] which can serve as a nice comparison point to judge its accuracy. We show that the system size is not fully converged even up to a box containing 128 water molecules, and despite DFT fails to generate an accurate absorption spectrum, it can qualitatively capture the temperature dependent spectral red-shift.

1.4 Hydrated Electrons in Electrolyte Solution

One important yet largely unexplored property of the hydrated electron is its behavior in electrolyte solutions. Experimentally, the hydrated electron's absorption spectrum is known to blue-shift in aqueous electrolyte solutions.[57–59] The magnitude of the shift increases with higher salt concentrations and saturates when the salt reaches its solubility limit. The magnitude of the spectral shift is also dependent on ion species: higher-valent cations induce a larger shift, and perchlorate anions produce a larger shift than chloride. The overall magnitude of the blue-shift, however, is relatively small: 5 m NaCl only shifts the spectrum by 70 meV. Interestingly, the shape of the spectrum stays unchanged regardless of salt concentration or ion species. Although electrolyte-induced blue-shifts of the hydrated electron's spectrum were reported two decades ago, there is still no explanation for why ions cause the blue-shift, how concentration affects its magnitude, and why it depends on ion species.

In previous work, Coudert et al. employed MQC simulations with the TB model and simulated how the hydrated electron pairs with a single Na^+.[60] These workers concluded that the excess electron undergoes a strong pairing with Na^+, which induces the spectral blue-shift. They also calculated the free energy profile of e^-_{aq} –Na^+ pairing and found a well that is more than $\sim 6k_BT$ deep. This implies that when a Na^+:e^-_{aq} pair is formed, it will not dissociate at room temperature. Reflective of the strong pairing, the predicted blue-shift in the absorption turns out to be more than a magnitude larger than that observed in the experiment. These workers were unable to provide

an explanation as to why the TB electron produces such an erroneously large shift.

Recently, we have decided to interpret the ion-pairing behavior of hydrated electrons using the language of the Hofmeister series.[61] In the series, ions are divided into two different groups. Structure-making ions (kosmotropes) are known to facilitate the formation of a water H-bond network and show negative entropies of hydration. On the other hand, structure-breaking ions (chaotropes) break the adjacent water H-bond network, which leads to a positive entropy of hydration. Usually, ions with a higher charge density tend to show more kosmotropic behavior whereas ions with lower charge density are mostly chaotropic. Kosmotropes are known to pair well with kosmotropes as there is a strong enthalpic incentive to put two kosmotropes close to each other. Similarly, chaotropes pair well with chaotropes as it is entropically favorable to solvate two adjacent chaotropes rather than solvating them separately. This is why salts with a chaotrope-kosmotrope combination tend to show higher solubility in water, as they tend not to pair with each other when dissolved.

The hydrated electron, in the Hofmeister language, is known to be the champion chaotrope as it shows the largest positive entropy of hydration compared with any other ions.[62, 63] This means that when an electron is solvated in an aqueous electrolyte solution, it should more strongly pair with chaotropic cations, such as Cs^+, and less strongly pair with kosmotropic cations, such as Na^+. Thus, the small magnitude of the blue-shift in NaCl solutions makes sense, as kosmotropic Na^+ should not pair well with the hydrated electron. This also explains the reason why the simulation by Boutin et al. shows an erroneously large blue-shift; the strong simulated Na^+:e^-_{aq} pairing is not a good representation of the experimental environment, likely because the TB electron may be too chaotropic, thus overestimating the blue-shift.

Given that the TB model is not able to capture the correct ion-pairing interactions, what improvements can we make to reproduce the correct magnitude of the blue-shift? Is it due to Na^+ being too chaotropic, e^-_{aq} too kosmotropic, or both? These questions can be answered by adjusting different interactions in the MQC simulations. First, we can tweak the Lennard-Jones parameters of Na^+, which changes its interactions with waters (i.e. kosmotropicness). Exploring this property is the main idea of chapter 4, where we show that slight adjustments to Na^+ parameters can result in a huge contact pair stability variation. This also means that slightly changing Na^+ parameters can notably shift the magnitude of the spectral blue-shift. Another way is to use different electron–

water pseudopotentials, which will effectively tweak the chaotropicness of the hydrated electron. In chapter 5, we introduce a new MQC model that generates a more chaotropic electron, which yields the correct magnitude of the blue-shift.

Having explored systems with only a single Na^+ added, there still remains a question of why the hydrated electron's spectral blue-shift depends on salt concentration and ion species. We answered this question in Ref. 64 and 65, work that is not included in this thesis. To provide a brief idea, we simulated different concentrations of NaCl solution using the MQC-based TB model and found that the electron pairs with multiple Na^+ cations.[64] The blue-shift gets larger with higher concentration due to the fact that the electron on average pairs with more Na^+. Because there is a limit to how many Na^+ can simultaneously interact with a hydrated electron, the blue-shift saturates at high concentrations. The ion species dependence can be explained using the the idea of competitive ion-pairing.[65] Na^+, which is a kosmotropic ion, pairs well with Cl^-, but not with ClO_4^-. Thus, in NaCl solutions, Cl^- pairs well with Na^+, mitigating e_{aq}^-–Na^+ interactions and reducing the blue-shift. Conversely, in $NaClO_4$ solution, ClO_4^- anions do not pair well with Na^+ which maximizes the direct interaction between Na^+ and e_{aq}^-, causing a larger blue-shift. Overall, the Hofmeister series serve as an important framework to explain the hydrated electron's interaction with ions.

For all of this effort, however, there still is uncertainty on whether the MQC simulations are generating the correct hydrated electron structures. Slight adjustments to the pseudopotential dramatically change the simulated hydrated electron's structure, and small tweaks in Na^+ LJ potential can change the free energy of contact pair formation by $\sim$4 k_BT. Due to this extreme sensitivity, it is difficult to clearly conclude that MQC simulations are correctly representing all interactions. Is the picture of the hydrated electron interacting with multiple cations an artifact or is it real? To address this question, we have to go beyond MQC simulations and check with ab intio models. Thus in chapter 5, we explore how DFT-based hydrated electrons pair with a single Na^+ and examine whether ab initio simulations can reproduce the accurate spectral blue-shift. We show that DFT produces hydrated electron structures that are too kosmotropic and shifts the spectrum to the opposite direction, clear proof that DFT is generating incorrect structures.

1.5 Summary of Chapters

Following the introduction, Chapter 2, reprinted with permission from Sanghyun J. Park and Benjamin J. Schwartz "Evaluating Simple Ab Initio Models of the Hydrated Electron: The Role of Dynamical Fluctuations" *J. Phys. Chem. B* **2020**, *124*, 9592–603, tests the DFT-based minimalist 0 K hydrated electron model consisting of 4-16 waters molecules with an excess electron surround by the polarizable continuum model (PCM). Using this model as a basis, we run room-temperature molecular dynamics and examine how the structure shifts as thermal energy is added to the system. We show that PCM is not capable of replacing explicit water molecules due to the fact that it does not provide adequate repulsion for the excess electron, allowing the electron to ooze out towards vacuum at room temperature. This creates a system that resembles more of a surface-bound anionic water cluster than the bulk hydrated electron, showing a rather poor agreement with experiments. Overall, this work highlights the importance of thermal fluctuations and entropic effects when modeling a room-temperature fluctuating object like the hydrated electron.

In chapter 3, reprinted with permission from Sanghyun J. Park and Benjamin J. Schwartz "Understanding the Temperature Dependence and Finite Size Effects in Ab Initio MD Simulations of the Hydrated Electron" *J. Chem. Theory Comput.* **2022**, *18*, 4973–82, rigorously tests the fully periodic DFT-based hydrated electron model by exploring its temperature dependence and finite size effects. We show that the system size is not converged even up to the largest box containing 128 waters. Both structural and electronic properties shift as the box size is increased, an indication that a larger box is required to generate accurate properties of the hydrated electron. We also explore the absorption spectrum and its temperature-dependent red-shift. For the steady-state absorption spectrum, DFT generates a too broad spectrum with a peak that is strongly blue-shifted, proving that it is not generating accurate hydrated electron structures. Surprisingly, DFT is able to qualitatively capture the red-shift of the absorption spectrum with increasing temperature, although the shift is a factor of two too large compared to experiment.

In chapter 4, reprinted with permission from Sanghyun J. Park, Wilberth A. Narvaez and Benjamin J. Schwartz "How Water-Ion Interactions Control the Formation of Hydrated Electron:Sodium Cation Contact Pairs" *J. Phys. Chem. B* **2021**, *125*, 13027–13040, explores how changing the Na^+ solvation affects the pairing between the simulated hydrated electron and Na^+

and ultimately the induced spectral blue-shift. With the MQC-based TB model, the e^-_{aq} and Na^+ form a tight contact pair that produces a spectral blue-shift that is more than an order of magnitude larger than experiment. By slightly tuning Na^+–water parameters to be stronger or weaker, the free energy of contact pair formation varies by more than 4 k_BT. This proves that all the interactions in this system are subtly balanced, so that slightly tuning them can dramatically shift the ion pairing behavior and thus the spectral blue-shift. Specifically, we show that by using a stronger Na^+–water potential, Na^+ causes water molecules to be unfavorably oriented to the electron, which results in weaker e^-_{aq}–Na^+ pairing. Stronger Na^+ solvation also produces a more accurate and smaller blue-shift, in better agreement with experiment.

Chapter 5 of the thesis explores how the DFT-based hydrated electron handles Na^+:e^-_{aq} pairing and examines whether this model can predict an accurate spectral blue-shift. We also make rigorous comparisons with multiple MQC models to specify the structural features that are important to get the blue-shift right. In this work, we use the language of the Hofmeister series to explain the ion-pairing behavior. The hydrated electron is known to be the king of chaotropes and should not pair well with a kosmotrope like Na^+. In the DFT-based hydrated electron simulation, surprisingly, an erroneous red-shift is observed when paired with Na^+. We show that this is because DFT produces a too kosmotropic electron that prefers to strongly interact with water to the point that it imposes its hydration structure on Na^+, leading to an unphysical spectral red-shift. We also show that by using a strongly chaotropic MQC model, it is possible to simulate the spectral blue-shift accurately, an indication that the correct hydrated electron structure must be chaotropic and that DFT is generating incorrect structures that are far too kosmotropic.

In summary, this thesis attempts to answer two critical questions about the hydrated electron. First, can DFT predict the correct structure of the hydrated electron? Although DFT is considered to be a higher-level theory than MQC, it does not necessarily show a better accuracy when comparing it with experiments. Second, what is the mechanism behind the hydrated electron interacting with ions to produce the spectral blue-shift? The electron is known to pair with Na^+, but its paring behavior turns out to be strongly sensitive to both electron's and ion's hydration structure. By answering these questions, it will be possible to determine the true structure of the hydrated electron.

Chapter 2

Evaluating Simple Ab Initio Models of the Hydrated Electron: The Role of Dynamical Fluctuations

2.1 Introduction

The hydrated electron is one of the simplest possible condensed-phase quantum mechanical systems, consisting of an excess electron solvated by water molecules. Hydrated electrons play an important role in chemical reactions such as ionization and electron transfer as well as in radiation chemistry.[5–7] Despite their importance, there are still a number of unanswered questions concerning basic features of hydrated electrons, such as the local structure of the water molecules that stabilize the excess charge. There is strong evidence suggesting that hydrated electrons have little occupancy in the water molecular orbitals, so that the majority of their charge density lies primarily between the water molecules in the bulk liquid.[66, 67] But the manner in which water reorganizes around an excess electron and the details of the corresponding electronic structure are

still the subject of a great deal of debate.

The standard structural picture developed over the years is that the excess electrons occupy a cavity in the water, locally expelling water from a volume midway in size between a chloride and bromide ion. This picture was supported by both early mixed quantum/classical MD simulations[11, 12, 32, 68, 69] as well as by more recent *ab initio* simulations,[34–36, 53, 70] although we note that some of these simulations present only snapshots,[36] and others present pair distribution functions without other ways of characterizing the hydrated electron's structure.[34, 35, 70] Other simulations, however, have suggested that the excess electron contains a significant number of interior water molecules,[33] so that its charge density has significant overlap with the surrounding water. We note that significant overlap of the electron's spin density with the surrounding water, an idea that is supported by EPR experiments,[50, 71] also occurs in some simulations in which the electron does have a central cavity.[34, 66]

Part of the reason for the controversy is that different structural models of the hydrated electron predict observables that agree with experiment about equally well – or equally poorly – depending on the experiment in question. Nearly every model is able to correctly predict the hydrated electron's room-temperature absorption spectrum,[11, 33, 68, 72] which is directly related to its radius of gyration.[44] Simulation models that predict that the electron resides in a cavity are also usually able to correctly predict the hydrated electron's molar solvation volume[45, 46] and some are also able to predict the resonance Raman spectrum,[41] but most fail (or never attempt) to reproduce the temperature dependence of the electron's absorption spectrum[10] or excited-state lifetime,[26, 43] the fact that the electron's absorption spectrum is homoegeneously broadened,[23, 73] or the experimentally-measured time-resolved photoelectron spectroscopy (TRPES).[42] Non-cavity simulation models, on the other hand, reproduce the temperature-dependent properties, the homogeneity of the absorption spectrum, and the TRPES and behavior of the hydrated electron near interfaces well,[26, 42, 43, 45] but predict the wrong sign for the molar solvation volume as well as miss (depending on the level of theory) the resonance Raman experiments.[15, 41, 45] And unfortunately, of the few fully *ab initio* models that have been explored, the computational expense is so high that it is nearly impossible to include enough water molecules or to produce enough statistics to provide meaningful comparisons with any of the above experiments.[35, 36, 70]

A few years ago, Kumar *et al.* proposed a simple density functional theory (DFT)-based *ab*

initio model of the hydrated electron consisting of only four quantum mechanical water molecules plus an excess electron surrounded by a polarizable continuum (PCM).[53] The idea of using only four water molecules came from starting with the initial octahedral cavity structure proposed by Kevan,[74] which was found to optimize into a locally tetrahedral cavity structure around the excess electron regardless of the calculation method of choice. These workers also explored the use of an additional explicit solvation shell, with a total of 16 water molecules plus PCM, and saw no change to the basic tetrahedral cavity structure, suggesting that this simple tetrahedral model correctly captures the quantum mechanical essence of the hydrated electron largely independent of the DFT functional used.[53] The zero-Kelvin tetrahedral structure seen by Kumar et al., shown in Fig. 2.1a, is indeed reminiscent of that seen in many traditional cavity model simulations, but has more overlap of the electron's charge density with the explicitly-treated waters than most such models.[53]

After optimizing the geometry of their 4- and 16-water molecule systems to obtain a tetrahedral cavity structure, Kumar *et al.* then tuned the size of the central tetrahedral cavity in order to explore the relationship between the cavity size and the experimental vertical detachment energy (VDE) of the hydrated electron. [16–19, 53] This simplistic zero-K model performed remarkably well when compared to a diverse set of experimental observables, including the room-temperature thermodynamic properties, suggesting that the hydrated electron indeed has a single average structure that seems to be dominant in the room temperature. We were surprised that a static model could correctly represent the room-temperature fluctuating object, which is why in this work, we extend the Kumar *et al.* hydrated electron model by using it as a basis for Born-Oppenheimer molecular dynamics (BOMD), so that entropic effects are explicitly accounted for. Because the model is relatively inexpensive, having either only four or 16 quantum mechanically-treated waters, we are able to run long trajectories (tens to hundreds of ps duration) and to test the model using different DFT functionals. In this way, we can understand the effects of thermal motions and fluctuations on the properties of this minimalistic *ab initio* model of the hydrated electron. There is a past study that used the minimalist model as a basis of molecular dynamics to explore the effect on reduction of the DNA basis,[75] but the structure of the hydrated electron itself was never explored dynamically. We are also able to run the simulations with an optimally-tuned range-separated hybrid functional, which provides a significant advance over other DFT-based simulations that use

more standard hybrid functionals.[34, 35, 53, 70]

For the minimalist 4-water BOMD model of the hydrated electron, we find that when dynamics and thermal motions are introduced to the system, the excess electron is not effectively confined by the four water molecules and PCM, but instead oozes out away from the explicit waters. The initial tetrahedral arrangement of the four water molecules is also destroyed by thermal motions, with the positions of the four waters becoming highly fluxional. Moreover, the average geometry for this model near room temperature exhibits a planar arrangement of water molecules reminiscent of the gas-phase water tetramer, emphasizing how important dynamics and fluctuations are to the hydrated electron system. We also find that the average structure of this simple *ab initio* BOMD model more closely resembles previous non-cavity models rather than the traditional cavity model, and thus this model suffers from all the same problems as non-cavity models. We introduce a set of structural parameters that can be used to numerically quantify how cavity-like (or not) a particular hydrated electron model is. Finally, we calculate the simulated steady-state absorption spectra, photoelectron spectrum and resonance Raman spectra of the model and show that the thermally fluctuating structures do indeed behave somewhat similarly to the experimental hydrated electron, although there is significant deviation due to the fact that four-water system overly fluctuates.

We then extended the model with 12 additional explicit water molecules to serve as a second solvation shell. We find, however, that the local structure of the electron is basically the same as what we observed with only four explicit waters: the electron has little direct interaction with the majority of the additional explicit waters. In fact, the results of our 16-water BOMD trajectories strongly resemble those run without PCM to simulate small water anion clusters,[76] with the excess electron preferring to reside at the cluster surface (where it is stabilized by H-bonds) rather than in the cluster interior. This means that PCM cannot be used as a substitute for explicit waters when considering the properties of the hydrated electron. All of the results suggest that the bulk hydrated electron is a statistical object that requires the interaction of many waters – likely hundreds – in order to correctly describe its experimental properties. The use of small numbers (i.e., tens of waters) provides a better representation of water cluster anions, which do not behave like the bulk hydrated electron at this size.[76–79] Most importantly, we see that fluctuations are critical for understanding the nature of the hydrated electron, and having only a handful of explicitly-treated waters is not sufficient to pin down the correct fluxional behavior.

2.2 Methods

All of our *ab initio* dynamics calculations were performed using the Q-Chem software package.[80] The coordinates of Kumar *et al.*'s model, optimized using the B3LYP functional, were used for the initial geometry for both the 4- and 16-water systems.[53] We also used the IEFPCM[81] (integral equation formalism polarizable continuum model) chosen by Kumar *et al.*, with the constants chosen to represent the dielectric behavior of bulk liquid water. The PCM cavities are built around the Van Der Waals radius of each atom. For calculating VDE's using the PCM, we used non-equilibrium solvation calculations, which separate the fast and slow part of the ionization process.[82] We chose a relatively large triple-ζ basis set, 6-311++G(d,p), which we verified was sufficiently big for our relatively small systems; we note that other groups have used smaller basis sets in hydrated electron simulations and were able to obtain cavity-structure hydrated electrons,[36] so the size of our chosen basis set is not structurally-limiting. The effect of possible insufficient basis set at the center cavity was checked and shown in the SI where addition of a ghost atom did not provide much of a difference in the electron center-of-mass and ionization energy. The nuclei, including the water protons, were treated classically, with the Born-Oppenheimer molecular dynamics (BOMD) propagated via the velocity Verlet algorithm with a time-step of 0.5 fs. The four-water model was propagated in the microcanonical ensemble and the 16-water model was propagated in the canonical ensemble using the Nose-Hoover chain thermostat to restrain the system to room temperature. [83] The average temperature of the four-water system also was $\sim$300 K, but with large fluctuations as expected for the small number of classical particles in the system, as shown in the Supporting Information (SI). The VMD software package was used to visualize the molecular trajectories including the electron spin density.[84] Further calculational details, including those of the mixed quantum/classical models run for comparison purposes, are also given in the SI.

Our first set of trajectories were run using the standard hybrid B3LYP functional,[81] as this was one of the main functionals used by Kumar *et al.* to analyze their zero-Kelvin structure of the four-water hydrated electron. We ran three 10-ps B3LYP-based BOMD trajectories with four explicit waters plus PCM and and an excess electron and found that all three trajectories were unbound: no matter what we chose for the initial condition, after a relatively short period of time, one of the four water molecules always moved away to a point where it no longer interacted with the excess

electron. In other words, even though the zero-Kelvin minimum with the B3LYP functional has a well-defined tetrahedral cavity geometry with all four waters stabilizing the electron, the thermal energy available at roughly room temperature is enough to completely break the four-water system apart, as described in more detail in the SI.

Given the difficulties in producing any physically meaningful geometries with the B3LYP functional, we turned next to a more sophisticated range-separated hybrid functional, the BNL functional;[85, 86] as far as we are aware, this is the first time an optimally-tuned range-separated hybrid function has been used to simulate the hydrated electron. We successfully used the BNL functional, with the same triple-ζ basis set used here, in the past to predict the photoelectron spectra of water cluster anions with four to six water molecules, and found that with the appropriate choice of the range separation parameter, we could reproduce water cluster anion VDEs calculated at the eom-IP-CCSD level of theory (with a quad-*zeta* basis plus diffuse functions) with better than 1% accuracy.[76] Thus, for the current work including four waters and PCM, we optimized the range-separation parameter to a value of 0.08 bohr^{-1} to satisfy Janak's theorem,[87] as described in the SI, and then ran a full set of BNL-based BOMD trajectories. Dispersion corrections were not applied since all available corrections were not empirically optimized for the BNL functional. We found that indeed, the BNL-based four-water plus PCM and excess electron system remained intact with thermal fluctuations averaging around room temperature, so these trajectories form the basis for all of the results presented below. We also chose the BNL functional for our 16-water BOMD trajectories, re-optimizing the range separation parameter for this larger system to a value of 0.065 bohr^{-1}. For both systems, we chose uncorrelated configurations separated by at least 100 fs for our calculations of ensemble-averaged properties, which are discussed in the next section. We also ran mixed quantum/classical simulations of the hydrated electron using both the Turi-Borgis (TB) and Larsen-Glover-Schwartz (LGS) pseudopotentials for comparison to the limits of cavity and non-cavity models, respectively, as described in the SI.

2.3 Results and Discussion

For all of the controversy over the structure of the hydrated electron, it has not been clear how one can calculate the full range of experimental properties from *ab initio* simulations that of ne-

cessity have limited numbers of water molecules and/or short trajectory times. Given the success of Kumar *et al.*'s model at zero Kelvin,[53] we thought that extending the model to include dynamics would provide an interesting test of the role of fluctuations and entropy in the calculated properties of the hydrated electron, particularly as we have recently shown that entropic effects are important in determining the properties of mixed quantum/classical hydrated electron models.[88] As described in the previous section, however, the four-water *ab initio* model whose properties were largely independent of the choice of functional at zero Kelvin becomes highly dependent on the choice of functional when dynamics are included. In fact, as mentioned above, we found that the BOMD trajectories we ran were unstable to dissociation of a water molecule when using the B3LYP functional, but that the four waters and electron plus PCM held together when using the range-separated hybrid BNL functional. This provides the first indication that the minimalist *ab initio* model isn't entirely robust, and as we show below, the results emphasize the importance of including fluctuations as critical to understanding any calculated properties of the hydrated electron.

2.3.1 Structure of Minimalist Room-Temperature BOMD Models of the Hydrated Electron

We start by examining the results of our BNL-based four-water-plus-PCM BOMD trajectories of the hydrated electron. The most significant thing we observe is a large change in average structure from the zero-Kelvin geometry. The zero-Kelvin tetrahedral structure, which we optimized including a constraint to hold the tetrahedral geometry (see the SI for details on what happens when this constraint is relaxed), is shown in Fig. 2.1a. As discussed by Kumar et al.,[53] the zero-K excess electron largely occupies a cavity between the molecules; the distances between the electron and other atoms correspond to the delta functions in the pair distribution function shown in Fig. 2.2d. In contrast, the average structure of the room-temperature four-water BOMD model has the four water molecules tending to reside inside the bulk of the electron's charge density, as seen in the red and blue curves in Fig. 2.2a. As a comparison to the extremes in possible hydrated electron structures, we also show in Figs. 2.2b and 2.2c, respectively, the pair distribution functions of the closest four water molecules for the Turi-Borgis (TB) cavity[11] and Larsen-Glover-Schwartz (LGS) non-cavity[33] mixed quantum/classical hydrated electron models. Clearly, when fluctuations are

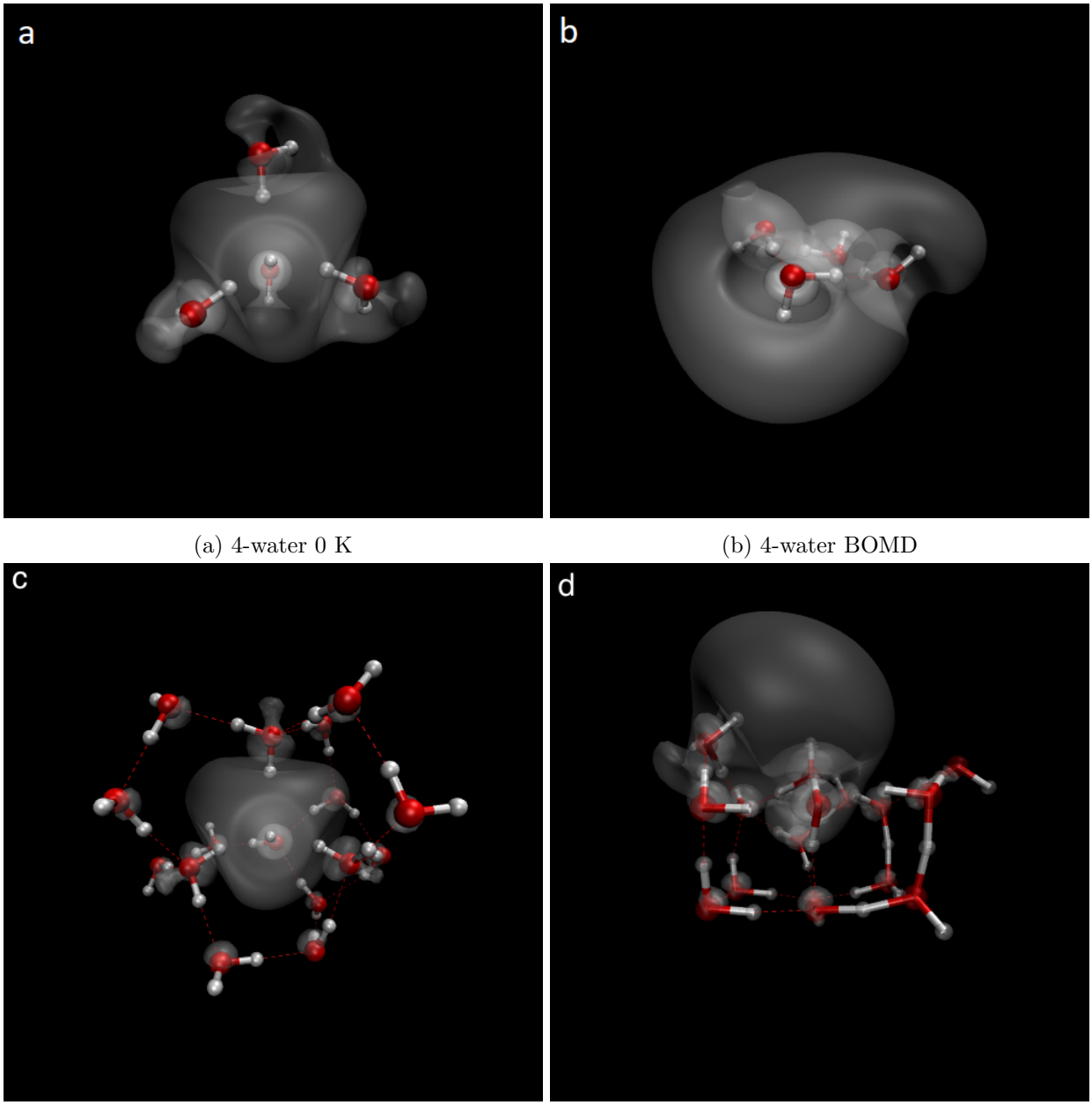

(a) 4-water 0 K

(b) 4-water BOMD

(c) 16-water 0 K

(d) 16-water BOMD

Figure 2.1: (a) The four-water + PCM, zero-Kelvin, tetrahedral hydrated electron geometry of Kumar *et al.*,[53] optimized using the BNL functional. The optimization was done by applying geometric constraints to ensure a tetrahedral water geometry. (b) A representative snapshot from the room-temperature BNL-based four-water BOMD trajectories. (c) The optimized 16-water + PCM, zero-Kelvin, tetrahedral hydrated electron geometry of Kumar *et al.* (d) A representative snapshot from the room-temperature BNL-based BOMD trajectories using 16 water molecules. For all four panels, the gray surface represents the 70% contour of the spin density. Clearly, the initially-tetrahedral zero-K geometry surrounding the excess electron changes drastically when dynamics are applied, with the waters favoring hydrogen bonding to each other more than with the excess electron. Thermal motions also cause the excess electron density to move outwards in a fashion not seen at zero Kelvin, emphasizing the importance of fluctuations in determining the hydrated electron's structure.

included, the zero-K *ab initio* cavity-like model becomes much more reminiscent of the LGS non-cavity model than the more traditional TB cavity model.

To test the effect of system size, we also carried out a similar analysis for the version of the model with 16 explicit waters. Starting from the optimized structure by Kumar *et al.* with a tetrahedral cavity around the excess electron, shown in Figs. 2.1c and 2.2h, we find that the average structure of the room-temperature collapses in much the same way as with the four-water version, as seen in Figs. 2.1d and 2.2e. For comparison, we also calculated the radial distribution functions of both the TB and LGS models using only the 16 closest water molecules, shown in Figs. 2.2f and 2.2h. Clearly, like the 4-water model, the radial distribution function of the 16-water room-temperature BOMD is much more similar to the LGS non-cavity model than to traditional cavity models. This suggests that *ab initio* BOMD models of the hydrated electron with minimalist numbers of waters plus PCM suffer from all the same problems as the LGS model, which is not well-accepted in the literature.[33, 46, 66]

Figure 2.1b shows a representative snapshot from the four-water room-temperature BOMD trajectories, respectively. Unlike the zero-Kelvin structure, which had the water molecule H atoms pointing towards the electron's center-of-mass (i.e., H-bond solvation of the electron), the dynamical structure suggests that with thermal energy, the water molecules prefer to make H-bonds with each other rather than with the excess electron. The preference is strong enough that the four waters on average adopt a flat, ring-like geometry reminiscent of the gas-phase water tetramer[77, 89] rather than an arrangement that looks like the zero-Kelvin tetrahedral cavity structure. This preference to maintain the water-water H-bonds is also consistent with what is known from studies of non-cavity models, which suggest there is a temperature-dependent free energy penalty for creating empty volume and breaking the pure water H-bonding network.[33, 66, 88]

The 16-water snapshot seen in Fig. 2.1d, on the other hand, bears a striking resemblance to what we saw in previous simulations of water anion clusters (using the same DFT functional) with similar numbers of water molecules but without the use of PCM.[76] The electron clearly prefers to sit on the surface of the cluster, stabilized by H-bonds of the few waters in the cluster that are adjacent to it. The other waters in the cluster make H-bonds with each other, and the addition of PCM seems to make little difference to the overall outcome, as we verified with a set of calculations using the same uncorrelated configurations, but without the use of PCM. We explore what happens

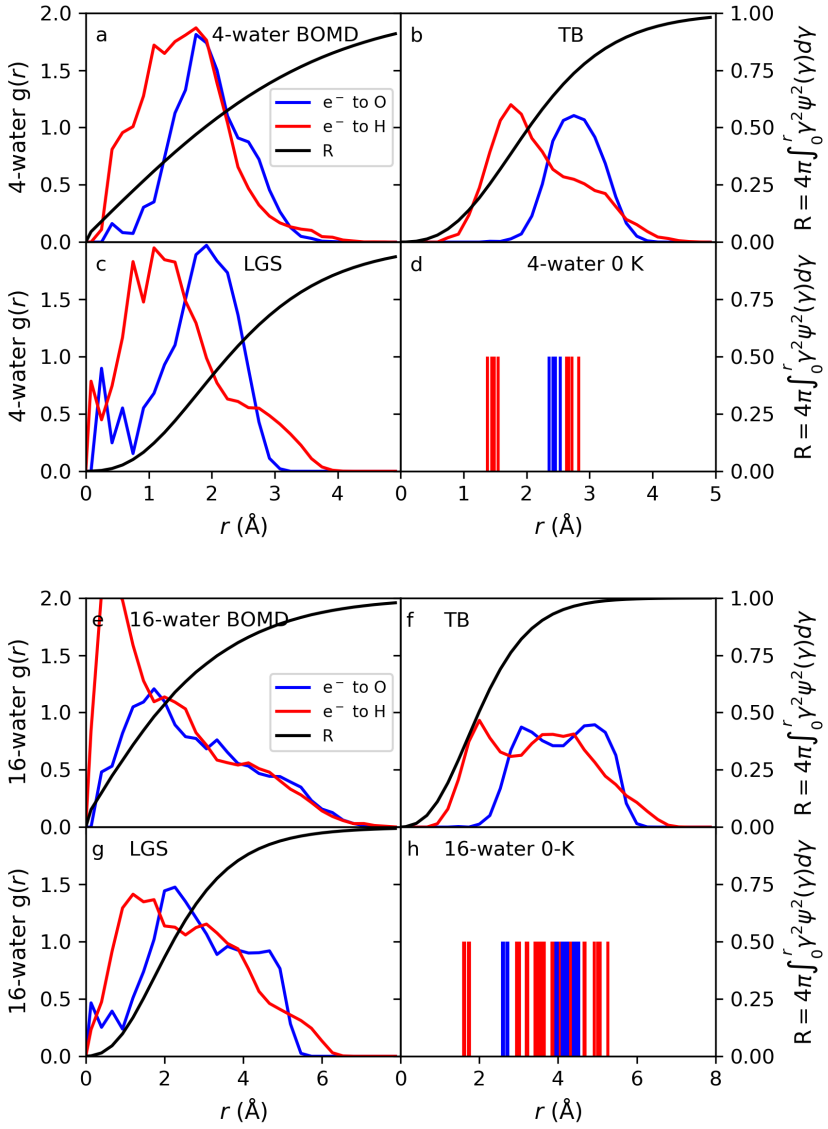

Figure 2.2: Radial distribution functions (RDFs) from the excess electron's center-of-mass for water hydrogen (red curves) and oxygen atoms (blue curves) for (a),(e) the BNL-BOMD (this work), (b),(f) the TB[11] and (c),(g) the LGS[33] hydrated electron models. The red and blue vertical lines coming up from the abscissa in (d),(h) represent the distance between the electron's center-of-mass and the hydrogen and oxygen atoms for the waters in the zero-Kelvin tetrahedral model whose structure is shown in Figs. 2.1a and 2.1c. The top and bottom sets of plots correspond to the four- and 16-water room-temperature BOMD models, respectively. All of the RDFs were normalized by using the number density of bulk water and calculating the volume of 4 or 16 water molecules. The results show clearly that the room-temperature BNL-BOMD models' excess electron more closely resembles the non-cavity LGS model than the TB cavity model, and bear little resemblance to the zero Kelvin structure. The black curves in each panel show $4\pi \int_0^r \gamma^2\psi^2(\gamma)d\gamma$ where $\psi(\gamma)$ is the wavefunction/spin density of the excess electron for each model.

without PCM in detail in the SI, but the general result is that the average distance between the center of mass of the electron and the center of mass of the cluster is largely unaffected by the presence of PCM. The cluster ionization energy does shift in the presence of PCM, as expected, but as discussed below, the amount of this shift is not nearly enough to recover the experimental ionization energy of the bulk hydrated electron. Thus, PCM simply shifts the electron binding energy but does not alter the structure to mimic a bulk system instead of that of a small cluster anion. This shows explicitly that PCM cannot be used as a substitute for explicit water molecules when simulating the properties of the bulk hydrated electron. Since it is well known that water anion clusters in the size range of a few tens of water molecules do not have the properties of the bulk hydrated electron,[78, 79] this result strongly suggests that *ab initio* simulations that also use only a few tens of water molecules are missing important physics underlying this object. We believe that hundreds of waters are necessary for a correct description of this object, something that is unfortunately currently out-of-range in terms of computational cost for BOMD simulations.

As a way to help quantify the arrangement of the water molecular orientation relative to the electron's center-of-mass, we calculated the asphericity A of the four closest water molecules in each simulation to the electron, defined from the positions of the water O atoms as:

$$< A >= \frac{< (\mathrm{Tr}^2 - 3M) >}{< \mathrm{Tr}^2 >}, \tag{2.1}$$

where $\mathrm{Tr} = R_1^2 + R_2^2 + R_3^2$ and R_1, R_2 and R_3 are the eigenvalues of the gyration tensor, and $M = R_1^2R_2^2 + R_1^2R_3^2 + R_2^2R_3^2$.[90] With this definition, A is zero for a three-dimensionally symmetric arrangement of the water molecules, 0.25 for a two-dimensionally symmetric arrangement, and 1.0 for a linear one-dimensional arrangement. Indeed, for the 4-water zero-K structure of Kumar et al., we calculate $A = 0.008$, a value near zero as expected. For the room-temperature BOMD trajectories, A never approaches zero but instead fluctuates around an average value of 0.34 for the four-water model (Fig. 2.3a) and 0.48 for the 16-water model (Figure 2.3b), suggesting an average local geometry of the waters near the electron that is closer to flat, consistent with the snapshots shown in Figs. 2.1b and d.

Figure 2.3c show the distribution of angles between the vectors connecting the electron's center-of-mass to the four closest water O atoms for the four- and 16-water BOMD models, respectively,

which for the zero-K tetrahedral arrangement both had a value very close to 109.5°. When thermal fluctuations are included, the average angle is closer to 70° for both BOMD models, another signature of the fact the water molecules prefer to make H-bonds with themselves rather than with the excess electron at room temperature. Overall, Fig. 2.3 indicates clearly that when fluctuations are accounted for, the local molecular geometry is not even approximately tetrahedral, so that the zero-K structure is not a good indicator of the average structure at room temperature.

One subject of current interest in the literature is how much the hydrated electron's wavefunction overlaps with the closest surrounding water molecules. In previous work, we calculated the 'direct overlap' Θ of the hydrated electron for different simulation models, defined as the fraction of the excess electron that resides within a certain distance r_c of the O atom on each of the surrounding water molecules:[66]

$$\Theta = \Big\langle \sum_{i=1}^{n_{\text{molcs}}} 4\pi \int_0^{r_c} r_i^2 |\Psi(r_i)|^2 dr_i \Big\rangle, \tag{2.2}$$

where r_c was chosen to be 1.0 Å, the same as the water O–H bond length and thus a good measure of the size of water's core molecular orbitals. The results for the room-temperature BOMD models as well as for the four instantaneously closest waters in the TB and LGS models are given in Table 2.1 as the '4-water direct overlap'. Not surprisingly, the TB cavity model shows a small direct overlap, indicating that the electron is strongly repelled from the water molecular cores, with little fluctuation in overlap as expected for such a strongly repulsive model.[88] In contrast, the four-water BOMD results have an average value and standard deviation that are quite similar to that of the non-cavity LGS model, suggesting that when thermal fluctuations are included, the electron becomes more likely to overlap the nearby waters. It is worth noting that the BNL-based cavity structure at zero Kelvin also has a high direct overlap with the explicit waters. This likely reflects the fact that the water molecules at zero K strongly interact with the excess electron due to a lack of hydrogen bonding with each other (or any exterior water molecules), and indicates that the nature of the zero-Kelvin *ab initio* hydrated electron model is fundamentally different than the TB model, even though both have central cavities.

Table 2.1 also shows that the 16-water BOMD simulation has a smaller direct overlap when both the closest four and all 16 water molecules are considered. For comparison, we also calculated

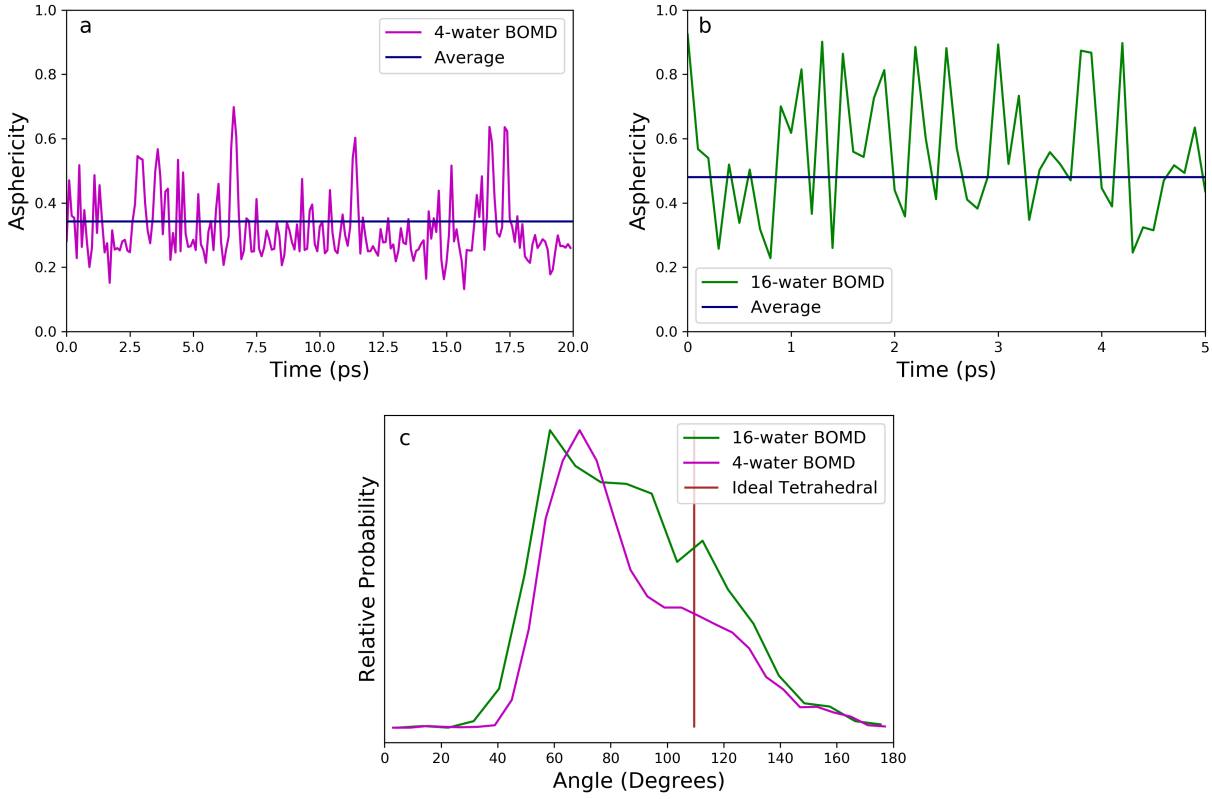

Figure 2.3: (a),(b) Asphericity A (see text for definition) of the room-temperature 4-water and 16-water BOMD model of the hydrated electron, with values calculated from uncorrelated configurations every 100 fs along a 20-ps and 5-ps trajectory. The navy horizontal line shows the average ashpericity value of 0.34 for the 4-water model calculated from five 20-ps long trajectories and 0.48 for the 16-water model calculated from four 5-ps long trajectories. Clearly, thermal fluctuations destroy any tetrahedral memory of the zero-K structure, as the asphericity value never approaches zero. (c) Distribution of angles between vectors connecting the electron's center-of-mass to the water O atoms for the same uncorrelated configurations in (a) and (b). If the O atoms are arranged perfectly tetrahedrally from the electron's center-of-mass, as in the zero-K structure, the distribution is a delta function at 109.5°. The fact that the room-temperature average is far from this value reflects the more planar average structure seen in Figure 2.1b and 2.1d.

Table 2.1: Direct overlap Θ, Eq. 2 (with n_{molcs} running over either the 4 or 16 closest water molecules), cavity order parameter q^{cav}, and radius of gyration of the experimental hydrated electron and the TB, LGS and room-temperature BNL-BOMD models. The values after the $\pm$ signs are the standard deviation for the fluctuating direct overlap and cavity order parameters. The results show that the as far as overlap is concerned, the four-water BOMD model resembles the LGS non-cavity model more than the TB cavity model and vice-versa for the 16-water BOMD model. The fact that the zero-Kelvin *ab initio* tetrahedral structure has such a high direct overlap 14.3% shows that the zero-K Kumar et al. model still behaves fundamentally differently than the traditional TB cavity model.

	4-water Direct Overlap	16-water Direct Overlap	Cavity Order Parameter	Radius of Gyration (Å)
Expt.	N/A	N/A	N/A	2.45
4-BOMD	8.65% ± 1.44%	N/A	0.766 ± 0.38	2.92
16-BOMD	3.15% ± 1.41%	4.25% ± 1.44%	0.768 ± 0.50	3.21
TB	2.98% ± 0.81%	4.57% ± 0.91%	0.012 ± 0.06	2.42
LGS	8.64% ± 2.77%	14.1% ± 2.85%	0.886 ± 0.43	2.5

the direct overlap with the 16 closest water molecules in the TB and LGS models, which shows that for the 16-water BOMD model, the direct overlap value is more similar to that of the TB cavity model. This is a direct reflection of the fact that in the 16-water model, the electron density is more water-anion-cluster-like, with the bulk of the electron density protruding into the PCM outside the water molecules, as seen in Fig. 2.1d. We believe that this behavior is unrepresentative of the bulk hydrated electron, as EPR experiments suggest that there should be reasonable overlap of the hydrated electron with the nearby waters.[50, 71] Thus, for minimalist simulations in this size range, adding more waters to the BOMD simulation doesn't necessarily improve things as far as representing the bulk object is concerned.

Finally, we also characterized the cavity/non-cavity nature of different hydrated electron models using a cavity order parameter that we recently introduced in another context.[88] The order parameter q^{cav} is defined as:

$$q^{\text{cav}}(\boldsymbol{R}^N) = \sum_{i=1}^{N} S(|\boldsymbol{R}^i - \boldsymbol{r}_e|), \tag{2.3}$$

$$S(r) = \frac{1}{\exp[\kappa(r - r_e)] + 1}, \tag{2.4}$$

where R^i is the distance of the i^{th} water molecule's O atom from the electron's center-of-mass. This function essentially integrates the number of water molecules within the distance of r_e of the electron's center. If we take the four instantaneously closest waters in the TB and LGS models as limits of cavity and non-cavity behavior, respectively, then the choice of $r_e = 1.75$ Å and $\kappa = 10$ Å^{-1} gives a value of q^{cav} of 0.89 for LGS and essentially zero for TB. This means that q^{cav} provides a nice distinction between different possible hydrated electron structures, as summarized in Table 2.1. The results show that the minimalist BOMD models have a similar q^{cav} as the LGS model, demonstrating that thermal energy is able to drive water molecules into the interior of what was otherwise a stable zero-K cavity structure. The fact that the 16-water BOMD model has a similar value of q^{cav} but a different value of Θ as the four-water model serves to emphasize that the presence of interior waters does not necessarily imply significant overlap and vice-versa. The large standard deviation in q^{cav} for both the LGS and BOMD models indicates that the number of waters residing close to the electron's center is highly fluxional, so that entropy places a large role in the cavity or non-cavity structure of the excess electron. The TB model shows essentially no fluctuations of water into the cavity interior, and we have argued in previous work that it is these fluctuations that are responsible for the temperature dependence of the hydrated electron's absorption spectrum and excited-state lifetime.[43, 88]

Overall, when thermal energy is added to the minimalist *ab initio* model of Kumar *et al.*, entropic contributions modify the overall structure from cavity-like to more non-cavity-like. Going from four to 16 water molecules makes little difference other than producing a smaller direct overlap value, which may actually increase the disagreement with experiment. In fact, in the presence of thermal fluctuations, the dynamical version of Kumar *et al.*'s model behaves quite a bit like the mixed quantum/classical LGS model and thus likely suffers from the same shortcomings, such as giving the wrong sign of the molar solvation volume based on the average number of interior waters.[45, 46] We note that most previous *ab initio* simulations of the hydrated electron, most of which used more water molecules than we use here, only minimally characterize the structure produced in their simulations: they usually plot only the radial distribution function,[34, 35, 70] or in some cases present only a few snapshots[36] to conclude that the excess electron resides in a cavity.[34–36, 53, 70] With the various structural parameters employed in this section, A, Θ, q^{cav}, etc., it is possible to numerically compare the structures of different hydrated electron models, and

we hope that parameters like these can be used by other groups in the future. To understand the importance of a hydrated electron model's structural details, we turn in the next section to testing the BOMD models against multiple different experiments. But the most important conclusion is that for any hydrated electron model, a zero-Kelvin or average structure is inadequate to explain the properties of the hydrated electron: clearly, thermal fluctuations are an extremely important part of the behavior of this statistically fluctuating quantum object.

2.3.2 Experimental Predictions of Minimalist BOMD Models

One of the successes of the zero-Kelvin version of Kumar *et al.*'s minimalistic *ab initio* model of the hydrated electron is that when the distances of the four water molecules were adjusted to match the experimental VDE, which was reported to be around 3.3 - 3.7 eV,[16–19] the resulting cavity size and absorption spectrum were in good agreement with experiment.[53] This leads to the question of how well that agreement persists when thermal fluctuations are added to the model and the presence of the central cavity is effectively destroyed.

We begin by examining the VDE of the minimalist BOMD hydrated electron models by calculating what would be expected in a photoelectron spectroscopy experiment. Since we optimally tuned the range-separation parameter of the BNL functional used in the simulations, as described in the SI, the singly-occupied molecular orbital (SOMO) energy is by construction equal to the ionization energy for each simulated configuration. Thus, we simply binned up the SOMO energies of uncorrelated configurations to simulate the steady-state photoelectron spectrum, the results of which are shown in Figure 2.4. The figure show that when thermal energy is added to the system, there is a large shift of the VDE toward lower binding energies relative to the 3.2-eV value of the zero-K four-water plus PCM structure. Clearly, thermal motions drive a lot of repulsive overlap between the excess electron and the nearby water molecules, making it easier to detach the electron, leading to a predicted VDE that is in contrast with experiment. Surprisingly, increasing the number of BOMD waters from four to 16 makes little difference in the predicted VDE, which is another sign that these minimalist models do not adequately represent the nature of the experimental bulk hydrated electron.

Next, we turn to the hydrated electron's resonance Raman spectrum. Experimentally, the hydrated electron's resonance Raman spectrum looks much like that of bulk water's, but with a

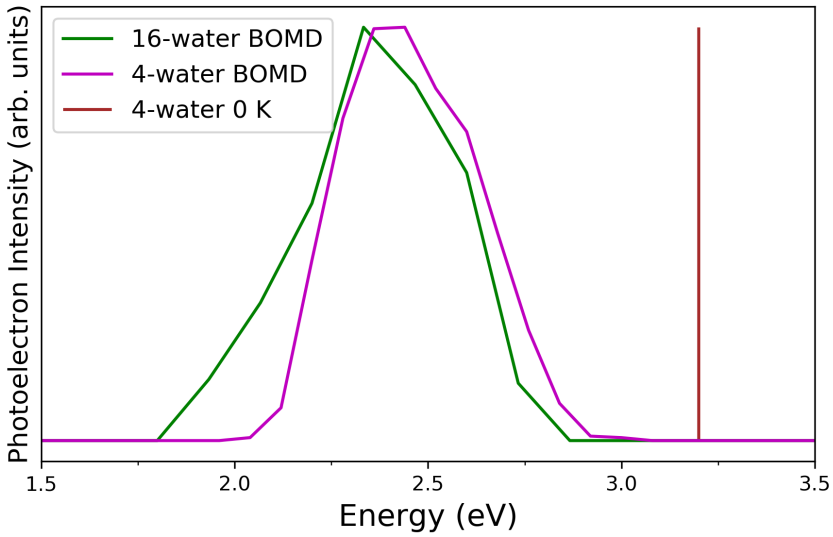

Figure 2.4: The photoelectron spectra simulated by binning the SOMO energies from uncorrelated configurations drawn from the room-temperature BOMD trajectories of the 4-water plus PCM BOMD model (magenta curve), and the 16-water plus PCM BOMD model (green curve). Compared to the experimental VDE value of 3.4-3.7 eV and the 4-water zero-Kelvin calculated VDE of 3.2 eV, represented as a brown vertical line, it is clear that thermal motions significantly reduce the binding of the excess electron for both *ab initio* dynamic models.

red-shifted and broadened O–H stretch.[4] In previous work,[15] we estimated the resonance Raman spectrum of mixed quantum/classical models of the hydrated electron using a frequency/electric field map parameterized to reproduce the Raman spectrum of bulk water,[91–93] and found that the LGS non-cavity model provided excellent agreement with experiment whereas the TB cavity model showed a qualitatively incorrect (blue-shifted and narrowed) O–H stretch.[15] A set of recent QM/MM calculations, however, has shown that cavity model hydrated electrons can qualitatively reproduce the Raman spectrum of the hydrated electron, presumably due to a small amount of occupation of the water LUMO by the excess electron that cannot be accounted for in mixed quantum/classical simulations.[41] These calculations also showed that a cavity hydrated electron structure could also provide an explanation for the isotopic splitting of the water bend that is missed by the LGS model.[41]

To calculate the resonance Raman spectrum of any object, the various vibrational normal modes need to be weighted by how much they are displaced upon electronic excitation. We have shown previously, however, that the average displacement of the O–H stretch upon excitation of the electron is roughly constant for water molecules that are within 4 Å of the electron's center, and

fairly negligible for waters outside this distance.[15] If we take advantage of this fact, we can estimate the resonance Raman spectrum for the room-temperature BOMD simulations by calculating the *ab initio* frequencies of the waters in this range and simply binning them with equal weight, as shown in Fig. 2.5. For the water molecules outside of the 4 Å range, instead of simply excluding them from the Hessian matrix calculation, we employed a vibrational subsystem analysis[94] in which vibronic interactions between the included and excluded molecules are implicitly folded into the calculation. We note that the Q-chem software we used for these simulations does not support Hessian matrix calculations with the IEFPCM model, so for calculation of the normal modes for our selected uncorrelated configurations, we used CPCM (conductor-like PCM) instead.[95]

Figure 2.5a shows that both the 4-water BOMD and experimental resonance Raman spectra have a similar peak O–H stretch peak location near 3100 cm^{-1}, an agreement which is better than most other models in the literature.[15, 41] The 16-water BOMD resonance Raman spectrum in Fig. 2.5b shows a peak that is further red-shifted, so that the addition of the 12 explicit water molecules actually makes the agreement with experiment worse. However, we also see that both the 4-water and 16-water BOMD calculated spectra are far too broad compared to experiment. We believe that this is a reflection of the fact the large fluctuations of the hydrated electron's structure in these models are also causing large fluctuations of the calculated normal mode frequencies. Thus, like the LGS model,[88] the broad width of the calculated resonance Raman spectra demonstrates that the room-temperature BOMD model overly fluctuates compared to the experimental hydrated electron. In contrast, the 4-water zero-K cavity structure has a predicted *ab initio* Raman spectrum that is too blue-shifted compared to experiment,[53] suggesting that neither the H-bonding environment of the waters nor the overlap of the electron's wavefunction with the water is captured correctly at zero Kelvin.

As mentioned in the introduction, one of the most standard experimental benchmarks of hydrated electron models is the optical absorption spectrum. The absorption spectrum is directly related to the radius of gyration of the electron's ground-state wavefunction, as explicitly connected through spectral moment analysis.[44] Since DFT-based simulations do not provide reliable excited states for calculating the transition dipole matrix elements underlying the optical absorption, we calculated the lowest 10 excited states using time-dependent DFT (TD-DFT) using the same optimally-tuned BNL functional on a series of uncorrelated configurations from each of the

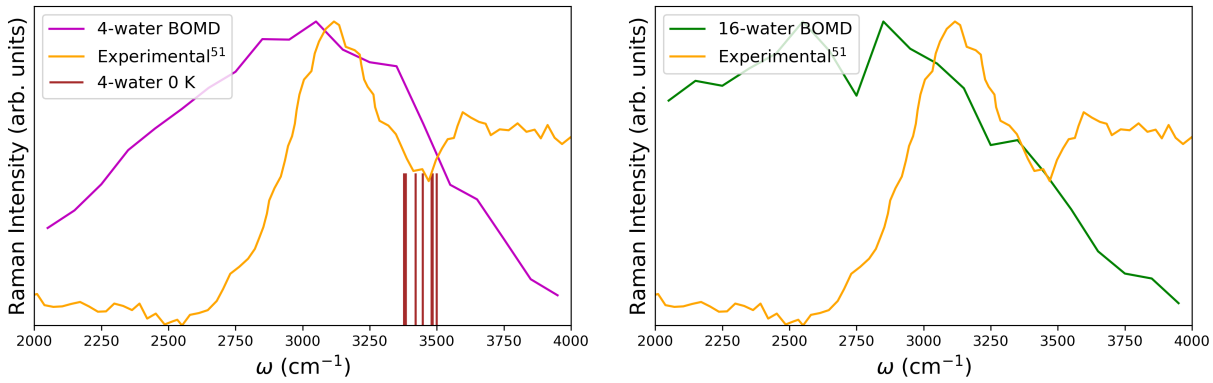

(a) 4-water BOMD

(b) 16-water BOMD

Figure 2.5: The resonance Raman spectra calculated from (a) the four- (magenta curve) and (b) 16-water (green curve) room-temperature BOMD simulation (see text for details) and measured by experiment (yellow curves in both panels).[4] The high fluctuations of both the geometry and electron density in the BOMD trajectories causes the calculated resonance Raman spectrum to be much broader than the experimental spectrum. For comparison, the red delta functions in panel (a) represent the normal modes of the 4-water zero-Kelvin tetrahedral structure, which are significantly blue-shifted compared to experiment, suggesting that the zero-K four-water model does not adequately reproduce this feature of the experimental hydrated electron.

BOMD ground-state trajectories. The transition dipoles between the ground and excited states were then computed and binned according to their energy gaps, producing the calculated spectrum shown in Fig. 2.6. The general shape and width of both the four- (panel a) and 16-water (panel b) room-temperature BOMD spectra are similar to the experimental spectrum,[10] but the positions are significantly red-shifted, reflecting the fact that the average radius of gyration of the room-temperature BOMD electrons is too large, as discussed further below. As is typical with nearly every hydrated electron model, the calculated spectra are dominated by transitions to the first three excited states, so-called *s*-to-*p*-like transitions.

To verify the reasons for the red-shift of the room-temperature-BOMD-simulated *ab initio* hydrated electron absorption spectra, we calculated the excess electron's radius of gyration using the spin density, as summarized in Table 2.1. The results indicate that unlike the more standard TB and LGS mixed quantum/classical models, whose predicted absorption spectra agree generally well with experiment,[11, 33] the radius of gyration of the BOMD models is indeed larger than the experimental value. This is because the polarizable continuum model is simply unable to confine the excess electron as much as Pauli exclusion from explicit water molecules, allowing the BOMD

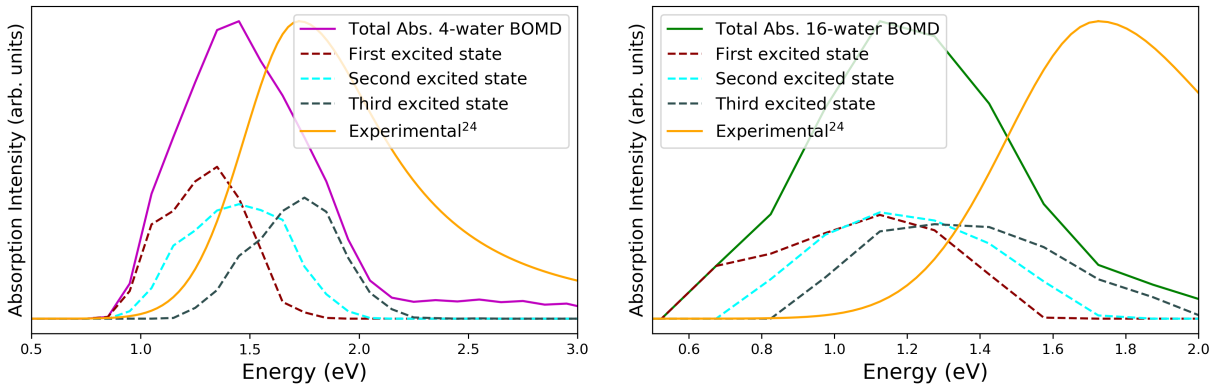

(a) 4-water BOMD

(b) 16-water BOMD

Figure 2.6: Room-temperature BOMD model predicted absorption spectra, calculated by via TD-DFT using the BNL functional on uncorrelated snapshots along the ground-state trajectory for (a) the 4-water + PCM minimalist BOMD model (magenta curve), and (b) the 16-water + PCM minimalist BOMD model (green curve), respectively. Transition dipoles to the lowest 10 excited states were used to build the calculated absorption spectrum. The dark red, cyan and grey curves represent the contributions of transitions to the first, second and third excited states to the total absorption spectrum, respectively. The orange curve in each panel shows the experimental absorption spectrum. The BOMD absorption spectra are red-shifted relative to experiment in both models due to a too-large radius of gyration caused by inadequate electron confinement of the PCM.

electron to balloon into the region where there are no explicit waters present. This idea not only explains the red-shift of the calculated absorption spectra, but also the decreased VDE, as it is well known that the VDE varies inversely with the hydrated electron's radius of gyration.[34, 72]

We note that other *ab initio* simulations also produce a radius of gyration that is somewhat too large,[34, 36] suggesting that it is quite difficult for DFT-based BOMD to correctly capture the true spatial extent of the hydrated electron. This is because it is challenging to accurately account for the small amount of mixing of the electron's wavefunction into the surrounding water LUMOs, which has a large effect on the radius of gyration because these waters have molecular orbitals whose charge density resides far from the electron's center-of-mass, and because it is difficult to properly capture thermal fluctuations with unrealistically small systems and limited sampling. Overall, we believe that the rough agreement of the zero-Kelvin minimalist model with experimental values such as the radius of gyration, VDE, vibrational spectrum and ESR coupling is largely a coincidence, as the dynamically fluctuating versions of this model show very different behavior than the single, unrepresentative zero-K snapshot.

2.4 Conclusions

In this paper, we have extended Kumar *et al.*'s zero-Kelvin minimalist water-plus-PCM *ab initio* model of the hydrated electron[53] to include thermal fluctuations at room temperature via BOMD. We find that even though the zero-K model is in good general agreement with experiment for the VDE and radius of gyration (but not the resonance Raman spectrum), when thermal motions are included, this simple model is inadequate to correctly capture the physics of the hydrated electron. Unlike at zero Kelvin, the BOMD models becomes highly dependent on the choice of DFT functional employed, with the common B3LYP hybrid functional actually leading to detachment of one of the four waters. With the optimally-tuned BNL range-separated hybrid functional, which did an excellent job reproducing the properties of small water anion clusters,[76] we find that the minimalist BOMD hydrated electron model behaves more like the non-cavity LGS model than any traditional cavity model in terms of its structure. The details of the BOMD model, such as the amount of electronic overlap of the excess electron with the surrounding water, do depend on how many waters are treated explicitly, but the general trend is that no central cavity is observed. This means that minimal BOMD models have all the same flaws as the LGS non-cavity model, including giving the wrong sign of the molar solvation volume,[45, 46] in addition to a too-large radius of gyration that leads to a red-shifted absorption spectrum and lower VDE than experiment.

It is worth noting previous DFT-based hydrated electron simulations using 32 QM water molecules showed a cavity-like structure,[34] while the 16-water simulations performed here show no sign of cavity behavior. This suggests that the transition to cavity-like behavior happens between 16 and 32 water molecules, which seems unlikely given that there is no sign of this transition in experiments on water cluster anions,[78, 96]or the use of MM waters and/or the use periodic boundary conditions approximate bulk behavior very differently than the PCM model used in Kumar et al.'s model and our extension of it here. We are not aware of any systematic exploration of finite-size effects in hydrated electron simulations using periodic boundary conditions, but the simulations presented here show that even 16 waters are nowhere near enough to capture the correct bulk behavior, even with the addition of PCM.

Given that the minimalist model works reasonably well at zero Kelvin, why does it fail at room temperature? In the zero-Kelvin version of the minimalist model, Kumar *et al.* found that

adding up to a dozen more water molecules made little difference to the calculated excess electron's properties. Yet, when thermal motion is added to the model, it becomes clear that the PCM is unable to provide adequate confinement of the excess electron, even when up to 16 explicitly-treated waters are used. The use of PCM merely shifts the electron binding energy, although not enough to be in agreement with experiment, and is not capable of altering the structure of the excess electron relative to what would have been observed in a small water cluster anion. Even if we were to use additional explicitly-treated waters in a BOMD model, however, it still remains unclear that DFT, even with an optimally-tuned range-separated hybrid functional, provides a sound basis for the quantum chemistry of the bulk object. Non-DFT-based *ab initio* simulations of the hydrated electron have been performed,[36] but the computational expense even with a limited number of water molecules (to date less than 50) precludes sufficient statistics to make meaningful comparisons with experiment. Our results indicate that whatever model is used to simulate the hydrated electron, replacing water molecules outside of the first two solvation shells with the PCM is not adequate for correctly capturing the physical behavior of this object.

The most important conclusion of this work, however, is the importance of fluctuations in determining the properties of the hydrated electron. The dramatic structural and electronic changes we observed between the zero-Kelvin and room temperature versions of the four- and 16-water models show that thermal motions are critical to any proper description of the hydrated electron. Even for cavity models, treating the electron as a quasi-halide ion doesn't make sense, as the size, shape and amount of overlap of the electron with the nearby waters is constantly fluctuating due to thermal motions.[88] Most of the *ab initio* simulations in the literature have not addressed the effects of fluctuations,[34–36] many of which can be simply captured with parameters such as the direct overlap Θ or q^{cav} coordinate, described above. Entropy is clearly the key to the temperature-dependent properties of hydrated electrons that are not well described by cavity models,[26, 42, 43, 88] so that any model of the hydrated electron, no matter how minimalist, must include temperature-driven fluctuations in order to provide a faithful picture of this fascinating object.

Chapter 3

Understanding the Temperature Dependence and Finite Size Effects in Ab Initio MD Simulations of the Hydrated Electron

3.1 Introduction

The nature of the hydrated electron, an excess electron solvated by liquid water, is still the subject of debate despite its apparent simplicity. Until recently, much of the theoretical work studying the hydrated electron was based on mixed quantum/classical simulations, where the electron is treated quantum mechanically but the water molecules are treated classically.[11–13, 40, 43, 69] The structure and properties of the hydrated electron obtained in such simulations are highly sensitive to the pseudopotentials used to describe the electron–water interaction.[11, 13, 97] To

date, most MQC simulations (but not all[13]) have concluded that the hydrated electron occupies a cavity in the water.[11, 12, 32] However, MQC simulations have been unable to explain all of the experimental properties of the hydrated electron, including the temperature dependence of the electron's absorption spectrum,[15, 47, 48] resonance Raman spectrum,[4, 15] and molar solvation volume:[46, 98] MQC models that predict some of these properties correctly usually fail dramatically in their predictions of the others.

Because of the failures of MQC models, recent efforts have focused on *ab initio* simulations of the hydrated electron. The first QM/MM treatment of the hydrated electron was described by Uhlig *et al.*, who embedded 32 quantum mechanical water molecules and an excess electron in a box with 992 classical waters and ran dynamics using density functional theory (DFT) for the quantum subsystem.[54] The results yielded a hydrated electron with a somewhat fluxional structure[88, 97] characterized by a central cavity that is smaller than those seen in traditional MQC simulations. The central cavity seen by Uhlig *et al.* contained only ∼40% of the excess electron's spin density.[54] A few years later, Ambrosio *et al.* ran *ab initio* dynamics using a hybrid DFT functional in a periodic system with 64 water molecules and an excess electron and also concluded that the electron occupies a cavity.[35] With certain approximations that will be discussed further below, these workers claimed that such simulations correctly predicted the experimental vertical detachment energy (VDE) and absorption spectrum of the hydrated electron.[35] More recently, Wilhelm *et al.* performed *ab initio* simulations of the hydrated electron using the MP2 method.[36] Because MP2 is much more expensive than DFT, their calculations were limited to a periodic box with only 47 water molecules and a total of ∼3 ps of dynamics.[36] Snapshots from this work show a cavity-like structure, but the computed bandgap was notably blue shifted compared with the experimental absorption spectrum.[36] Other *ab initio*[41, 70] and QM/MM[99] simulations also have explored different aspects of the hydrated electron's behavior.

Although essentially every *ab initio* calculation has concluded that the hydrated electron is associated with a cavity in the water, no calculations presented to date have provided any detailed analysis or characterization of the electron's behavior. Occasionally, such work characterizes the electron's structure using pair distribution functions,[35, 54] but there has been little discussion concerning the shape of the electron's wavefunction, its overlap with the surrounding water, or any fluctuations that may be crucial for understanding the temperature dependence.[88] Vertical

detachment energies, which are perhaps the easiest value to extract from simulations that can be compared with experiment, are unfortunately not trivial to calculate in periodic systems that do not have a well-defined zero of energy. In addition, of computational necessity, *ab initio* simulations have been limited to very small system sizes, with little exploration of finite size effects.[35] Finite size effects have been shown to be important in MQC simulations of the hydrated electron with over 200 water molecules.[13] Thus, it is not clear whether *ab initio* simulations can truly capture the experimental properties of the hydrated electron, either due to inadequacies in the level of theory employed for the quantum mechanics (particularly DFT), the small system sizes that are computationally available, or both.

One of the most basic properties of the hydrated electron that has yet to be satisfactorily explained theoretically is its temperature dependence. Experiments have shown that the absorption spectrum of the hydrated electron red-shifts with increasing temperature by 2.2 meV/K, independent of the water density.[48] Moreover, spectral moment analysis indicates that the electron's radius of gyration increases at higher temperatures,[47] but the electron's molar solvation volume does not show any significant changes over the same temperature range.[46] This suggests that somehow the cavity structure associated with the hydrated electron is not strongly temperature dependent, but the diffuseness of its wavefunction and thus the overlap with the surrounding water increases as temperature is increased. MQC simulations in which the hydrated electron resides in a cavity do not show any temperature dependence (although a non-cavity model does),[15, 43] and to date, there has been no attempt to simulate the temperature dependence of the electron's properties using *ab initio* methods.

Thus, in this paper, we present a careful exploration of *ab initio* simulations of the hydrated electron to understand the roles of both finite size effects and temperature in the calculated structural and electronic properties. We perform DFT-based periodic simulations with box sizes of 47, 64 and 128 waters, and find that although the calculated VDE extrapolated to infinite box size it is in good agreement with experiment, the structural and energetic properties of the hydrated electron are not converged even with 128 waters. We also explore the *ab initio* behavior of the hydrated electron at temperatures ranging from 298 to 375 K and calculate the spectroscopy using time-dependent density functional theory (TD-DFT) with an optimally tuned range-separated hybrid functional.[100] We find that the calculated spectrum indeed red-shifts with increasing tem-

perature accompanied by only a modest change in the cavity structure, but the magnitude of the temperature-dependent spectral shift is overstated, and the simulated spectral shapes and positions do not agree well with experiment. We also fully characterize the hydrated electron's electronic and structural properties, allowing for a detailed comparison between different *ab initio* and MQC methods. We conclude that to date, no *ab initio* simulation method has had a high enough level of theory on a system of sufficient size to truly capture the nature of the hydrated electron.

3.2 Methods

To perform *ab initio* molecular dynamics of the hydrated electron, we ran trajectories using the CP2K program suite.[101] We explored a total of 5 different systems with varying box sizes and temperatures. For the box size variation, periodic boxes containing 47, 64 and 128 water molecules at 298 K were used, and for the temperature dependence, we used the 64-water simulation box and explored temperature points at 298 K, 350 K and 375 K. Much of our work follows methodology that is largely similar to that previously published by Ambrosio *et al.*,[35] but with important differences as noted below. For running dynamics, we used the PBE0 functional with Grimme's DFT-D3 correction.[102] We note that CP2K uses Goedecker-Teter-Hutter pseudopotentials to represent core electrons, so only the valence electrons were accounted for in the quantum chemistry.[103] A triple-ζ quality basis set that is optimized to be used with the GTH pseudopotential (TZVP-GTH) was employed with a grid cutoff of 500 Ry; we verified that energy convergence was reached with this cutoff. Our chosen basis set is larger than that used by Ambrosio *et al.*[35] The Hartree-Fock (HF) exchange in the DFT functional was calculated with a truncated scheme where the cutoff was half of the box length. To accelerate the HF exchange calculation, the auxiliary density matrix method was employed with an auxiliary cFIT3 basis set.[104] All trajectories were propagated for at least 20 ps with a 0.5-fs time step in the NVT ensemble with the Nose-Hoover chain thermostat used to maintain the desired temperature.[83] We set the system volume to give the experimental water density at room temperature and pressure, and held the density constant even as the temperature was changed to exclude density-based effects from our analysis of the temperature dependence.[15, 48, 105] Initial configurations were taken from an equilibrated MQC simulation using the cavity-forming Turi-Borgis pseudopotential[11], and the first 5 ps of each $\geq$20-ps trajectory was not used

for analysis to ensure equilibrium under *ab initio* propagation. Ensemble-averaged quantities were calculated using at least 100 uncorrelated configurations drawn every 100 fs for each system.

Surprisingly, there has been little work using *ab initio* simulations to calculate the absorption spectrum of the hydrated electron. The only such effort of which we are aware is that by Ambrosio *et al.*,[35] who simply binned the excited-state Kohn-Sham orbital energies from the periodic DFT calculation with respect to the ground-state energy to estimate the absorption spectrum; this procedure yielded what appears to be good agreement with experiment. We note, however, that if one performs this same calculation but uses transition dipole matrix elements between the low-lying orbitals, the agreement with experiment becomes substantially worse because the spectrum becomes highly structured, as we document in the Supporting Information (SI). We also note that the application of standard hybrid functionals to the hydrated electron produces low-lying Kohn-Sham excited states with charge-transfer character, a general problem of charge delocalization that is well known with DFT; these low-lying states were simply ignored in the work of Ambrosio *et al.*, who used a radius-of-gyration-based criteria to select only those states that were confined near the central cavity for their spectral analysis.[35]

It is worth noting that previous work has shown that the level of theory used by Ambrosio *et al.* is expected to be inadequate for calculating the observed spectroscopy of the hydrated electron. Uhlig *et al.* argued that when analyzing hydrated electron configurations generated from periodic simulations, it is important to use TD-DFT to calculate the excited states needed to generate a simulated absorption spectrum.[100] Moreover, these workers also showed that the calculated spectroscopy was extraordinarily sensitive to the choice of functional used in the calculation, and that the most reliable way to calculate the spectrum was to use TD-DFT with a range-separated hybrid functional whose range separation parameter was optimally tuned to satisfy Janak's theorem.[87, 100]

Thus, for our calculations of the hydrated electron's absorption spectrum, we extracted uncorrelated configurations from our *ab initio* trajectories with the hydrated electron's center of mass set at the origin and performed non-periodic TD-DFT calculations on these configurations using the QChem program suite.[106] To prevent the excess electron from spilling into the vacuum at the edges of the non-periodically-treated configurations, we surrounded the quantum mechanical waters with 26 replicated simulation boxes containing simple point charge (SPC) waters to represent

the periodically-treated water molecules. We chose the LRC-ωPBE functional, a range-separated version of the PBE functional used for the dynamics, for our spectral and other analyses; we found that this choice removed low-lying spurious charge-transfer excited states that are commonly observed with standard hybrid functionals like PBE0, including those that had to be removed by Ambrosio *et al.*,[35] as discussed in the SI.

As suggested by Uhlig *et al.*,[100] we optimized the range separation parameter ω in the LRC-ωPBE functional to satisfy Janak's theorem[87] by taking uncorrelated configurations and determining the value of ω that led to the best average match of the ionization and SOMO energies for each of the 5 different simulation conditions. The optimized ω values that we employed are shown in the last row of Table 3.1, below, and details are given in the SI. It is worth noting that the optimized ω values are different for trajectories with different box sizes and temperatures, which shows that caution should be used if attempting to use the default ω value or when assuming that ω is roughly constant across different simulation conditions. For the TD-DFT calculations, we tested the convergence of the basis set (see the SI for details) and chose 6-31++G* as the best compromise between computational efficiency and accuracy.

Once the TD-DFT calculations for uncorrelated configurations from each condition were complete, we calculated the hydrated electron's absorption spectrum by taking the 10 lowest-lying TD-DFT excited states and binning them weighted by their oscillator strength from the ground state. Each bin was then convoluted with the Gaussian kernel according to:

$$I(E) = \langle \sum_{i=1}^{N} |\mu_{0,i}|^2 \Delta E_{0,i} \sqrt{\alpha/\pi} \exp(-\alpha(E - \Delta E_{0,i})^2) \rangle, \tag{3.1}$$

where α was chosen to be 25 meV. To verify this methodology, we also generated the absorption spectrum using configurations generated via MQC simulations using the cavity-forming TB potential,[11] which indeed do a reasonable job reproducing the experimental spectrum, as shown in the SI.[100] We used the SOMO generated from the TD-DFT calculations to best represent the hydrated electron's ground state in the various optical transitions, and we used the square of the TD-DFT SOMO to represent the ground-state charge density. We note that many other simulations have used the spin density for calculations and/or visualization,[36, 54] but the spin density tends to have a larger radius of gyration than the square of the SOMO. This means that the radius

of gyration of the electron based on the spin density will not be consistent with the sum rules used to determine the electron's size by spectral moment analysis,[47] as discussed in more detail in the SI.

3.3 Results and Discussion

3.3.1 Finite Size Effects in *Ab Initio* Simulations of the Hydrated Electron

Although there has been a lot of *ab initio* work on water cluster anions,[76, 107–109] which are precursors to the bulk hydrated electron, relatively little *ab initio* work to date aimed at simulating the bulk hydrated electron using periodic boundary conditions has been performed. The use of periodic boundary conditions, in turn, means that finite-size effects that alter the system properties could be important if the simulation box is too small.[13] However, the computational expense associated with *ab initio* dynamics severely limits the system size, with the largest equilibrium simulation to date by Ambrosio *et al.* having only 64 quantum mechanical water molecules.[35] In their work, Ambrosio *et al.* did perform limited calculations using a 128-water box, but they presented no analysis using the larger simulation size other than extracting a VDE to use in a two-point extrapolation to infinite box size.[35] As mentioned in the introduction, even MQC simulations of the hydrated electron show finite-size effects at box sizes greater than 200 waters,[13] much larger than what was used by Ambrosio *et al.* or the 47-water MP2-based simulations of Wilhelm *et al.*[35, 36] Thus, in this section, we present a detailed exploration of how the simulation box size affects the calculated properties of periodic *ab initio* simulations of the hydrated electron.

To examine the effects of finite size, we used three different box sizes to simulate the hydrated electron containing 47, 64 and 128 water molecules. We begin our exploration of box size effects by examining the vertical detachment energy (VDE), which is perhaps the most easily-computed quantity that can be directly compared to the ∼3.5-eV value measured experimentally.[17–19] We note, however, that calculating VDEs is not trivial when periodic boundary conditions are employed because there is no well-defined zero of energy; thus, the VDE cannot be simply computed as the difference in energy between neutral and anionic configurations. Because of this issue, Ambrosio *et al.* estimated the VDE from their simulations by integrating the SOMO energy by occupation and assuming that Janak's theorem holds for the hybrid functional employed in their simulations.[35]

Since we used a similar hybrid functional as that employed by Ambrosio *et al.*, we tested the accuracy of Janak's theorem but found that it does not hold. We also note that Ambrosio *et al.* shifted their calculated SOMO value by an arbitrary amount (which was not reported) to represent the energetic offset from the water valance band edge,[35, 110] so we believe that the excellent agreement reported between the simulated and experimental VDEs in their work is largely a coincidence.

To avoid the complexities of computing VDEs from periodic calculations, we computed the VDE using non-periodic TD-DFT calculations on configurations extracted and extended from the periodic trajectories, as described above. Since we use a range-separated hybrid functional for these calculations that is optimally tuned to satisfy Janak's theorem, we can easily extract VDEs by taking the calculated SOMO energies, as shown in Table 3.1. We checked the validity of using the optimized long-range-corrected SOMO value by also computing the VDE by subtracting the energy of identical anionic and neutral configurations, and we obtained similar results, as shown in the SI. Table 3.1 shows that for all the system sizes we studied, including the 128-water box, the calculated VDEs are strikingly smaller than the experimental value. However, if we use the information from the three box sizes to extrapolate to infinite box size by plotting the calculated VDEs as a function of the inverse box length, we find better agreement with experiment, as shown in Fig. 3.1. The fact that the calculated VDE at the largest box size differs from experiment by well over an eV suggests that even with 128 waters, the simulations are not close to converged with respect to box size.

After the VDE, the next-easiest hydrated electron quantity that can be compared between simulation and experiment is the absorption spectrum. The absorption spectrum, however, is not terribly sensitive to the details of the hydrated electron's structure, as both cavity and non-cavity MQC models with similar radii of gyration predict absorption spectra that are in good agreement with experiment.[11, 13] The only *ab initio* simulation we are aware of that has attempted to compute the hydrated electron's absorption spectrum is that by Ambosio *et al.*[35] As mentioned above, these workers calculated the spectrum by simply binning the energy differences between SOMO and unoccupied Kohn-Sham orbitals obtained directly from their periodic 64-water DFT-based simulation. They also manually removed the contributions of low-lying states by arguing that such states are likely artifactual.[35] When we perform similar periodic calculations using

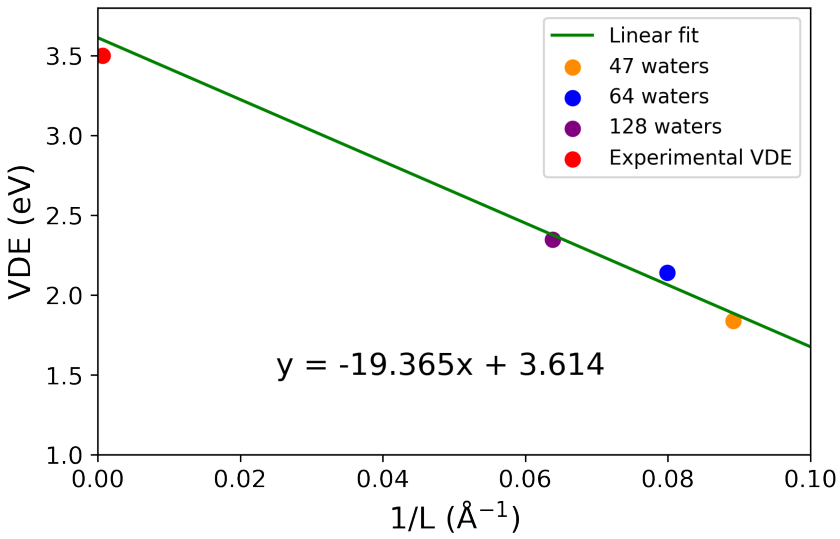

Figure 3.1: Vertical detachment energy of the hydrated electron calculated with non-periodic TD-DFT using an optimally-tuned range-separated hybrid functional on configurations extracted and extended from periodic *ab initio* simulations at three different box sizes, plotted against the inverse of the simulation box size. The ∼3.6-eV intercept of the best-fit line, which extrapolates the calculated VDEs to infinite box size, is in good agreement with experiment. However, the calculated VDE is more than an eV different from experiment even at the largest box size (Table 3.1), showing that 128 water molecules are not sufficient to converge the simulated properties of the hydrated electron.

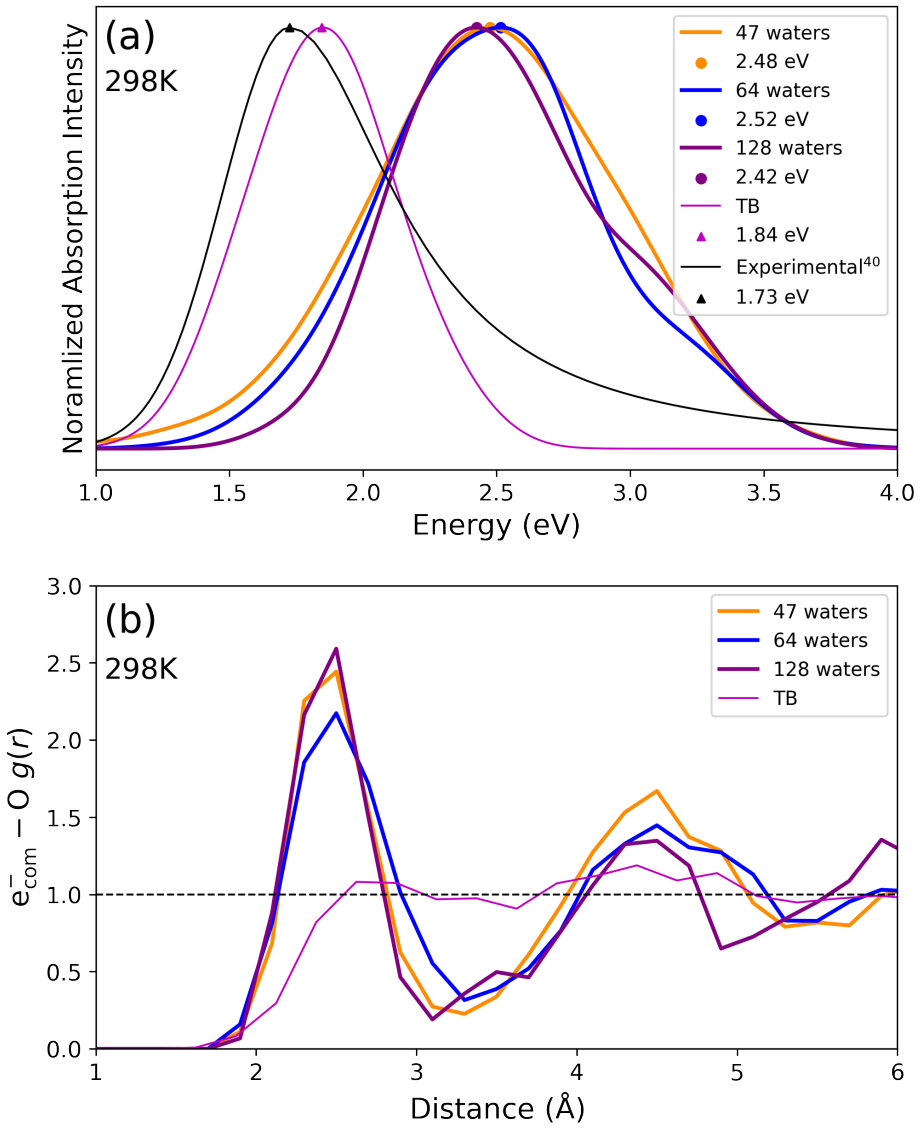

Figure 3.2: (a) Absorption spectrum of the hydrated electron calculated using configurations extracted and extended from periodic *ab initio* trajectories using TD-DFT with an optimally-tuned range-separated hybrid functional using three different simulation sizes; the yellow, blue and brown curves represent simulation boxes with 47 (yellow curve), 64 (blue curve) and 128 (purple curve) H_2O molecules. The experimental absorption spectrum (taken from a Gauss-Lorentzian fit) at room temperature is shown as the thin black curve,[10, 111] and the absorption spectrum calculated in the same manner using configurations taken from a MQC simulation run with the Turi-Borgis pseudopotential[11] is shown as the thin pink curve for reference. For the *ab initio* simulations, although the spectral position is not strongly size-dependent, the spectral width decreases with increasing box size due to a decrease in first-shell solvent coordination fluctuations (see text). The general agreement between the experimental and *ab initio*-generated spectra is poor. (b) Hydrated electron center-of-mass to water oxygen pair distribution functions, $g(r)$, at different *ab initio* simulation box sizes. The simulated structure around the central cavity is much more pronounced than in previous MQC simulations (thin pink curve), and monotonic box size effects are most prominent in the second solvation shell.

the PBE0 functional but using TD-DFT and computing transition dipoles between the states, the resulting absorption spectrum is strongly red-shifted, broadened and more structured compared to experiment, as shown in the SI.

Due to these issues with using Kohn-Sham orbitals without transition dipoles to estimate the spectroscopy of the hydrated electron,[35] we elected to use TD-DFT calculations based on an optimally-tuned range-separated hybrid functional, as outlined by Uhlig *et al.*,[100] and described above. The results for the three different box sizes we used at room temperature are shown as the yellow, blue and purple curves in Fig. 3.2(a). We see that the spectral peak location does not appear to be terribly sensitive to the simulation box size, but the spectral shape and particularly width are box-size dependent. Moreover, the calculated absorption spectra are substantially blue shifted and broadened compared both to experiment (thin black curve) and a standard cavity-model MQC simulation (thin pink curve).[11] Indeed, when we calculate the radius of gyration of the simulated hydrated electron (using the square of the TD-DFT SOMO), as shown in Table 3.1, we obtain an average value of $\sim$2.3 Å, which is substantially smaller than the 2.45 Å obtained experimentally through spectral moment analysis.[47] Since neither the radius or gyration nor the spectrum appear to be converging toward experiment with increasing box size, the representation of the hydrated electron with this level of theory is inadequate.

We analyze the structure associated with the hydrated electron via electron center-of-mass to water oxgyen pair distribution functions in Fig. 3.2(b). We see that the *ab initio* hydrated electron (yellow, blue and purple curves) is associated with a central cavity, but one whose size is smaller and whose structure is more pronounced than that obtained from the standard cavity-forming Turi-Borgis MQC model (thin pink curve).[11] The height of the first-shell peak near 2.5 Å is also notably larger than that observed in the DFT-based QM/MM calculations of Uhlig *et al.* but the computed cavity size is similar.[54] Interestingly, the *ab initio*-computed pair distribution functions do not show any significant size dependence, other than perhaps a slight decrease in the height and area of the second solvation shell near 4.5 Å with increasing box size. Electron center-of-mass to water H atom pair distribution functions, as well as several other structural characterizations of the hydrated electron, are shown in the SI.

To better delve into the structural changes that are responsible for the hydrated electron's VDE and spectral behavior with box size, we further examine aspects of the hydrated electron's structure

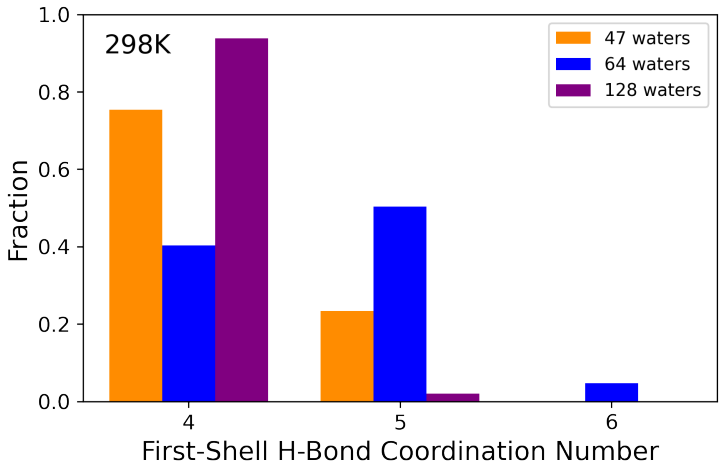

Figure 3.3: Fraction of *ab initio* hydrated electron configurations with different first-shell water coordination numbers (defined as those first-shell waters with H-bonds pointing at the electron's center-of-mass; see text) at different simulation box sizes. The coordination number does not show monotonic trends with system size. The average 5-coordination with 64 waters agrees with Ref. 35. For the largest 128-water box size, the coordination number is nearly precisely 4 with few fluctuations, possibly explaining the narrower absorption spectrum at this box size seen in Fig. 3.2(a).

in Fig. 3.3. Here, we show the average e^-–water coordination number, defined as the number of water molecules whose oxygen atoms are within 3.5 Å of the electron's center-of-mass that also have an H atom within 2.5 Å of the center-of-mass; i.e., the number of first-shell water molecules that are solvating the electron via H-bonding (see the SI for the corresponding angular distributions of the first-shell waters). For the 64-H_2O box, the average coordination number turns out to be ∼5, in good agreement with the observations of Ambrosio *et al.*[35] However, we also see that the degree of water coordination is highly box-size dependent. Both the smaller and particularly the larger box size show a stronger preference for electron coordination by only 4 waters. The larger fluctuations in coordination number in the smaller box sizes are likely the cause of the broader absorption spectra for these sizes seen in Fig. 3.2(a). The fact that we do not see a monotonic trend in coordination number with box size is another factor that suggests that structure of the electron is not converged even with the 128-water box.

To further characterize the behavior of the *ab initio* hydrated electron, we compute several quantities associated with its charge density. First, we examine the interactions between the electron and adjacent solvent molecules via the 'direct overlap', Θ, given by:[40, 109, 112]

$$\Theta = \Big\langle \sum_{i=1}^{n_{\text{molcs}}} 4\pi \int_0^{r_c} r_i^2 |\Psi(r_i)|^2 dr_i \Big\rangle, \tag{3.2}$$

where the angled brackets represent an ensemble average, Ψ is the normalized TD-DFT-calculated SOMO using the optimized range-separated hybrid functional, the sum runs over all of the water molecules, r_i is the distance between the electron and the i^{th} water oxygen atom, and r_c is a constant that roughly represents the size of the water molecular core orbitals, here chosen to be 1.0 Å.[40] The direct overlap thus represents the fraction of the hydrated electron's charge density that lies directly on top of (as opposed to in between) the surrounding water molecules; the results for different simulation sizes are given in Table 3.1. Within error, there is no box size dependence to the direct overlap, but what is striking is that the *ab initio* value of $\Theta \sim 21\%$ is much larger than the ∼6% obtained from cavity-model MQC simulations, suggesting that the pseudopotentials used in such simulations are much too repulsive.[40, 88, 97, 109]

Given that roughly 21% of the *ab initio* hydrated electron sits directly on top of the water, it is also interesting to determine what fraction of the electron sits out of the central cavity between the water molecules. To quantify this, we computed the 'radial overlap', Φ, defined as:[40]

$$\Phi = 4\pi \int r^2 g(r) |\Psi(r)|^2 dr, \tag{3.3}$$

where $g(r)$ is the electron center-of-mass to water oxygen pair distribution function (cf. Fig. 3.2(b)). With this definition, Φ measures the fraction of the electron's charge density that resides at the same distance from the electron's center-of-mass as the surrounding water molecules; the difference between this value and 100% roughly gives the fraction of the electron that resides in the central cavity. Values of Φ for the different simulation box sizes are given in Table 3.1. For all box sizes, the radial overlap is roughly 53%, meaning that less than half of the electron resides in the central cavity, a result in decent agreement with previous QM/MM estimates based on the spin density.[54] The amount of radial overlap is much larger than the ∼30% seen in cavity-model MQC simulations, again consistent with the idea that the pseudopotentials used in such simulations overly confine the electron to the central cavity.[40, 88, 109]. In the SI, we show several other measures of the cavity nature of the hydrated electron, along with measures of the shape of the electron's wavefunction.

Overall, the fact that few of the structural quantities we calculate are strongly dependent on

Table 3.1: The radius of gyration, direct overlap (Θ, Eq. 2), radial overlap (Φ, Eq. 3), VDE and range separation parameter (ω) for all *ab initio* simulations of the hydrated electron explored in this work, including varying the box size and temperature. The quoted errors are ± 1 standard deviation of the corresponding fluctuating quantity.

	64-298K	64-350K	64-375K	47-298K	128-298K	TB (298K 500)
Radius of gyration (Å)	2.35 ± 0.09	2.54 ± 0.19	2.62 ± 0.24	2.34 ± 0.12	2.31 ± 0.08	2.42
Direct Overlap (%)	21.84 ± 2.16	21.01 ± 2.27	20.80 ± 2.52	21.99 ± 2.19	21.67 ± 2.13	5.7
Radial Overlap (%)	52.95 ± 3.31	55.95 ± 4.04	57.86 ± 4.92	53.14 ± 4.05	52.34 ± 3.60	31.1
VDE (eV)	2.14 ± 0.36	1.81 ± 0.37	1.95 ± 0.38	1.84 ± 0.35	2.35 ± 0.30	3.12
Optimal ω	0.175 a_0^{-1}	0.165 a_0^{-1}	0.160 a_0^{-1}	0.200 a_0^{-1}	0.185 a_0^{-1}	0.145 a_0^{-1}

box size makes it difficult to determine why the VDE appears to converge to the experimental value when extrapolated to infinite box size. Clearly, long-range electrostatic forces help to stabilize the hydrated electron, but given that the Onsager length in room-temperature water is only ∼7 Å, long-range electrostatics is not enough to fully explain the behavior of the VDE with box size. The change in water coordination number might be responsible, but the observation that the average coordination number decreases in the largest box size indicates that there must be subtleties in the number of coordinating water molecules and the strength with which they stabilize the hydrated electron. All of the results indicate that even 128 waters is not enough to converge the simulated properties of the hydrated electron. The simulated spectroscopy of the electron agrees poorly with experiment at all box sizes, suggesting that the level of theory chosen for the dynamics based on a hybrid DFT functional is likely inadequate. This is perhaps not surprising as it is hard to imagine a single hybrid functional correctly representing the valence electrons in the water molecular orbitals, the water-water H-bonds, water-water dispersion interactions, and the excess electron, of which ∼79% sits in the cavity and interstitial spaces between the water molecules. With MP2 and other wavefunction methods currently out of reach for the necessary simulation sizes and durations, there is clearly work to be done to describe the bulk hydrated electron using *ab initio* MD simulations.

3.3.2 Temperature Effects on the Hydrated Electron

As discussed in the Introduction, the temperature dependence of the hydrated electron's absorption spectrum has never been satisfactorily explained by theory. Non-cavity MQC simulations that do show a temperature-dependence reminiscent of experiment predict the wrong sign for the electron's molar solvation volume, while cavity MQC simulations that get the molar solvation volume about right do not show any temperature dependence whatsoever.[15, 43] Although the analysis above suggests that *ab initio* simulations based on a hybrid DFT functional with a small number of waters are likely not up to the task, it is still instructive to see if this level of theory can explain why the radius of gyration of the electron increases with temperature[47] but the molar solvation volume, which is presumably closely connected to the cavity size, does not.[46] Thus, we ran simulations with 64 waters at fixed density at three different temperatures – 298, 350 and 375 K – to draw insights into what features of *ab initio*-simulated hydrated electrons change with temperature.

Figure 3.4(a) shows the calculated absorption spectrum of the *ab initio* hydrated electron, using the same optimized range-separated hybrid functional TD-DFT methodology described above, at the three different temperatures. The most striking feature of this data is that there is indeed a nearly 200 meV red-shift of the calculated absorption spectrum as the temperature is increased from 298 to 375 K. Although the absolute positions of the calculated spectra do not match experiment, the magnitude of the T-dependent shift of the absorption maximum is comparable to (but larger) than that observed experimentally.[48] The data also show, however, that the width of the calculated spectrum, which is already too broad at room temperature, increases even further at higher temperatures, a feature that is not observed in experiment.[47] There are also significant T-dependent changes in the calculated spectral shape, with the shoulder on the blue side at room temperature becoming a shoulder on the red side as T is increased (and of course, there are no shoulders present in the experimental spectrum of the hydrated electron). Thus, even though the basic temperature-dependent red-shift is in rough agreement with experiment, the spectral details are in rather poor agreement.

To understand how the observed red-shift of the *ab initio* hydrated electron's spectrum is connected to its underlying structure, in Fig. 3.4(b) we show electron center-of-mass to water oxygen pair distribution functions at the three different simulation temperatures. As the temperature is

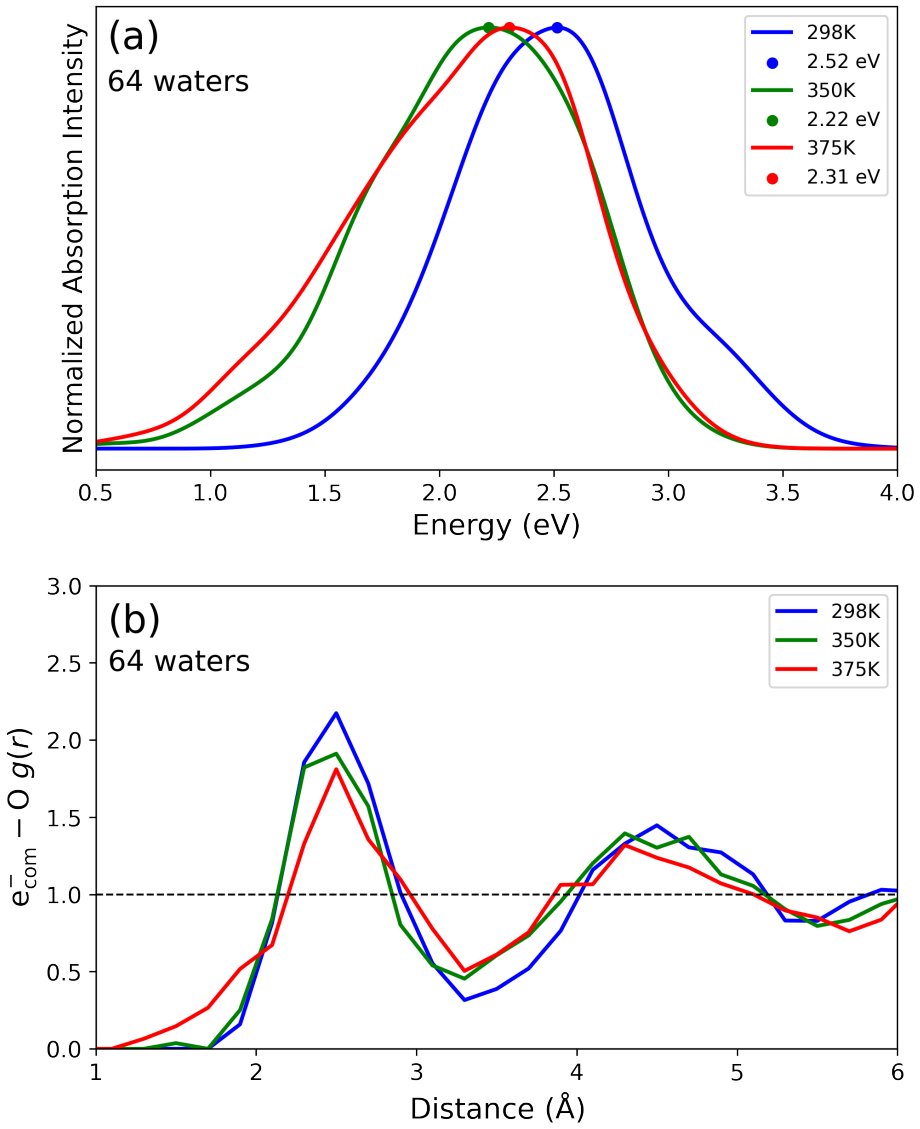

Figure 3.4: (a) Optimally-tuned range-separated hybrid functional TD-DFT-calculated *ab initio* absorption spectrum of the hydrated electron at three different temperatures: 298 K (blue curve), 350 K (green curve) and 375 K (red curve). Although the spectra are in the wrong position and are broader than experiment, the magnitude of the observed red-shift with temperature is comparable to (but about twice as large as) that seen experimentally. (b) Electron center-of-mass to water oxygen pair distribution functions at different temperatures. Increasing temperature moves waters from the well-defined first solvation shell both into the central cavity and into the interstitial space between the first and second solvation shells.

increased, we see that the first-shell solvation peak decreases in amplitude and increases in width, while the interstitial space between the first and second shells slightly fills in. This suggests that at higher temperatures, the first-shell waters are much more fluxional and thus more likely to reside either slightly closer to or farther from the electron's center-of-mass. Perhaps most importantly, there is significant penetration of waters into the central cavity at the highest temperature, suggesting that the spectral properties indeed reflect the nature of a T-dependent central cavity structure.[43, 88]

Additional detail about how the solvent coordination changes with temperature is given in Fig. 3.5. Panel (a) shows that as the temperature is increased, the most prominent coordination number shifts from 5 to 4. This results from the facts that there are both fewer first-shell waters and that fewer of the first-shell waters maintain a favorable H-bonding geometry with the hydrated electron at higher temperatures. The change in the prevalence of favorable H-bonds with temperature is shown in Fig. 3.5(b), which tabulates the number of first-shell coordinating waters that make either 1 or 2 H-bonds to the hydrated electron. The data clearly show an increase in the number of doubly-coordinating waters with increasing temperature, showing that the structure of the cavity and the local water H-bond network are becoming less well-defined. This idea is extended in Fig. 3.5(c), which shows the angular distribution of the first-shell water O–H bonds relative to the electron's center of mass for 4-coordinate configurations. As temperature increases, the distribution not only broadens, but shifts to lower angles, indicating that there is less preference for a tetrahedral H-bond geometry[52, 109] and thus a higher likelihood to find dipole solvation or other motifs. It is the combination of the change in number of first-shell molecules and their angular distribution that results in the broadening and shape change of the simulated spectrum with temperature.

To understand how the temperature-dependent changes in the local water structure affect the electronic properties of the hydrated electron, we also analyzed the radius of gyration and the direct (Θ, Eq. 2) and radial (Φ, Eq. 3) water overlaps,[40] all of which are summarized in Table 3.1. As expected, the electron's radius of gyration is roughly inversely correlated with the position of the absorption spectrum and monotonically increases with temperature. More surprisingly, the direct overlap slightly decreases with increasing temperature; apparently, the greater conformational space available to the nearby waters at higher temperatures allows them to avoid enthalpically unfavorable

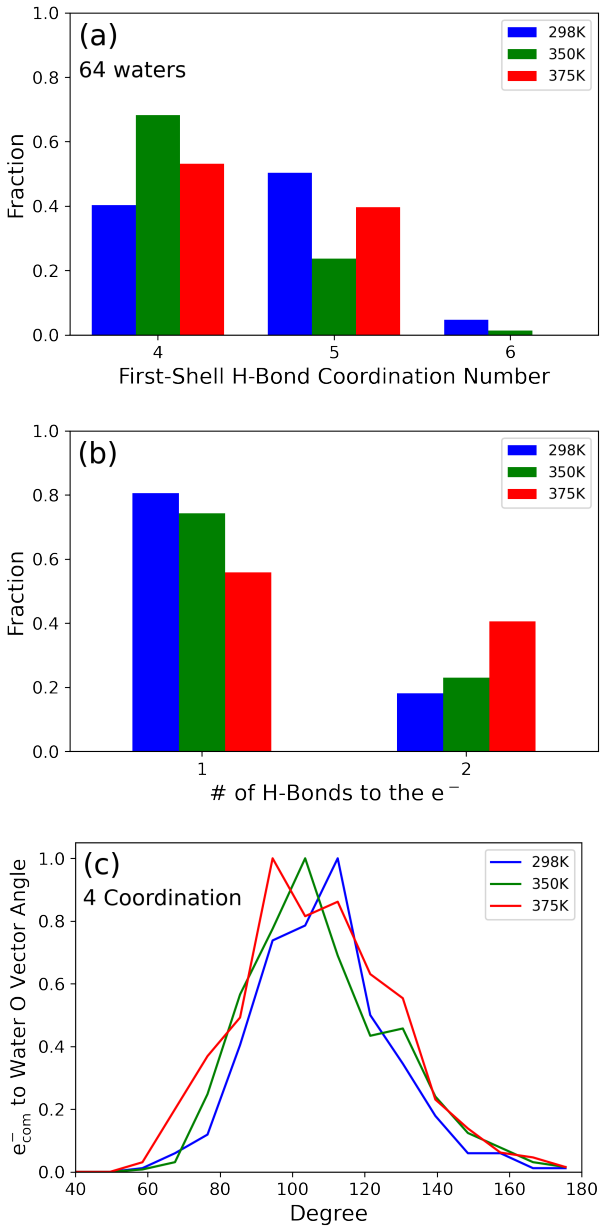

Figure 3.5: (a) Fraction of *ab initio* hydrated electron configurations with different first-shell water coordination numbers (defined as those first-shell waters with H-bonds pointing at the electron's center-of-mass; see text) at different simulation temperatures. As the temperature increases, the average coordination number at first decreases due to increased entropy, and then increases because the number of waters close to the electron's center-of-mass increases (cf. Fig. 3.4(b)). (b) Fraction of first-shell waters making either 1 or 2 H-bonds to the hydrated electron at different temperatures. The number of waters making 2 H-bonds (dipole solvation rather than H-bond solvation) increases with increasing temperature, again the result of increased entropy. This effect also contributes to the increase in 5-coordination observed at the highest temperature. (c) Angle distribution between vectors connecting electron's center-of-mass (ecom) and the water oxygen atoms of the first-shell waters for 4-coordinate configurations at 3 different temperatures. The angular distribution, which is largely tetrahedral at room temperature, becomes both broader and less tetrahedral as the temperature increases.

overlap interactions with the electron. The radial overlap, in contrast, increases with increasing temperature for two reasons. First, the increased radius of gyration puts more of the solvated electron outside the central cavity and into the region between the first and second solvation shells. Second, the radial overlap also increases because of penetration of the water into the central cavity region at high temperatures. Taken together, the results all suggest that the structure that defines the cavity containing the hydrated electron weakens with increasing temperature. The central cavity remains roughly the same size, however, so that the simulations are roughly consistent with the experimental observations that the radius of gyration increases with temperature[47] but the molar solvation volume is roughly temperature independent.[46]

Finally, Table 3.1 also shows that the calculated VDE decreases with increasing temperature. This prediction is in sharp contrast to traditional MQC cavity models of the hydrated electron, which show no change in VDE or absorption spectrum with temperature.[11, 15] The decreased VDE of the *ab initio* hydrated electron reflects the lower coordination number and loss of the well-defined stabilizing H-bonded solvation structure, as well as the increased radius of gyration, as the temperature increases. Although the computed temperature-dependent VDE decrease is only ∼200 meV between 298 and 375 K, the fact that our 64-water simulations are not converged with respect to box size means that the VDE change with temperature extrapolated to infinite box size would likely be larger, and thus measurable by experiment. As far as we are aware, the hydrated electron's VDE has only been measured at room temperature,[19] so the roughly few-hundred meV decrease in VDE with increasing temperature over water's stability range at 1 atm is a prediction of this work.

3.4 Conclusions

In summary, we have shown that periodic *ab initio* simulations of the hydrated electron are not converged, even for our largest box containing 128 H_2O DFT-treated water molecules. The calculated VDE is still over an eV lower than experiment at this box size, although the agreement with experiment improves when the calculated value is extrapolated to infinite box size. When we use established methodology to calculate the hydrated electron's absorption spectrum using TD-DFT with an optimally-tuned range-separated hybrid functional that suppresses spurious low-lying ex-

cited states and accounts for the transition dipoles between the ground and different excited states, the agreement with experiment is poor. The calculated absorption maximum is off by more than 0.5 eV, the calculated spectral width is too large, and the calculated spectrum shows structure that is not seen experimentally. This suggests that the configurations generated by this level of theory are likely not correctly representative of those of the experimental object.

One reason for the failure of this level of theory to correctly capture the behavior of the hydrated electron are excessive fluctuations that occur with small system sizes. Both $g(r)$ and the H-bond coordination of the hydrated electron change non-monotonically with system size, at least up to 128 waters, indicating that simulations at this size are likely not converged. The magnitude of the fluctuations observed in the first-shell solvation structure is large at small system sizes, but these fluctuations appear to decrease in simulations with 128 waters, so it is possible that the size needed to accurately capture the properties of the hydrated electron may only be a few hundred waters, provided that the level of electronic structure theory used is up to the task.

One interesting feature is that our *ab initio* model is qualitatively able to reproduce the red-shift of the hydrated electron's absorption spectrum with increasing temperature. Although many spectral details, such as the spectral position, broadness, and spectral structure do not match experiment, the simulations do predict a net spectral red-shift as the temperature increases from 298 to 375 K at constant density. The magnitude of the predicted redshift is roughly double that seen experimentally, consistent with the idea that the small simulation box size produces configurations that are too fluxional. The simulated red-shift results from an increase in the electron's radius of gyration at higher temperatures, which occurs because some of the ∼47% of the electron density in the central cavity at room temperature moves out into the region occupied by the first shell waters and beyond. The water structure around central cavity becomes less well defined but the cavity size is mostly maintained at higher temperatures, which is consistent with the observation that the molar solvation volume of the electron is roughly temperature independent over this range.[46] Thus, to the extent that these simulations do reflect experiment, the temperature dependence of the hydrated electron's properties results primarily from changes in the water structure around the central cavity: in other words, fluctuations are important.[43, 88, 109]

Overall, despite this qualitative agreement with experiment, all of the results indicate that *ab inito* simulations still have a ways to go to properly explain the properties of the hydrated

electron. DFT-based simulations have a tough time getting the structure and dynamics of liquid water correct,[113, 114] so the properties of water in the presence of an excess electron, where fine details of the structure, dynamics and fluctuations are critical to understanding experiment, are still a challenge for this level of theory, particularly given that at least a few hundred waters and many tens of ps are needed for convergence. Comparing the VDE obtained from periodic simulations that do not have a well-defined zero of energy to experiment requires approximations that have not been well tested, although our use of an optimally-tuned range-separated hybrid functional at least seems to extrapolate well to the experimental value. Comparing the calculated absorption spectrum to experiment is also not straightforward, particularly given the difficulty of obtaining meaningful excited states even with TD-DFT; the way that transition dipoles and potentially spurious excited states that result from the charge delocalization error inherent with DFT also present challenges. We believe that better benchmarking for this class of simulations is needed to ensure that the results obtained are experimentally relevant and do not simply agree by coincidence.

Chapter 4

How Water-Ion Interactions Control the Formation of Hydrated Electron:Sodium Cation Contact Pairs

4.1 Introduction

When an excess electron introduced into liquid water, the resulting solvated object is known as a hydrated electron. Despite the importance of the hydrated electron in many fields, especially radiation chemistry,[5, 7] there is still not a unifying underlying picture that can explain all of its properties, such as the temperature dependence of the electron's absorption spectrum[10, 15, 43, 47, 48] and EPR g-factor,[46, 71, 115, 116] the fact that the electron's molar solvation volume does not appear to be temperature dependent[46, 98] but the radius of gyration from spectral moment analysis does,[117] etc. One particularly interesting feature of the hydrated electron that has received somewhat less attention is that its properties also depend on whether or not there are other ions present in the aqueous solution. Experimental work by Mostafavi and co-workers

demonstrated that the steady-state absorption spectrum of the hydrated electron blue shifts in the presence of electrolytes.[58, 59] The magnitude of the blue shift depends on the concentration of the electrolyte and the identities of not only the salt cation but also the anion.

Although the experimental observation of how the spectrum of the hydrated electron changes in the presence of electrolytes was presented over 15 years ago, there have been only limited attempts to understand the origins of the salt-dependent shifts from a theoretical perspective.[60, 118] Although much of the recent efforts in the literature are focused on performing *ab initio* simulations of the hydrated electron,[34–36, 41, 72, 100, 119] computational expense limits such calculations to at most a few tens of water molecules and a few tens of ps of dynamics. This means that *ab initio* simulation of an aqueous system with a high concentration of electrolytes and an excess electron is prohibitively expensive: the number of atoms needed is well into the hundreds, and capturing the slow diffusive motions of the ions is simply out of reach, even with relatively inexpensive methods such as DFT. Thus, with current technology, this is a question that can only be addressed by approximate methods.

The main theoretical effort in area of hydrated electrons in aqueous electrolytes to date comes from Boutin and co-workers, who examined the potential of mean force (PMF) between a single Na^+ cation and a hydrated electron.[60, 118, 120] These researchers used mixed quantum/classical (MQC) molecular dynamics (MD) simulations, where the water molecules and sodium cation were treated classically and the quantum-mechanically-treated electron interacted with the classical particles via pseudopotentials. Even with this level of theory, calculating an electron-ion PMF is challenging because the ability to restrain the distance between a quantum electron and a classical sodium cation requires evaluating forces on all of the water molecules that determine precisely where the hydrated electron's center-of-mass is located. Boutin and co-workers accomplished this with a perturbation-theory-based method,[121] and found that the PMF consists of a well that is $\sim$5 k_BT deep with an energetic minimum located at an e^-–Na^+ distance of $\sim$2 Å: in other words, they found that Na^+ forms a stable contact pair with the hydrated electron.[60]

Boutin and co-workers then went on to examine how the absorption spectrum of the MQC-simulated hydrated electron varies as a function of distance from the Na^+ cation. They found that proximity to a sodium cation indeed led to a blue-shfit of the electron's calculated spectrum, and that the magnitude of the spectral shift varied roughly inversely with the sodium-electron

distance.[60] This suggested that the blue-shift of the hydrated electron's spectrum is largely due to the electrostatic interaction between the cation and the electron, and that chemical interactions (i.e., orbital overlap) between the electron and sodium cation or an altering of the local solvation structure of around the hydrated electron when it is in the proximity of the cation play less important roles.

For all of the success of the MQC model in explaining the spectral blue-shift of hydrated electrons in aqueous electrolytes, the simulations still failed to capture many aspects of the experiment. First, the calculated blue-shifts[60] were significantly larger than those observed experimentally.[58] In addition, the experiments found that although the spectrum of the hydrated electron blue-shifted in the presence of salts, the shape of the spectrum remained invariant.[58] Boutin and co-workers' MQC simulations, however, found that the hydrated electron's spectrum changed shape quite a bit when in a contact pair with a sodium cation. [59, 60] Finally, when Boutin and co-workers attempted to mimic the concentration dependence of the electron's spectrum by varying the electron-cation distance,[60] the spectral behavior had a different dependence than that seen experimentally.[58]

These discrepancies mean that something in the MQC simulations is not capturing the correct experimental behavior. The differences could be because the simulations looked at only a single cation rather than a high concentration of neutral salt consisting of multiple cations and anions. They also could arise because one of the interactions in the simulation is not properly tuned to correctly understand the properties of the system. The interactions include the pseudopotential between the electron and water, for which Boutin and co-workers chose the Turi-Borgis (TB) potential, which yields a hydrated electron in a well-defined cavity in the water.[11, 13, 40, 69] The simulations also include a pseudopotential between the electron and sodium cation,[38, 122] as well as classical interactions of the water molecules with each other and with the sodium cation.[123] This leads to the central question addressed in this work: presuming that the MQC level of theory is sufficient to draw insights into this system, which interactions are most important in determining the behavior of hydrated electrons in the presence of aqueous electrolytes?

In this paper, we revisit MQC simulations of a hydrated electron interacting with a single sodium cation in liquid water. We explore the PMF between a hydrated electron and a sodium cation using a new method for quantum umbrella sampling.[124] Although *ab initio* methods have provided some success in reproducing the experimental features associated with the hydrated electron,[41, 72]

performing umbrella sampling with *ab initio* methods is currently not feasible: even with DFT, the computational cost of running numerous trajectories at different values of the umbrella parameter is prohibitive, and as of yet, there has been no quantum umbrella sampling method that works with *ab initio*-generated wavefunctions or spin densities. This is why we focus on using MQC simulations to generate hydrated electron:sodium cation PMFs to explore how the interplay between the quantum and classical interactions affect the formation of the contact pair and the blue shift of the absorption spectrum. Although the accuracy of the MQC simulation is inferior to *ab initio* calculations, MQC simulations still successfully capture most of the features observed experimentally, including the blue-shift of the electron's absorption spectrum from the addition of cations.

Here, we specifically explore how changing the classical interactions between the water and the sodium cation, leaving all the pseudopotentials and the water–water interactions constant, affects the PMF governing e^-:Na^+ contact pairs. We find that sodium cation–hydrated electron contact pair stability is heavily affected by the choice of classical Na^+-water interaction. We show that contact pair stability is determined by a subtle balance between the classical and quantum interactions, including electron solvation, cation solvation and the cation-electron attraction. We find that even a slight tipping of this balance can lead to dramatic changes in the way hydrated electrons behave in the presence of electrolytes. Stronger cation–water interactions lead to more unfavorable solvation structures and thus a net destabilization of Na^+:e^- contact pairs. Thus, to properly simulate objects like cation:electron contact pairs, it is important to correctly describe the classical solvation of the ion as well as the quantum mechanics of the solvated electron.

4.2 Methods

To investigate the role that classical cation-water interactions play in the properties of hydrated electron:cation contact pairs, we used MQC MD simulations. The methods we use closely follow our previous work simulating the hydrated electron, as well as the work of Boutin and co-workers.[40, 60, 124] Our simulation box contained 497 classical SPC/flex water molecules,[37] one classical Na^+ cation, and a quantum mechanically treated electron. The dynamics were run in the canonical (N, V, T) ensemble. The wavefunction of the excess electron was represented in a basis of 24 $\times$ 24 $\times$ 24 grid points centered in the simulation box. Following the work of Boutin and co-

Table 4.1: The Na^+–water oxygen Lennard-Jones parameters used in this work. The Aqvist parameters show the largest ion radius with shallowest energy well. The Dang and Koneshan parameters are similar with Koneshan showing the smallest ion with Dang with the deepest energy well.

	Dang[38]	Koneshan[39]	Aqvist[41]
σ_{Na-O} (Å)	2.758	2.728	3.247
ϵ_{Na-O} (kJ/mol)	0.595	0.560	0.086

workers, we used the TB pseudopotential to treat the electron-water interactions.[11, 69] We used our previously-developed pseudopotential to represent the electron–Na^+ interaction.[38, 122] The classical sub-system was propagated using the velocity Verlet algorithm with a 0.5-fs time step,[125] and forces from the quantum mechanical electron were evaluated every time step via the Hellman-Feynman theorem.[126] The system density was fixed at 0.997 g/cm^3 and the temperature was held constant at 298 K using the Nose-Hoover chain thermostat.[83]

The main thrust of this study is to examine the effects of choosing different classical Na^+–water interactions on the properties of the MQC system. We thus explored three different sets of parameters representing the interactions between the classical sodium cation and the flexible SPC water. The first set of Na^+–O parameters is taken from work by Dang *et al.*, who chose the Lennard-Jones (LJ) parameters for this interaction by fitting them to match the experimental enthalpy of gas-phase ion-water clusters.[127] The second set of water–ion parameters is taken from Koneshan *et al.*,[128] who refitted an earlier potential due to Pettitt and Rossky[129] into the Lennard-Jones form. Finally, the third set of cation-water LJ parameters were taken from the work of Aqvist *et al.*, who adjusted the parameter values to reproduce the experimental $\Delta G_{\text{hydration}}$ of different ions.[130] All three sets of parameters are summarized in Table 4.1.

Even though these sets of parameters are designed to simulate the same system – a sodium cation in liquid water – the sets of parameters are noticeably different as they were optimized using different targets. The Aqvist parameters have the largest sodium size with a shallow energy well. This implies that the sodium-water interactions that are relatively weak compared to the other parameter sets. The Dang and Koneshan parameters look more similar to each other, but do have minor differences; the Dang parameters have the deepest energy well while the Koneshan parameters yield the smallest sodium cation size.

The principal focus of this work is see how different ion-water interactions affect the potential of mean force (PMF) between the hydrated electron and the cation. To do this, the distance between the electron's center-of-mass and the sodium cation needs to be restrained so that the free energy can be calculated. Although this is standardly done by umbrella sampling in all-classical simulations, it is not straightforward to extend umbrella sampling to quantum mechanical particles because the quantum Hamiltonian does not commute with the umbrella potential.[121] To circumvent this problem, the umbrella potential can instead be applied to an expectation value of the quantum subsystem, so that the quantum degree of freedom is integrated out. In our case, this will be the expectation value of the electron's position, or center-of-mass.

The difficulty with restraining quantum expectation values in MQC simulations is that the forces that restrain the quantum expectation value have derivative terms that involve how the expectation value changes with motion along each of the classical coordinates. Borgis and co-workers used a perturbation-theory approach to evaluate these derivatives, a method referred to as sum-over-states quantum umbrella sampling (SOS-QUMB).[121] This method has the advantage that it can be relatively inexpensive to calculate the required forces, but has the disadvantage that it is only exact when all possible quantum eigenstates are incorporated into the calculation, and the convergence properties when truncating the sum are unknown. Thus, in this work, we take advantage of a method that we previously developed that evaluates the necessary derivatives by using the coupled-perturbed response equations.[124] Although somewhat more expensive than calculating only a few terms of the SOS-QUMB expansion, the coupled-perturbed quantum umbrella sampling (CP-QUMB) method can evaluate the exact forces on the classical coordinates needed to restrain a quantum expectation value. In previous work, we have successfully applied CP-QUMB to restrain the position of a hydrated electron relative to the air/water interface,[45] and also to restrain the number of water molecules within a given distance of the hydrated electron's center of mass,[88] so we use this method for all of the calculations described below.

To calculate PMFs for each set of ion–water LJ interaction parameters, we first employed 15 simulation windows for different restrained electron–ion distances: one every 0.25 Å, starting from 0 Å separation to 4 Å separation of the Na^+–e^- center-of-mass distance. For electron–ion distances beyond 4 Å, it appeared that the PMFs had largely reached their asymptotes, so we only ran three additional simulation windows separated by 0.5 Å. The restraining harmonic umbrella potential

had a force constant of 1.5 eV/Å^2 in all our simulation windows. With this choice of the umbrella force constant, we found good overlap of the distributions for neighboring simulation windows, providing good statistics for constructing the PMF by connecting the data from each window using the multistate Bennett Acceptance Ratio method,[131] as described in more detail in the Supporting Information. Each simulation window was run for at least 25 ps, truncating the first 5 ps to ensure equilibrium. For the remaining 20 ps of data, uncorrelated configurations were drawn every 200 fs and used for data analysis.

4.3 Results and Discussion

4.3.1 Effect of Changing ion–water Interactions on Na^+–e^- Potentials of Mean Force

We begin our exploration of the effects of the role of cation–water interactions in determining how hydrated electrons interact with sodium cations by examining the cation–electron PMFs, calculated from the CP-QUMB method; the PMFs are shown in Fig. 4.1a. It is worth emphasizing that for these simulations, all interactions – the water–water, electron–water and electron–sodium interactions – are identical, and that the only difference between them is the choice of LJ parameters representing the Na^+–water interaction. Clearly, the choice of ion–water interaction makes a significant difference in the way the ions interact with the hydrated electron. In particular, although all three PMFs suggest that the electron does form a stable contact pair with the sodium cation, each PMF shows a different well depth and optimal distance for the contact pair. The Aqvist LJ parameters (green curve) produce a PMF with the deepest well ($\sim$8 $k_\mathrm{B}T$) and the shortest equilibrium distance between the Na^+ and the center of the hydrated electron. The Koneshan sodium-cation–water LJ parameters (blue curve), on the other hand, yield an electron–cation PMF with a shallow well that has only $\sim$2 $k_\mathrm{B}T$ stability relative to the energetic maximum at 3.5 Å separation, indicating a contact pair that is barely stable relative to free ions. Finally, the Dang ion–water LJ parameters (red curve) lead to an intermediate PMF, with a $\sim$6 $k_\mathrm{B}T$ well depth and an intermediate distance for the equilibrium separation.

We note that the previous work by Boutin and co-workers also used the Aqvist LJ parameters to describe the Na^+–water interaction, and the other interactions in their simulations were also

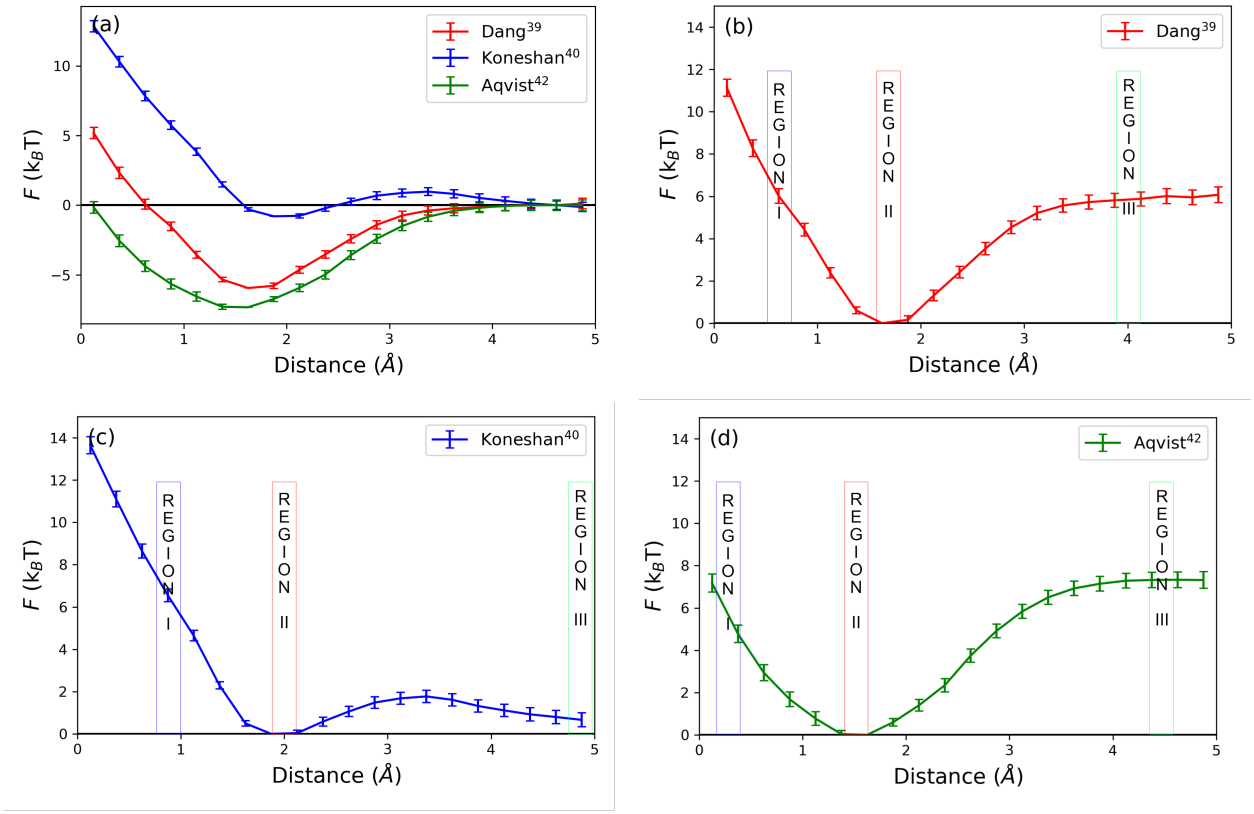

Figure 4.1: (a) Hydrated electron–Na^+ PMFs calculated using the CP-QUMB method with the TB model of the electron and identical simulation parameters except for the LJ parameters describing the water–Na^+ interaction, taken from the models of Dang et al. (red curve), Koneshan et al. (blue curve) and Aqvist et al. (green curve). All three PMFs show a free-energy minimum in the region between 1.5–2.0 Å, indicating that hydrated electrons form stable contact pairs with sodium cations. The three curves show remarkably different contact-pair stabilities, however, indicating that the ion–water interactions are important in determining the behavior of electron–ion contact pairs. (b)-(d) The same PMFs shown in panel (a), with the three regions chosen for further analysis (6 k_BT above the free-energy minimum, the free-energy minimum and along the long-distance asymptote) marked; the three regions occur at slightly different distances for each model because of the differences in the PMFs.

similar to ours except for the quantum umbrella sampling method. Boutin and co-workers indeed observed features in their calculated PMF that are similar to those generated in our work, with a $\sim 6k_BT$ deep free energy well whose minimum was at an electron center-of-mass to cation distance of ∼1.75 Å. At longer distances, however, the PMF by Boutin and co-workers showed a significant decrease in free energy, and the asymptotic region was not reached until distances of ∼9 Å. We note that Boutin and co-workers did not show error bars on their calculated PMF, so it's unclear if the barrier they observe and long-distance PMF fall-off is within the calculated error, or possibly might be a result of a convergence failure of the SOS-QUMB method they employed at longer distances.

The general features of the PMFs for the three models that we observe in Fig. 4.1a can be rationalized as follows. As the electron–ion distance approaches zero, the excess electron is forced to be centered on the sodium cation, so the system behaves effectively as a solvated neutral sodium atom. Neutral sodium atoms have the largest possible electronic stability, but they are also hydrophobic objects, and thus there is a net free-energy penalty to solvate them in liquid water. At long electron–ion distances, the Na^+ and hydrated electron are solvated separately with minimal electronic interaction, defining the zero of free energy. Finally, at intermediate electron–ion distances, there is some favorable electronic interaction between the electron and the sodium, and the partially-separated species, which has a significant dipole moment, is also reasonably well solvated, leading to stable contact-pair formation.

The presence and stability of electron–cation contact pairs is of critical importance in radiation chemistry, electrochemistry and other fields,[132–135] but the results in Figure 1 suggest that without careful consideration of how the ions interact with the water, we aren't able to have a good theoretical understanding of how such ions interact with excess electrons. Thus, the questions that form the focus of the remainder of this paper are: why do relatively minor changes in the water–Na^+ interactions make such dramatic changes to contact pair formation between the sodium cation and hydrated electron? What type of trade-off is there between hydrated electron solvation, cation solvation and electron–cation interactions that yields such vastly different behaviors with relatively subtle changes in the interactions? Can we compare the calculated properties of the different simulated cation–electron contact pairs to experiment?

To answer these questions, we examine the properties of the different simulated e^-:Na^+ contact pairs in three different regions of their respective PMFs. Region I is chosen to be at electron–

ion distances shorter than the contact-pair equilibrium distance at a free energy 6 $k_{\mathrm{B}}T$ above the minimum. Region II is chosen to be at the contact-pair free-energy minimum for each model, and region III is chosen at large electron–ion distances along the PMF asymptote. Because the PMFs for each model are so different, the precise electron–ion distances for each region are also different, as shown explicitly for each model Figs. 4.1b-d. One interesting feature in the Koneshan PMF is that there is a maximum at 3.5 Å making it difficult to determine the asymptotic region. Thus, for this model, we chose region III at the farthest distance we calculated as the best representation of asymptotic behavior.

4.3.2 The Solvation Structure of Hydrated Electron–Na^+ Contact Pairs

We begin our analysis of the three different simulation models by examining the solvation structures of the electron and sodium cation at different electron–ion distances. Figure 4.2 plots e^-–H (right side) and Na^+–O (left side) radial distribution functions, $g(r)$, for all three models in each of the three electron–ion distance regions outlined in Figs. 4.1(b)-(d); note that for the Na^+–O $g(r)$'s shown on the left, the y-axis scale is different in each panel. The e^-–O and Na^+–H $g(r)$'s shown in Fig. S3 in the SI closely follow the e^-–H and Na^+–O $g(r)$'s in Fig. 4.2 because the same water molecules are involved. The radial distribution functions in Figs. 4.2(e) and (f) show that at larger e^-–Na^+ distances (region III), the structures of the water around both the electron and sodium cation are similar to those of the isolated species for each model, which are shown in panels (g) and (h), respectively. This indicates that there is relatively little interaction between these species and their first solvation shells at separation distances farther than ∼4 Å, consistent with the flat PMF in this region.

Figure 4.3 shows integration of the first-shell peaks in $g(r)$ Fig. 4.2 (up to 3.0 Å for water oxygens around Na^+ and 3.5 Å and 2.5 Å for water O atoms and H atoms around the hydrated electron, respectively) to obtain the number of first-shell waters around each species. In region III, we see that there are roughly 3.7 waters in the hydrated electron's first solvation shell (panel b) and roughly 5.3 waters in the sodium cation's first solvation shell (panel a), which is only slightly less than the number of first-shell waters around the isolated species (4.5 and 5.6 waters, respectively, black bars). In summary, at the asymptotic region (region III), both the Na^+ and the electron are separated enough to be essentially independent.

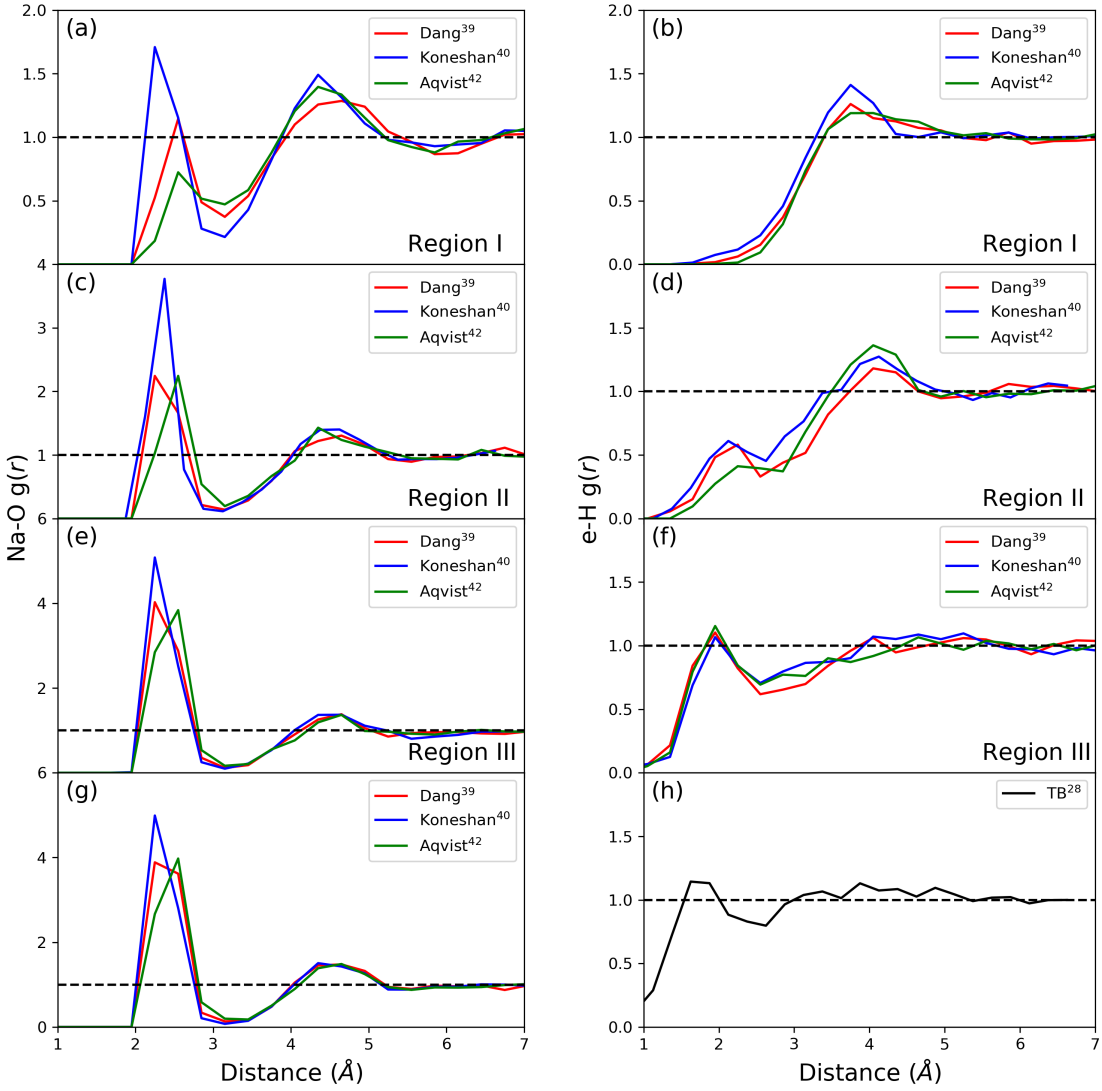

Figure 4.2: Radial distribution functions showing the probability to find water O atoms as a function of distance from the Na^+ (left column) and to find water H atoms from the center-of-mass of the hydrated electron (right column) for the three different models in each of the three regions delineated in Fig. 4.1. The colors of each curve represent the model used, the same is in Fig. 4.1, and the first, second and third row of panels show the behavior in regions I, II, and III, respectively. The bottom row shows the solvation structure for the isolated systems with only a Na^+ or a hydrated electron. As the Na^+–e^- distance reaches the PMF asymptote in region III, the solvation structures of both the electron and cation approach those of the isolated species. As the sodium cation is restrained to reside closer to the electron's center of mass, regions I and II, the solvation of the electron is strongly affected: the number of first-shell H atoms decreases dramatically, and a new e^--H peak appears at further distances. The number of first-shell waters around the cation (note the change in the y-axis scale between the different panels showing the Na^+–O distributions) also decreases as the cation is forced towards the electron's center. The Koneshan model Na^+ (blue curves), which has the strongest ion–water interaction, retains the most first-shell waters as the electron approaches, some of which are then forced to be in the first shell of the hydrated electron.

When the hydrated electron forms its stable contact pair with the sodium cation, region II, Figs. 4.2(c) and (d) show significant changes in the solvation structures of each species, as well as sharp differences between the different ion–water simulation models. The most obvious change is a significant decrease in the height of the first-shell solvation peak for Na^+, compared with panel (e) at region III: Fig. 4.3a shows that there are on average two fewer waters in the cation's first solvation shell in the region II contact pair than when the species are separated. This indicates that to form a stable electron–ion contact pair, the electron needs to displace roughly two waters from the cation's first solvation shell. Similarly, even though the number of water O atoms near the electron does not change dramatically between regions III and II (Fig. 4.3(b)), the number of H-bonds solvating the hydrated electron significantly decreases in region II (Fig. 4.3(c)). Moreover, and a new e^--H peak appears at longer distances in region II (Fig. 4.2(d)). All of this suggests that the first-shell water molecules around the electron in the contact pair are forced by cation–water interactions to orient with their H atoms pointing away from the electron.

Figures 4.2(c) and (d) and Fig. 4.3 also show that the Koneshan model has the highest number of solvating waters for both the Na^+ and the hydrated electron in region II. The Koneshan cation–water interaction parameters, summarized in Table 4.1, have the smallest Na^+–water distance (σ) among the three models. Thus, in this model, the cation hangs on much more tightly to its first-shell waters, as demonstrated by the sharp first peak shown in panel (g). Thus, even though the TB e^-–water pseudopotential is highly repulsive, the nearby electron is less able to displace first-shell waters from a cation described with the Koneshan LJ parameters than for cations represented by the other models. We will argue below that the increased number of waters in the electron's first shell for this model are those that are strongly bound to the sodium cation: these waters are literally forced into the electron's vicinity with an unfavorable orientation, and although they reside at a distance that is similar to the electron's natural first solvation shell, they do not help participate in solvation of the electron. This provides our first hint as to why the electron–ion PMF for the Koneshan model shows a much less stable contact pair than the other models we considered.

Finally, Figs. 4.2(a) and (b) show that when the sodium cation is forced to reside near the center of the electron, region I, there are further changes to the local solvation structure. The TB model of the hydrated electron has a radius of gyration of 2.45 Å, which is smaller than the diameter of the Na^+ ions in all three models. Even though the radius of gyration of the electron shrinks to around

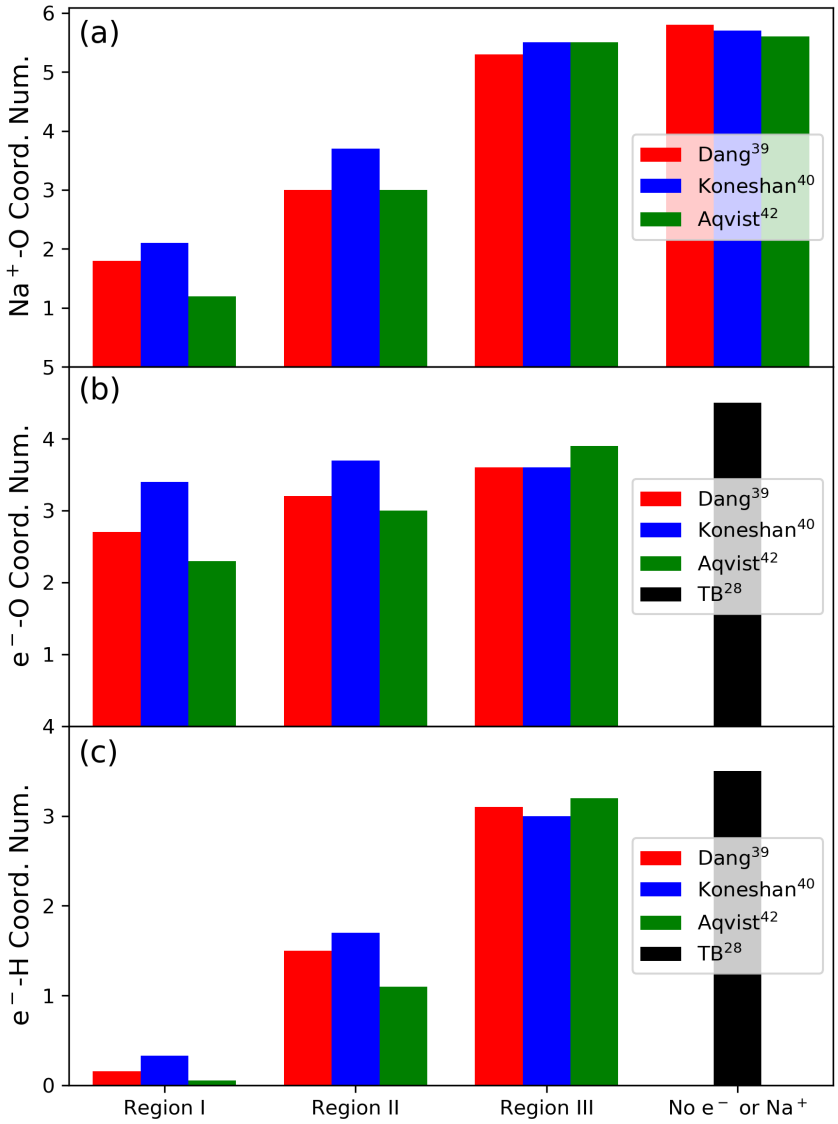

Figure 4.3: First-shell solvation coordination numbers of Na^+ and the hydrated electron for the three simulation models in each of the three regions defined in Fig. 1 (colored bars with the same scheme as Figs. 1 and 2), as well as for the isolated TB hydrated electron and aqueous Na^+ systems (black bars). The values were obtained by integrating the $g(r)$'s in Fig. 2. The first shells are defined as all water O sites within 3 Å of the Na^+ and 3.5 Å of the electron's center-of-mass, and all water H sites within 2.5 Å of the electron's center-of-mass. The overall trend is similar to what is observed in the radial distribution function with decreasing coordination number as the cation–electron distance is decreased. The fact that the O and H solvation numbers around the electron change differently in the different regions indicate a change in water orientation around the electron when it is in the vicinity of the sodium cation. The Koneshan model (blue bars). with its stronger cation–water interactions, produces higher coordination of both the cation and the electron.

2.2 Å when restrained to have the sodium cation inside of it, the repulsive electron prevents water molecules from residing at the distance where the natural first solvation shell of the ion would be, leading to the drop in cation coordination seen for all three models seen in Fig. 4.3(a). As above, the Koneshan model (blue curves), with the strongest ion–water interactions, is better able to keep waters in its first solvation shell than the other models. This ion–water attraction forces water to reside inside the first natural solvation shell of the electron, effectively creating a combined species that behave as an object with no net charge due to the presence of the interior cation. The disappearance of the first peak in the electron–hydrogen $g(r)$, Figs. 4.2(b) and 4.3(c), suggests that the first-shell H atoms are oriented away from the electron, emphasizing that the system is indeed behaving more like a solvated neutral sodium atom than a cation–electron contact pair.

Overall, what the data in Figs. 4.2 and 4.3 show is that there is a subtle interplay between solvation of a sodium cation and solvation of the hydrated electron when the two species approach to form a contact pair. In general, the repulsive electron displaces water from around the Na^+ to provide for a favorable electronic interaction, but the sodium cation also wants to maintain its favorable solvation environment in the water. Since Na^+ is solvated by the water O atoms, which are highly repulsive to the electron, the tighter a sodium cation hangs on to its first-shell waters, the more unfavorable the interaction between it and the hydrated electron. Because these interactions are all closely balanced, modest changes in the ion–water interactions can make relatively large changes in the solvation structure of the electron–ion contact pair.

4.3.3 The Electronic Structure of Hydrated Electron–Na^+ Contact Pairs

Now that we have seen how the solvation structure of hydrated electron–sodium cation contact pairs changes as a function of Na^+–e^- distance and ion–water interaction model, we turn next to exploring how this solvation structure alters the electronic properties of the contact pairs. Solvated electrons are interesting objects because their properties are entirely determined by their interaction with the surrounding solvent. A solvated electron–sodium cation contact pair, however, has a behavior somewhere between that of a solvated neutral sodium atom and a solvated electron, as exemplified by previous experiments and simulations studying solvated electron–Na^+ contact pairs in liquid tetrahydrofuran (THF).[136–139] The question we explore in this section is: for aqueous sodium cation–hydrated electron contact pairs, how do changes in the cation–water interactions

Table 4.2: The direct overlap (Eq. 1), radius of gyration and electronic eigenvalue for each of the three electron–Na^+ simulation models in each of the three regions defined in Fig. 1.

	Na^+ Direct Overlap	H_2O Direct Overlap	Radius of Gyration	Eigenvalue
Dang[38] Region I	47.17%	1.75%	2.22 Å	-3.73 eV
Dang[38] Region II	30.35%	2.15%	2.22 Å	-3.64 eV
Dang[38] Region III	2.37%	3.54%	2.42 Å	-3.03 eV
Koneshan[39] Region I	42.50%	2.12%	2.24 Å	-3.57 eV
Koneshan[39] Region II	24.10%	2.66%	2.24 Å	-3.39 eV
Koneshan[39] Region III	0.45%	3.52%	2.43 Å	-2.95 eV
Aqvist[41] Region I	50.69%	1.65%	2.21 Å	-3.79 eV
Aqvist[41] Region II	35.30%	2.02%	2.18 Å	-3.72 eV
Aqvist[41] Region III	1.24%	3.58%	2.41 Å	-2.99 eV
Hydrated e^- (no Na^+)	N/A	5.7%	2.43 Å	-3.08 eV
Gas Phase Na Atom	53.28%	N/A	2.26 Å	-4.02 eV

affect the pair's electronic properties?

We begin our examination of the contact pair's electronic structure by examining how the proximity of the sodium cation to the hydrated electron's center-of-mass affects the electronic interaction of the electron with both the sodium cation and the surrounding water molecules. We characterize this by examining the direct overlap, Θ, given by:

$$\Theta = \Big\langle \sum_{i=1}^{n_{\text{molcs}}} 4\pi \int_0^{r_c} r_i^2 |\Psi(r_i)|^2 dr_i \Big\rangle, \tag{4.1}$$

where the angled brackets represent an ensemble average, Ψ is the normalized wavefunction of the quantum-mechanically treated electron, the sum runs over either the single sodium cation or all of the water molecules, and r_i is the distance between the electron and the appropriate classical species. The parameter r_c is set to be 1.0 Å for water, a value we have used previously to compare different hydrated electron models to each other,[40, 109] and 2.0 Å for Na^+, to represent the average size of the Na $3s$ atomic orbital. The value of Θ thus gives the fraction of the electron residing on top of the centers of either the waters or the nearby sodium cation. The values of the direct overlap of the electron with both Na^+ and water for the three water–ion models at all three

different regions are given in Table 4.2.

Table 4.2 shows that in region III, the electron–water direct overlap is ∼3.5%, a little less compared with the isolated TB electron,[40] which is understandable due to the slightly decreased water-electron coordination discussed above. The electron's average eigenvalue is similar to what is observed in the bare TB electron, and the electron–Na^+ overlap in this region is essentially negligible. This indicates that at this distance, there is effectively no interaction between the electron and the sodium cation, and that we are truly in the asymptotic region.

In contrast, we see significant changes in electronic structure when the electron forms a contact pair with Na^+. In region II, the electron's direct overlap with the Na^+ dramatically increases, to about half that seen in a bare gas-phase neutral Na atom. The direct overlap of the electron with water decreases, a direct result of the structural changes that put less water in the electron's first solvation shell seen in Fig. 2. One way to think about the contact pair is that the sodium cation now lies within the electron's radius of gyration, creating a direct electronic interaction, so that Na^+ occupies space where water otherwise would have resided in the electron's first solvation shell.

The contact-pair interaction between the electron and sodium cation in region II, however, is highly dependent on the model used to represent the Na^+–water interactions. The Koneshan model, with its tight cation–water interactions, has the lowest electron–Na^+ overlap and highest electron–water overlap. This is because the cation in this model is holding more tightly onto its own first-shell waters, which in turn repel the electron from the region around the cation. We also believe that this is the reason why the PMF minimum for this model is observed at the longest ion–water distance; pulling Na^+ closer to the electron's center becomes more unfavorable as additional waters are forced to enter the electron's cavity. The electron's contact-pair eigenvalue is also significantly higher (less bound) for the Koneshan model compared to the other two, both because there is less stabilization from the sodium cation and because the electron has a more unfavorable solvation structure. All of this explains why this model has a much shallower PMF for the contact pair seen in Fig. 4.1.

In region I, as the sodium cation is forced to sit close to the electron center-of-mass, the direct overlap of the electron on the Na^+ is 40–50%, consistent with the idea that the system is approaching the behavior of a solvated neutral Na atom, which in the gas phase has a direct overlap of 53%. The direct overlap of the electron with the water decreases; this is because the first-shell waters

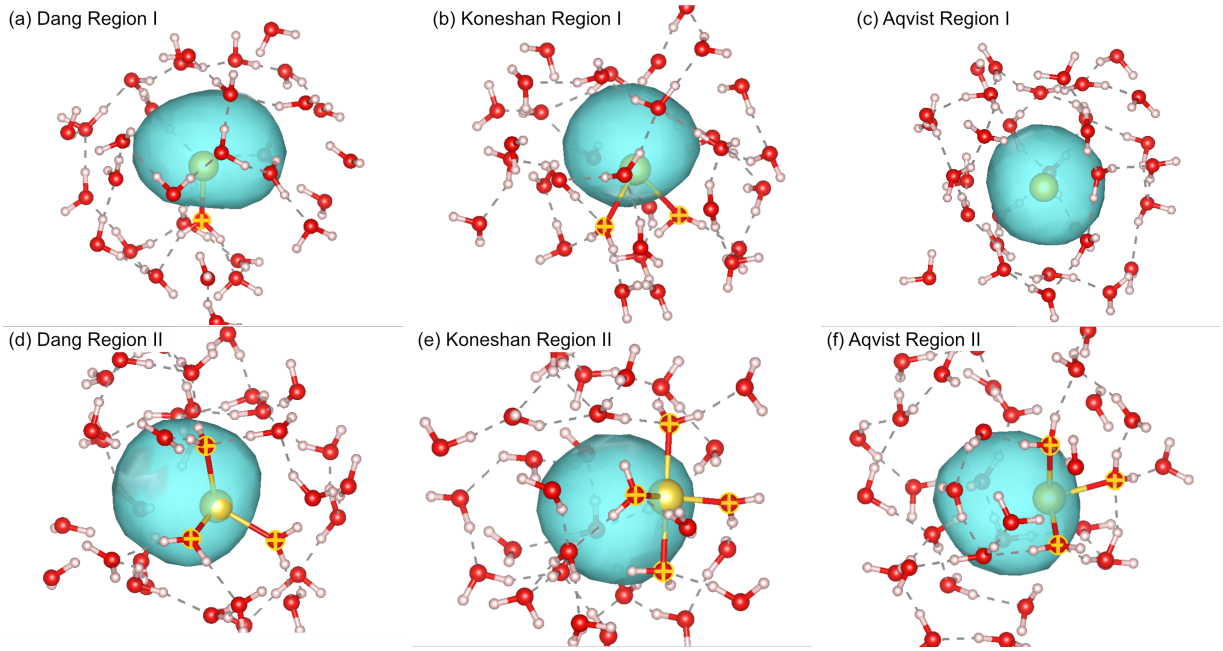

Figure 4.4: Representative simulation snapshots of Na^+–hydrated electron contact pairs for regions I (panels a-c) and II (panels d-f) for all three ion-water models. First-shell water O atoms within 3 Å of the Na^+ are marked with yellow crosses. The Koneshan model cation manages to keep two waters in its first solvation shell in region I and four in region II, whereas the other models have either zero or one first-shell water in region I and only three in region II. The first-shell waters that stabilize the cation are oriented so that their H atoms unfavorably point away from the electron, providing a trade-off in net solvent stabilization of the contact pair. The Aqvist model shows an almost perfect clathrate solvation structure in region I.

are trying to solvate a neutral object and thus are forming a clathrate-like structure, as will be discussed further below. The electronic properties in region I are also strongly model-dependent, with the Koneshan model showing the least Na^+ overlap. Again, this is because the Koneshan Na^+ strongly attracts water, which in turn repels the electron, also leading to the highest eigenvalue of the three models. This explains why the Koneshan PMF shows the most unfavorable free energy in this region, reaching $\sim$14 k_BT as Na^+ is forced into the electron's center.

The structural and electronic changes that a hydrated electron undergoes in the vicinity of a sodium cation are visualized in Fig. 4.4, which shows representative snapshots of the system in regions I and II for all three models. Oxygen atoms are marked with yellow crosses if they are within the first solvation shell ($\leq$ 3 Å) of the sodium cation. Not surprisingly, all such O atoms are on waters that have their H atoms pointing away from the cation. There are few of these waters in region I, and the clathrate solvation structure of what is essentially a neutral Na atom is evident:

the closest water H bonds are preferentially directed around the cation/electron pair rather than toward or away from either species. In both regions I and II, it can be seen that the Koneshan model has a higher cation–water coordination number (cf. Fig. 4.3), forcing those waters to be in an unfavorable location and orientation with respect to the electron. Thus, the dramatic difference in contact pair stability for the different solvation models is a result of a slight shift in the balance of competing interactions between cation solvation, electron solvation and the direct cation–electron interaction.

To better understand how solvation of the Na^+ competes with solvation of the electron in the electron–ion contact pair, we examine the orientational distribution of the water molecules in the first solvation shells of both the electron and the cation in Fig. 4.5. These distributions were constructed by taking the dot product of the water dipole vector with the vector connecting first-shell water O atoms with either the sodium cation (left column of Fig. 4.5) or the hydrated electron center-of-mass (right column of Fig. 4.5). The bottom two panels show that the water O atoms point directly at the sodium cation when no electron is present (dot product of 1.0), and that water H bonds point towards the center of an isolated TB hydrated electron (dot product of $\sim$-0.75). Figures 5(c) and (g) show that in region III, the orientational distributions of the waters around each species are the same as when they are isolated, which is again consistent with the idea that by the time the species are separated by $\sim$5 Å, they are essentially independent.

In contrast, when the contact pair forms in region II, panels (b) and (f), the water orientational distribution around the Na^+ remains essentially unchanged, but the orientation of the waters around the hydrated electron changes significantly: there are now a significant number of waters pointing the 'wrong way', with their O atoms toward the center of mass. This indicates that contact pair formation is primarily a trade-off between losing favorable solvation of the electron and getting the maximal possible electron–cation interaction.

The most striking difference between the different cation–water models appears in region I, where the Koneshan model maintains the bare ion water orientational distribution to a much greater extent than either the Dang or Aqvist models. Thus, not only does the slight change in classical LJ parameters change the coordination number of the sodium cation, but it also helps to lock in the water orientation in the first solvation shell. The extra degree of favorable solvation of the cation in the Koneshan model, however, comes at a price: the waters around the cation

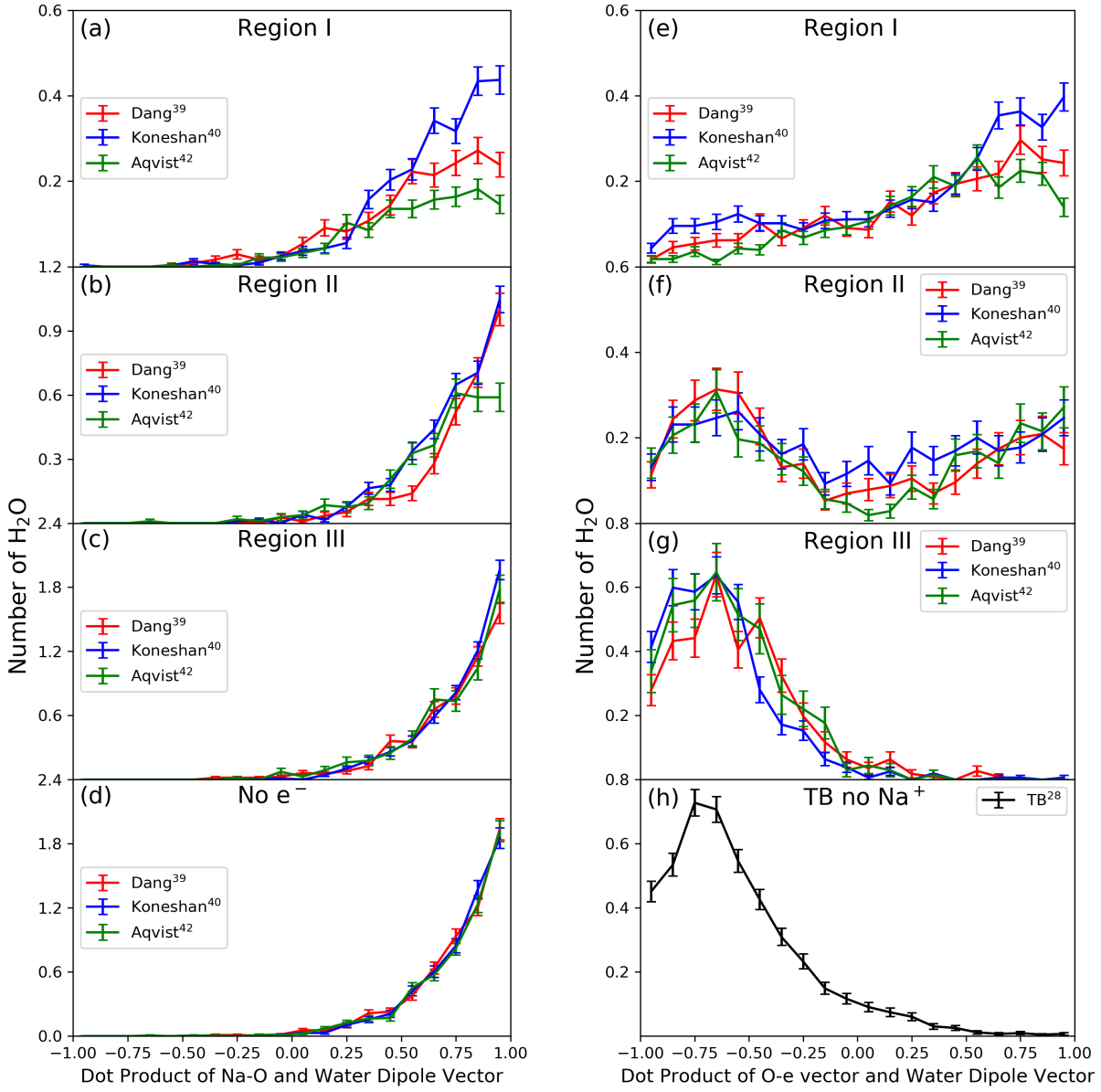

Figure 4.5: The distribution of dot products of the Na^+–O vector and water dipole vector for waters with O atoms that in the first solvation shell of Na^+ (panels a-c) for each of the three contact pair models in each of the three regions defined in Fig. 1. Panels (e-g) show the same distributions for first-shell waters relative to the electron's center of mass. Panel (d) and (g) show the same distributions for isolated Na^+ and TB hydrated electrons, respectively. The dot product is defined as 1.0 when the negative end of the water dipole points directly towards the species, and -1.0 when the positive end of the dipole points towards the species. With this definition, when water H bonds are oriented toward the electron, the dot product is around -0.75 . Clearly, the water orientation around Na^+ does not change significantly between the three regions, while that around the hydrated electron undergoes a dramatic change when present in a contact pair.

are clearly oriented unfavorably for the hydrated electron, and also hinder electron–cation overlap, so that the Koneshan model creates the least stable species in region I. These changes in relative solvation also affect the electron's radius of gyration and eigenenergy, which are plotted as a function of electron–cation distance for each of the three models in Fig. S4 in the SI.

4.3.4 The Calculated Spectroscopy of Hydrated Electron–Na^+ Contact Pairs

The calculations presented so far allow us to make sense of why subtle changes in the water–ion LJ parameters lead to such large changes in the stability of electron–ion contact pairs. This leads to the question of which of these models, if any, allow for the most direct connection to experiment. As mentioned in the Introduction, experiments have shown that when hydrated electrons are created in aqueous electrolytes, the spectrum of the electron blue shifts.[58] The magnitude of the observed blue shift depends on the salt concentration, and also the identities of the cation and anion, suggesting that the spectral shift reflects an interplay between solvation of the electron, solvation of the cation and the way that cation–anion contact pairs affect the formation of cation–electron contact pairs.

In previous work, Boutin and co-workers attempted to theoretically reproduce the concentration dependence of the electron's spectral shifts in the presence of salts via MQC simulation. These workers studied the electron's interaction with a single sodium cation and assumed that the concentration dependence could be accounted for by adjusting the distance between the cation and electron as the inverse cube root of the salt concentration.[60] They found that the electron's spectrum did blue shift in a manner that was inversely related to the electron-cation distance. They also saw that as the cation was brought close to the electron, a new shoulder appeared on the blue side of the electron's spectrum that was not observed experimentally.

To better understand how different choices of the ion–water interaction affect the spectroscopy of cation–electron contact pairs, we calculated the absorption spectrum for all three models in the three different regions summarized in Fig. 4.1. The absorption spectrum was generated in the inhomogeneous limit by calculating the oscillator strength between the ground and the three lowest electronic excited states and then binning the oscillator strengths according to the energy difference between them. The resulting histograms were then convoluted with a Gaussian kernel, resulting in a final expression for the spectrum of:

$$I(E) = \langle \sum_{i=1}^{N} |\mu_{0,i}|^2 \Delta E_{0,i} \sqrt{\alpha/\pi} \exp(-\alpha(E - \Delta E_{0,i})^2) \rangle, \tag{4.2}$$

where the Gaussian width α was chosen to be 50 eV^{-2} following the previous work from our group.[97] For each model and region, a minimum of 100 uncorrelated configurations were used to generate the spectra. The normalized absorption spectra calculated this way are shown in Fig. 4.6.

Figure 4.6(c) shows that in region III, the calculated spectra of the different model contact pairs are effectively the same as that of an isolated TB hydrated electron, consistent with the idea that the two species are essentially independent in this region. In region II, Fig. 4.6(b) shows that the calculated spectra are all significantly blue-shifted; as with the prior work of Boutin and co-workers,[60] the calculated blue shifts are an order of magnitude larger than those seen experimentally.[58] Surprisingly, Fig. 4.6(c) shows that the magnitude of the blue shift is not monotonic with the cation–electron distance: for the Dang model, there is no additional blue shift between regions I and II, and for the Aqvist model, the spectrum in region I is actually red-shifted from that in region II. This trend is consistent with what is observed for the electron's radius of gyration, seen in Fig. S4 in the SI, and likely reflects the shift in the energy of the excited state from that of a hydrated electron to something that more resembles the $3p$ state of a neutral Na atom.

The spectra shown in Fig. 4.6 are associated with the three different regions of the PMFs, and thus do not provide a direct way to compare to what would be measured experimentally. To better compare the simulations to experiment, we averaged the calculated absorption spectra from all of the simulated umbrella windows for each model and weighted them by the Boltzmann factor using the free energies from the calculated PMFs. These Boltzmann-weighted spectra are shown in Fig. 4.7a.

Even with this Boltzmann-weighted spectrum, a direct comparison with the experiment requires some finesse because the effective cation concentration is not well-defined for a single-cation system. In previous work, Boutin *et al.* attempted to use the inverse cube-root of the restrained cation–electron distance as an approximation to the experimental concentration.[60] This approximation fails, however, as the calculated spectral shift turns out to be non-monotonic with electron:cation distance (cf. Fig. 4.6) while the experimental shift is monotonic with cation concentration.[58] For our Boltzmann-weighted calculated spectrum, we averaged all the single-distance spectra together

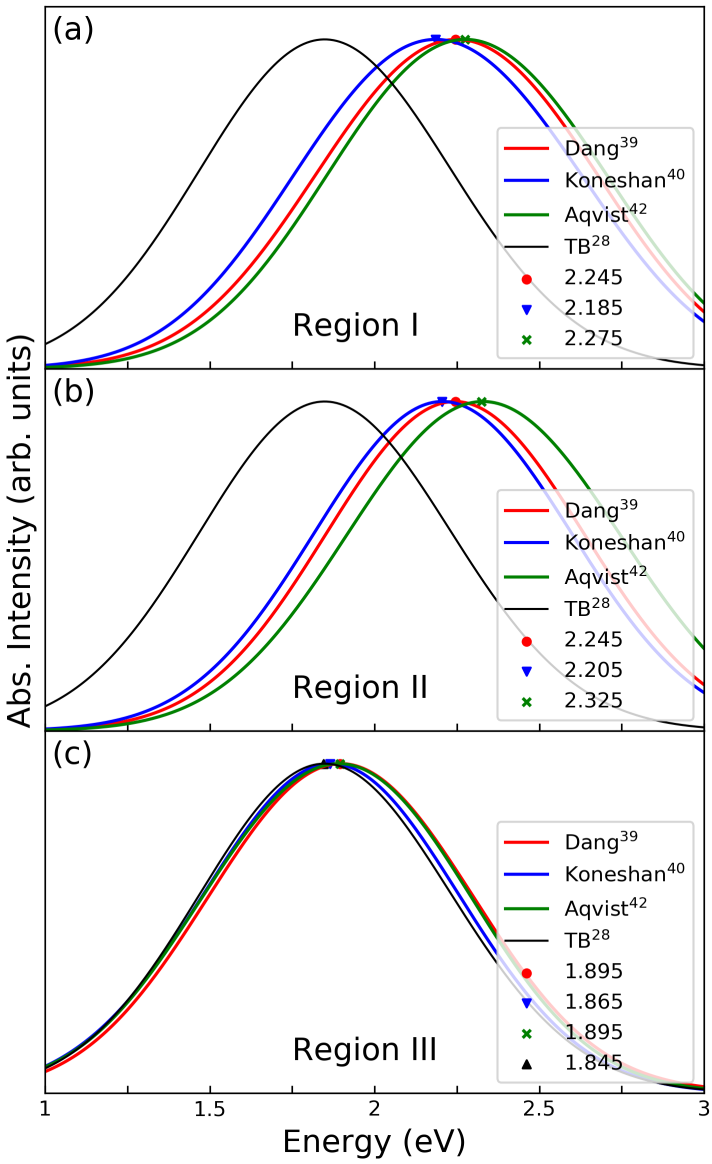

Figure 4.6: The absorption spectrum of each hydrated electron–cation contact pair model in each of the three regions described in Fig. 1. Panels (a), (b) and (c) depict the spectra in regions I, II and III, respectively. The different colors correspond to the different models, as in the previous figures. All three models predict a spectral blue-shift of the contact pair relative to the bare hydrated electron that is an order of magnitude larger than what is observed experimentally. The predicted blue shift is smallest for the Koneshan model, likely due to the fact that the electron–cation overlap is reduced in this model due to the tight hydration of the cation.

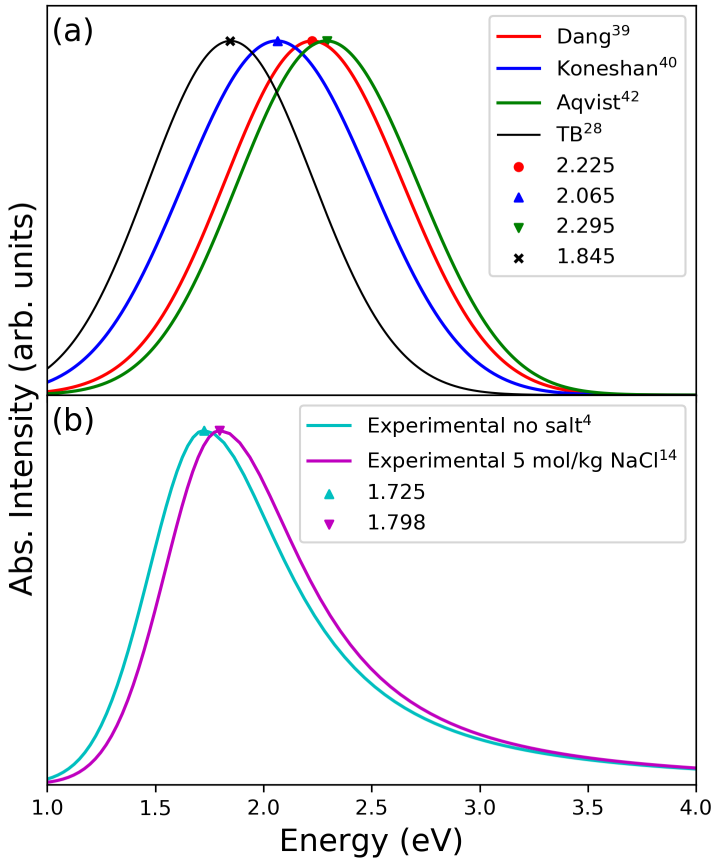

Figure 4.7: The absorption spectrum shown in panel (a) is calculated by weighing the absorption spectrum from all simulation windows by the Boltzmann factor. The red, blue and green curves represent the weighed spectrum for Dang, Koneshan and Aqvist, respectively. The spectra in panel (b) represent the experimental absorption spectra for the hydrated electron in different conditions. The cyan curve shows the hydrated electron without salts and the magenta curve shows the hydrated electron with 5 mol kg^{-1} NaCl.

up to a cation:electron separation of 5 Å (averaging to distances further than this leads to almost no change in the averaged spectrum because there is little Boltzmann weight to the configurations at the longer distances). If we assume that our effective concentration is one cation in the volume of a 5 Å-radius sphere, this would correspond to an experimental concentration of 3.2 M. The experimental spectrum of the hydrated electron, both in neat water (cyan curve) and in the presence of 5 kg mol-1 NaCl (magenta curve), are shown in Fig. 4.7b; the spectra are reproduced using the standard Gaussian-Lorentz form (see the SI for details) with the parameters measured by Mostafavi and co-workers.[10, 58] The experiments show that even at very high salt concentrations, the magnitude of the blue-shift is only 73 meV.

A comparison between the Boltzmann-averaged simulated spectra and the experimental spectrum shows that the MQC-calculated blue shift of the electron's spectrum in the presence of sodium relative to that in the absence of salt is significantly too large. Both the Dang and Aqvist models yield an averaged spectrum similar to that seen in region II, because the other regions have negligible Boltzmann weight. The Koneshan model, however, shows a smaller blue shift of the averaged spectrum compared to that in region II, because the shallower PMF for this model increases the relative Boltzmann weight of configurations at larger cation:electron separations, which have smaller spectral shifts. This makes the Koneshan weighted spectrum in somewhat better agreement with the experimental shift, although the blue shift for this model is still notably larger than the experiment. Overall, our MQC simulations fail to accurately reproduce the experimentally-observed blue-shift of the hydrated electron's spectrum in the presence of salt, indicating that some factor in the MQC calculations is improperly balanced and thus does not correctly describe the nature of Na^+:e^- contact pairs in water.

Overall, the Koneshan model shows the least blue-shifted absorption spectrum, while the Aqvist model produces the largest blue-shift. This is a direct reflection of the decreased electron–cation overlap in the Koneshan model. Since none of the models produce the correct order of magnitude for the blue-shift, it is not clear if the Koneshan model is in the best agreement with experiment (i.e., that there is relatively little overlap of hydrated electrons with sodium cations in solution) or not. It is entirely possibly that our MQC model misses some of the important physics of the system; for example, the TB model of the electron, although giving a structure in reasonable agreement with ab initio calculations,[11, 34–36] is so strongly cavity forming as to be unable to reproduce

the temperature dependence of the hydrated electron's spectrum.[15] It is also possible that the electron partially occupies the water LUMOs, changing the way the waters interact with the cations in a manner that is not well captured using pseudopotentials. Another factor might be that the experimental measurements occur at salt concentrations that are on the order of a few molar, so that the correct physics may involve interactions with multiple cations instead of only a single cation. Finally, we know experimentally that the anion also plays a role in the spectral blue-shift, and we plan to explore this in future work.

4.4 Conclusions

In summary, we have found that relatively modest changes in the interactions between a sodium cation and water have a large effect on the stability and properties of sodium cation:hydrated electron contact pairs. The free energy of these contact pairs and the equilibrium distance at which they prefer to reside change significantly between the different models, as evidenced by large changes in the electron-cation PMF. We argued that the differences result from the strength of the ion–water interaction: stronger ion solvation leads to poorer solvation of the electron in the contact pair and also reduces the direct interaction of the electron with the cation. This is because the solvation interactions with the cation are somewhat stronger than those with the electron, so that waters that accompany the cation are held near the electron in an unfavorable orientation. Thus, electron–cation contact pair stability arises from a delicate balance between competing effects, including electron solvation, cation solvation and cation–electron electronic interactions. Small changes in any of these interactions tip the balance, altering the nature of the electron–cation contact pairs.

We also found that despite the sensitivity of the simulated contact pair properties to the choice of ion–water interactions, all three models we explored predicted a spectral blue-shift of the contact pair that is an order of magnitude larger than that observed experimentally. This strongly suggests that the physics of the system is either not well represented by a single cation, or that quantum interactions that go beyond MQC play an important role. The fact that the experimental system shows only a relatively small spectral blue-shift ($\leq$100 meV shift of the electron's $\sim$1.7 eV absorption maximum) suggests that on the continuum of contact-pair behavior from isolated hydrated electron to solvated neutral Na atom, the experimental system behaves more like a

slightly-perturbed hydrated electron than a solvated neutral atom.

All of the above results suggest that obtaining a theoretical understanding of the behavior of solvated electron in aqueous electrolytes remains a serious challenge. Describing a system with hundreds of water molecules and tens of cations and anions with *ab initio* molecular dynamics is simply out of reach computationally, and MQC simulations are clearly highly sensitive to the choice of parameters used to describe the classical part of the system and also may miss quantum aspects that are important to the physics of contact pair formation. Given that hydrated electrons often appear in solutions containing electrolytes, we believe that this remains a fruitful area for study both experimentally and theoretically.

Chapter 5

Ab Initio Studies of Hydrated Electron:Cation Contact Pairs: Hydrated Electrons Simulated with DFT are too Kosmotropic

5.1 Introduction

The hydrated electron (e^-_{aq}), an excess electron dissolved in liquid water, is the primary species produced in radiation chemistry and is known to participate in a variety of radical and other chemical reactions.[8, 140–142] Hydrated electrons also serve as a paradigm system for comparing the results of quantum simulations with experiment. This is both because they are relatively easy to generate in the laboratory by pulse radiolysis or via the charge-transfer-to-solvent excitation of simple anions,[47, 143] and because they provide one of the simplest quantum many-body problems that can be readily tackled by modern simulation methods. Despite all the effort aimed at understanding the nature of hydrated electrons, however, there are still open questions concerning their basic features, particularly their solvation structure. The standard picture of the e^-_{aq} (although alternatives have been proposed[13]) is that it occupies a cavity in liquid water.[11, 12, 32, 35, 36, 54, 144] But the exact structure of the cavity and the orientation of the waters around the excess electron remain

as of yet unresolved.

The question of the solvation structure of the e^-_{aq} is not just academic: the rates of reactions involving hydrated electrons can vary over many orders of magnitude even when they have similar activation energies, which is not consistent with Marcus theory.[27] This implies that there is something about the reorganization of the waters solvating the e^-_{aq} that critically determines the way that hydrated electrons can interact with other chemical species in aqueous solution. The purpose of this paper is to use simulations to study the way that hydrated electrons with different solvation structures interact with other species in solution; in particular, we examine the pairing of a simulated e^-_{aq} with a simple ion, Na^+. The goal is to use experimental knowledge of e^-_{aq}–ion interactions to help determine which simulated structure of the hydrated electron, if any, best matches experiment.

What is known experimentally about hydrated electrons in the presence of electrolytes is that the absorption spectrum of the e^-_{aq} shifts to the blue when salts are present, with the magnitude of the blue shift dependent on the identities of both the cation and anion.[57–59] Salt does not cause the hydrated electron's spectrum to change shape, and the magnitude of the spectral blue shift increases with increasing electrolyte concentration.[58] For e^-_{aq}'s in high-concentration NaCl aqueous solutions, the spectrum shifts by only a few tens of meV.[58] The small magnitude of the spectral shift indicates that the presence of ions provides at most a subtle perturbation to the electron's hydration structure, and that any direct overlap of the e^-_{aq}'s charge density with the salt cation is quite small. In previous simulation work, we argued that the blue-shift of the e^-_{aq}'s spectrum in the presence of salt was not driven by the salt-induced change in dielectric constant, but instead results from electron-ion pairing.[64, 65, 112, 145] Electron-ion pairing, in turn, is a behavior driven by the interaction of the e^-_{aq}'s and ion's hydration structures,[64, 65, 145] which form the focus of this work.

Based on our previous simulations, we argued that the e^-_{aq} in aqueous salt solutions competes with other anions to undergo ion pairing with cations based on their relative positions on the Hofmeister series.[61] The Hofmeister series classifies ions as structure makers, or kosmotropes, when they have high charge-to-surface-area ratios and thus form tight hydration spheres with negative entropies of solvation; Na^+ and Cl^- are examples. Conversely, larger and more hydrophobic ions are classified as structure breakers, or chaotropes, which have less negative or even positive

entropies of hydration, such as Cs^+ and ClO_4^-. In general, kosmotropic ions tend to form pairs with other kosmotropic ions, as there is a favorable enthalpy to put two high charge density ions close together. Chaotropes also tend to pair with chaotropes, as there is a more favorable entropy to solvate a single large paired hydrophobic object rather than two separate smaller ones. Mixed kosmotrope/chaotrope salts, however, tend not to ion pair.[129, 146–150] Hydrated electrons have the largest known solvation entropy of any anion,[62, 63] and thus should be champion chaotropes; as such, they are expected to pair poorly with kosmotropes like Na^+.

Our previous simulations of e_{aq}^-/Na^+ pairing used mixed quantum/classical (MQC) methods, where only the hydrated electron was treated quantum mechanically and the water was treated classically, with the water–e_{aq}^- interactions described by a pseudopotential. We chose the standard cavity-forming Turi-Borgis (TB) pseudopotential for our previous work,[11, 69] and found that the TB hydrated electron experiences a strong interaction with Na^+; the simulations predicted a spectral blue shift of the ion-paired e_{aq}^- that is an order of magnitude larger than experiment.[64, 112] In addition, we found that subtle adjustments of the classical Na^+–water interactions that made the cation more or less kosmotropic produced significant changes in the e_{aq}^-–Na^+ pairing behavior, although the pairing was always too strong.[112] We believe that this overly strong interaction arises because the TB hydrated electron has a hydration structure (see Fig. 5.1(a), below) that is somewhat too kosmotropic, so that its pairing interactions with simulated kosmotropic Na^+ ions are too strong.

Recently, there has been a surge of interest in using ab initio approaches to determine the structure and behavior of the e_{aq}^-.[35, 36, 52, 54, 56, 70, 109, 144] To date, all such work has used DFT-based methods, and even though different functionals were employed, the work from different groups appears to yield a similar solvation structure, which is shown below in Fig. 5.1(c). (We note that the work in Ref. 36 is also predominantly based on DFT, with the atomic positions updated only every 6th time step via the MP2 method; these simulations also yielded a similar hydration structure, as shown in the SI of Ref. 56). To date, however, DFT models have not done a good job predicting the absorption spectrum or vertical detachment energy of the e_{aq}^-,[56] although it appears that DFT does qualitatively describe the hydrated electron's temperature dependence.[56, 144] All of this leads to the principle questions addressed in this work: does the hydration structure of a DFT-simulated e_{aq}^- interact with a Na^+ in a way that is consistent with experiment? If not, is

there an another simulation e^-_{aq} model whose solvation structure can predict the correct ion pairing behavior?

In this paper, we answer these questions by performing the first DFT-based simulations of a hydrated electron in the presence of a sodium cation. We then compare the results of the DFT calculations to MQC simulations of a e^-_{aq} paired with Na^+. Our MQC simulations use two different pseduopotentials, the TB pseudopotential mentioned above,[11] and an altered version of the TB pseudopotential with the polarization interactions optimized to better match the results of CCSD(T) quantum chemistry calculations, which we have referred to as the TBopt potential.[97] We find that the solvation structure of the DFT-simulated e^-_{aq} is so strongly kosmotropic that it actually imposes its hydration structure onto the nearby Na^+. As a result, the predicted spectrum of the DFT-simulated hydrated electron paired with Na^+ shifts to the red, the exact opposite of what is seen experimentally. The results indicate that the DFT-predicted hydration structure of the e^-_{aq} is far too kosmotropic to be correct. We also find that unlike MQC simulations using the TB pseudopotential, which as mentioned above predict an overly blue-shifted spectrum of the e^-_{aq}–Na^+ ion-pair, [64, 112] MQC simulations with the TBopt pseudopotential, which produces a much more chaotropic hydration structure for the e^-_{aq}, are able to predict the hydrated electron's spectral blue shift in the presence of Na^+ nearly quantitatively. Thus, it is not enough to simply conclude that the e^-_{aq} occupies a cavity: capturing the correct details of the cavity hydration structure are the key to understanding the spectroscopy and reactivity of this fascinating object.

5.2 Results and Discussion

The methodology used for both our MQC and DFT-based ab initio molecular dynamics simulations of hydrated electrons interacting with Na^+ follows that of our previous work,[56, 64, 65, 112] and details are given in the Methods section below and in the Supporting Information. We begin our exploration of how different simulation models of the e^-_{aq} undergo ion-pairing with Na^+ by first examining the hydration structure of each model. The dashed curves in Figure 5.1(a)-(c) show radial distribution functions, $g(r)$'s, for the TB, TBopt and DFT hydrated electron models without any ions added to the system, respectively; the blue curves show e^-_{aq} center-of-mass to water H atom $g(r)$'s, while the red curves show e^-_{aq}–O radial distribution functions. As is well known, the MQC-

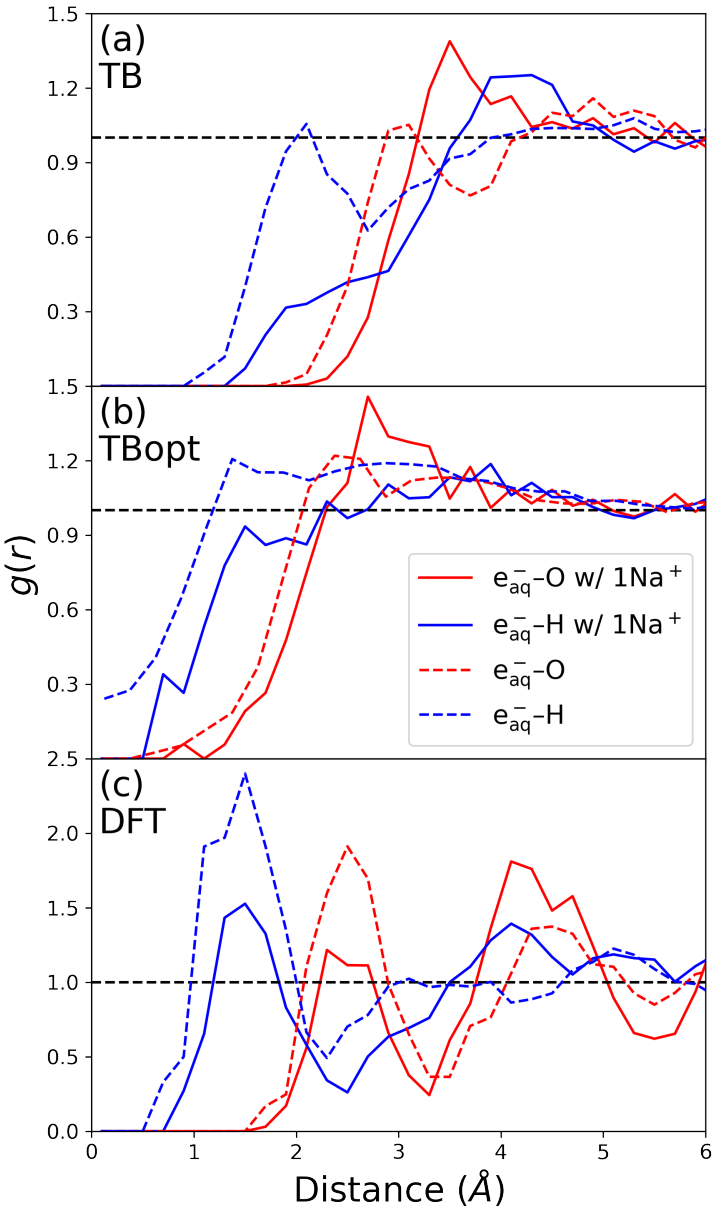

Figure 5.1: Hydration structure of different models of the hydrated electron. The e^-_{aq}–O and e^-_{aq}–H radial distribution functions are shown as the red and blue curves, respectively, with structures shown for the MQC TB, MQC TBopt, and DFT e^-_{aq} models in panels (a), (b), and (c), respectively. The dashed curves show the hydration structure of the e^-_{aq} without Na^+, and the solid curves represent the same system with a single paired Na^+. The TB model shows a distinct cavity with a modest hydration structure, and the addition of Na^+ notably decreases the e^-_{aq}–H first peak, indicating dehydration of the electron by the adjacent Na^+. The TBopt model is the most chaotropic, showing an indistinct hydration structure with a less well-defined cavity; the addition of Na^+ makes little change to this e^-_{aq}'s hydration structure. The DFT e^-_{aq} model shows a highly structured hydration shell that resembles a kosmotropic anion like Cl^-; upon the addition of Na^+, the highly structured solvation peak persists, another indication that the DFT electron is quite kosmotropic.

based TB model in Fig. 5.1(a) shows a distinct central cavity, with virtually no water O atoms approaching within 2 Å of the electron's center.[11] The TB model has a relatively poorly defined hydration structure, with modestly-clear first-shell e^-_{aq}–O and e^-_{aq}–H peaks, suggesting that this species behaves as a weakly kosmotropic or modestly chaotropic anion.

The dashed curves in Fig. 5.1(b) shows that the TBopt model has a smaller and more poorly-defined central cavity than the TB model. In previous work, we argued that this poorly-defined central cavity causes the TBopt e^-_{aq} to have a temperature-dependent structure that yields a spectral red-shift with increasing temperature that resembles experiment (although the magnitude of the predicted spectral shift is too small;[97] the TB model, in contrast, shows no temperature dependence whatsoever, a result that is not commensurate with experiment[15, 43]). The TBopt model also has a much less well-defined hydration structure than TB, with no visible e^-_{aq}–H first-shell solvation peak, suggesting that this species is more chaotropic.

The dashed curves in Fig. 5.1(c) show that the DFT-based ab initio model not only has a distinct cavity region that lies between TB and TBopt in size, but also has a very strongly structured first hydration shell (note that the height of the first-shell e^-_{aq}–H peak is ∼2.4, which is much larger than the 1.0-1.2 seen with the TB and TBopt models).[56] This type of hydration structure is typical of what is seen around anions such as Cl^- or Br^-, and suggests that the DFT e^-_{aq} is the most kosmotropic of the three models.

The solid curves in Fig. 5.1 show how the structure of the simulated hydrated electrons change in the presence of a single nearby Na^+ cation. After a Na^+ is added to the system, the TB model shows a dramatic decrease in the first peak of the e^-_{aq}–H $g(r)$ as well as a restructuring of the e^-_{aq}-O $g(r)$ to move waters from the first to the second solvation shell. We argued previously that this is because some water molecules that were involved in H-bonding with the e^-_{aq} reorient to solvate the nearby Na^+, leaving those waters pointing the 'wrong way' toward the hydrated electron.[112] In contrast, this desolvation phenomenon does not take place with the TBopt model, which shows only a slight decrease in its first-shell $g(r)$'s because Na^+ replaces a few water molecules, but otherwise little change is made to the TBopt electron's hydration structure. This is because the TBopt e^-_{aq} is more fluxional than TB, so that the TBopt electron can easily distort to help water maintain its natural H-bond network even when there is a paired cation nearby. Finally, the DFT-based e^-_{aq} model shows a hydration structure that is not at all perturbed by the presence of a nearby

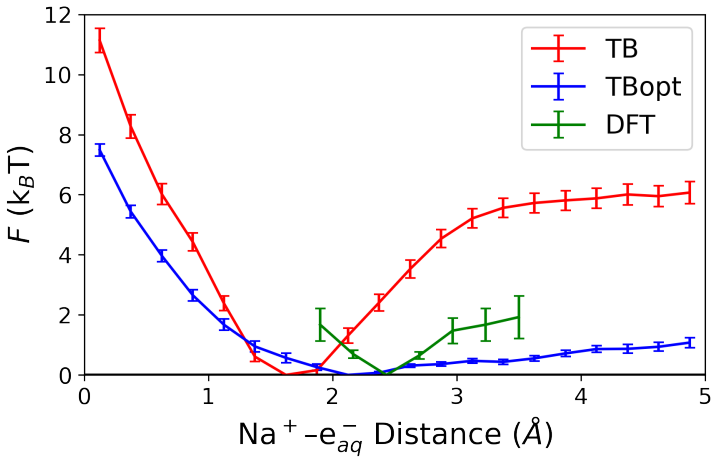

Figure 5.2: Na^+–e^-_{aq} potentials of mean force for the TB (red curve), TBopt (blue curve), and DFT (green curve) e^-_{aq} models. The TB model shows strong pairing between Na^+ and the e^-_{aq} with a relatively short equilibrium distance, whereas the TBopt model shows much weaker pairing with a longer equilibrium pairing distance. The PMF of the DFT model, which is limited by the simulation statistics, is in between those of the TB and TBopt models, showing a modest pairing strength and equilibrium distance. The stronger pairing seen with the TB and DFT e^-_{aq} models suggests that their hydration structure is more kosmotropic than the TBopt model.

Na^+, other than a general decrease in the number of first-shell water molecules due to displacement by the cation. The fact that the hydration structure of each e^-_{aq} model changes differently when Na^+ is added shows that indeed, ion-pairing is sensitive to the electron's solvation structure, which should allow us to compare the behavior of the different simulation models to experiment and thus determine which hydration structure makes the most physical sense.

In Fig. 5.2, we show potentials of mean force (PMFs) between the center-of-mass of each e^-_{aq} model and Na^+. The stability of the e^-_{aq}–Na^+ contact pair is quite different for each of the three simulation models. The red curve in Fig. 5.2 shows the PMF for a Na^+ interacting with the TB e^-_{aq}, which we have presented previously.[64, 65, 112] The contact pair has a stability of roughly 6 k_BT and an equilibrium distance of only ∼1.7 Å, which is smaller than the TB electron's 2.2 Å radius of gyration, thus leading to significant electron–cation overlap.[112] This PMF is strongly reminiscent of that between two fairly kosmotropic ions.[129, 147] In contrast, the blue PMF curve in Fig. 5.2 for the TBopt e^-_{aq} model shows a much shallower free energy well, only ∼1.5 k_BT deep, with a significantly longer ion-pair equilibrium distance. This means that the TBopt e^-_{aq} can fairly easily move away from Na^+ at room temperature, indicative of the type of weak ion-pairing that

might be expected between a kosmotropic cation and a chaotropic anion.[129, 146–150] This PMF is consistent with the fact that the presence of Na^+ minimally perturbs the TBopt e^-_{aq}'s hydration structure, as seen in Fig. 5.1. Since the parameters simulating the Na^+–water interaction are the same in the two MQC simulations, the difference in the two PMFs emphasizes how contact-pair stability is extraordinarily sensitive not only to the simulated hydration structure of the cation[112] but also the simulated hydration structure of the e^-_{aq}.

For comparison, the green curve in Fig. 5.2 shows the limited PMF results available for the DFT-based AIMD e^-_{aq} model. Although we were unable to explore what happens far from equilibrium and thus do not know the full depth of the well, the DFT e^-_{aq} appears to form a less stable ion pair with Na^+ than the TB model, with a shallower well and longer equilibrium distance. This is consistent with what we saw in Fig. 5.1(c), where the presence of Na^+ does not significantly alter the DFT hydrated electron's solvation structure. However, the DFT-based e^-_{aq} clearly forms a stronger ion pair with Na^+ than the TBopt model, with a similar equilibrium distance. We will argue below that these results show not only that the DFT e^-_{aq} is too kosmotropic, but also that the hydration structure of the DFT-simulated Na^+ is less kosmotropic than what is seen in the MQC simulations. The net result is that instead of the ion altering the hydration structure of the e^-_{aq}, the DFT hydrated electron alters the hydration structure of the cation, a result that we will argue below is inconsistent with experiment.

To delve deeper into the local solvation structures of the different hydrated electron and sodium cation models, we have examined the orientation of the first-shell waters around each species in the different simulated e^-_{aq}–Na^+ ion pairs. We define first-shell waters as those whose positions are closer than the distance of the local minimum past the first solvation shell peak in the electron–O $g(r)$ (see the SI for details). For the orientational analysis, we built distributions of the dot product between the dipole vector of a first-shell water molecule and the vector connecting the O atom of that water molecule to either the e^-_{aq}'s center or mass or the position of the Na^+. Figure 5.3(a) shows the water orientational distributions around each of the three e^-_{aq} models when no cation is present. All three models show a peak near -0.7, which corresponds to the angle expected when water is making an H-bond that points directly toward the e^-_{aq}'s center-of-mass. We note that the orientational structure is much less distinct for the TBopt model (dark blue curve), which is consistent with the idea that this model is more chaotropic and thus does not impose a strong

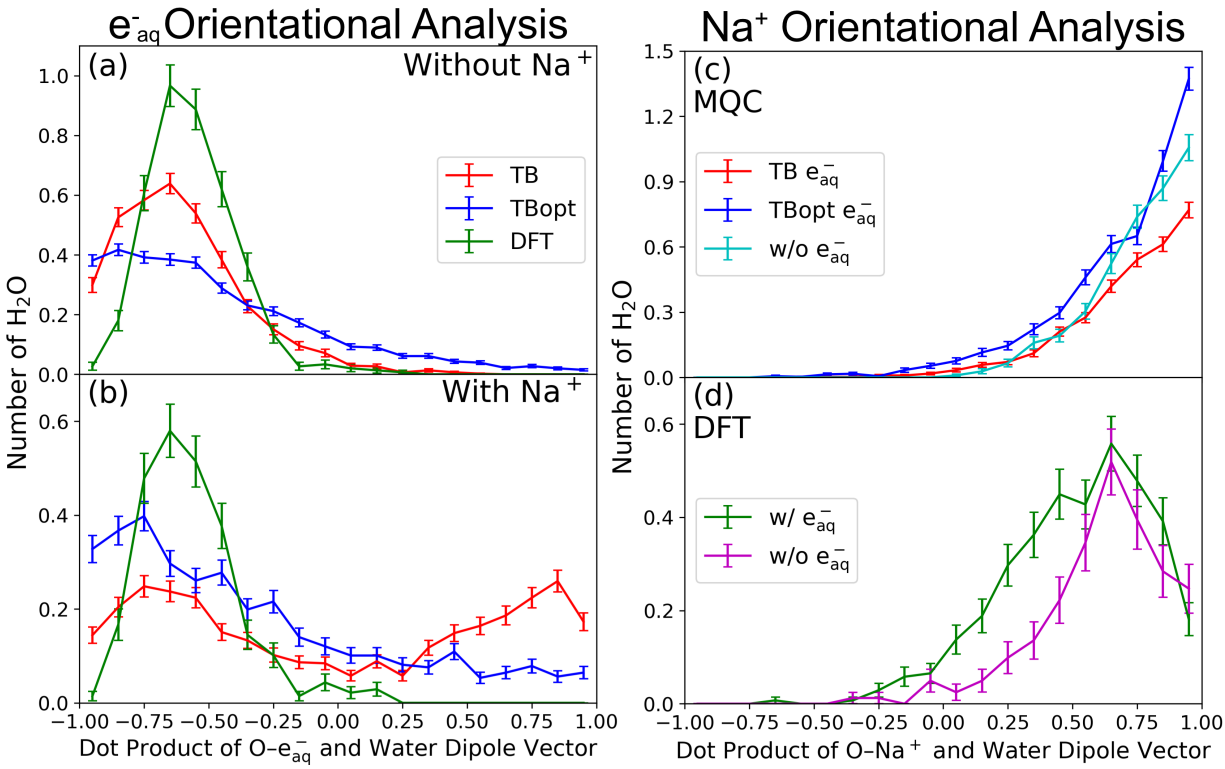

Figure 5.3: Hydration structure orientational distributions, calculated as the dot product between the dipole vector of first-shell water molecules and the vector connecting the water O and either the e^-_{aq} (panels (a) and (b)) or the Na^+ (panels (c) and (d)). The angular hydration structures of the TB, TBopt, and DFT models are represented by the red, blue, and green curves, respectively. Panels (a) and (c) show distributions for the different e^-_{aq} models when no Na^+ is present, and panels (b) and (d) show the distribution after the addition of a single Na^+. The data show that the TB e^-_{aq} becomes dehydrated when Na^+ is in proximity, so that some first-shell waters reorient into an unfavorable configuration. The TBopt e^-_{aq} first-shell water orientation is largely unaffected by Na^+, a sign of weak ion pairing. The DFT e^-_{aq} not only maintains its favorable water H-bond orientation in the presence of Na^+, but also imposes an unfavorable hydration structure on the paired cation, indicating that the DFT e^-_{aq} is actually more kosmotropic than DFT Na^+.

structure on the surrounding water molecules.

In addition to hydration of the e^-_{aq}, the cyan curve in Fig. 5.3(c) shows the orientational distribution of first-shell water molecules around a classically-simulated Na^+ without the presence of a e^-_{aq}; the peak at +1.0 shows that classical waters strongly prefer to have their dipoles pointing directly away from the sodium cation, so that the negatively-charged O atoms can sit as closely as possible to the cation, a signature of a strongly kosmotropic species. This distribution is quite different from when DFT is used to simulate hydrated Na^+ without a nearby e^-_{aq}, as shown by the magenta curve in Fig. 5.3(d). The DFT Na^+ hydration structure has a preferred first-shell water orientation with a significant tilt relative to what is seen in the classical simulations, indicating that the DFT first-shell waters have more of a preference to maintain their H-bonding with the second-shell waters than to strongly solvate the cation. This also suggests that the DFT-based Na^+ is less kosmotropic than what is seen in the classical simulations, a feature that is important to keep in mind when comparing the ion-pairing of the different simulation models.

With the water orientations around bare e^-_{aq}'s and Na^+'s established, we now examine how ion-pairing causes changes in the hydration orientation of the two species. Figure 5.3(b) shows the orientational distribution of the water molecules around the different e^-_{aq} models when they are at their equilibrium distance in a contact pair with Na^+. The red curve shows that for the TB e^-_{aq}, when Na^+ is present, there is a decrease in the number of water molecules making H-bonds to the electron (peak near -0.7) and an increase in water molecules that point their dipoles away from the e^-_{aq}'s center of mass (peak at +1.0). We argued previously that this occurs because the highly kosmotropic classical sodium cation 'outcompetes' the TB hydrated electron for imposing structure on waters that are in the first shells of both species; these waters prefer to solvate Na^+ and end up oriented in the 'wrong' direction for solvating the e^-_{aq}.[112] Indeed, the red curve in Fig. 5.3(c) shows that pairing with the TB e^-_{aq} has little effect on the water orientation in the first shell surrounding the classical Na^+, with a distribution that has a similar shape as for a bare classical Na^+ (with a slight decrease in the number of first-shell waters because of the presence of the nearby e^-_{aq}).

In contrast, the blue curve in Fig. 5.3(b) shows that the orientation of the first-shell water molecules surrounding the TBopt e^-_{aq} is largely unaffected by the presence of a nearby classical Na^+, other than perhaps a slight increase in the tail of the distribution at positive dot products.

This result is consistent with the $g(r)$'s in Fig. 5.1(b), which also argue that the TBopt e^-_{aq}'s hydration structure is largely unaffected by being in a contact-ion pair. Remarkably, the blue curve in Fig. 5.3(c) shows that the orientation of the first-shell waters around classical Na^+ is also unchanged by ion-pairing with the TBopt e^-_{aq}. How can water simultaneously maintain its favorable orientation around both species when they are paired? We believe that this is due to the chaotropic nature of the TBopt e^-_{aq}. Unlike with the TB model with its rigid cavity, the first-shell waters around the TBopt e^-_{aq}, which has a softer cavity, are more fluxional, as they do not have a tight hydration structure to maintain.[88] This provides them with the opportunity to find an orientation that can favorably solvate both the e^-_{aq} and the cation. We will show below that the fact that ion-pairing of the TBopt e^-_{aq} leads to little change in hydration structure also yields a smaller spectral shift that is in much better agreement with experiment than for the other hydrated electron models.

The green curves in Figs. 5.3(b) and (d) show the orientations of the first-shell waters around the hydrated electron and sodium cation, respectively, in the DFT-based ab initio simulations. Figure 5.3(b) shows that the DFT e^-_{aq} experiences no change in first-shell water orientation when placed into contact with Na^+, consistent with the fact that the first-solvation structure also doesn't change (cf. Fig. 5.1(c)). But strikingly, Fig. 5.3(d) shows that ion-pairing with a DFT e^-_{aq} changes the first-shell water orientations around the sodium cation: the number of water molecules solvating the Na^+ increases in the presence of the DFT electron, and the distribution of solvation angles broadens. This indicates that the DFT e^-_{aq} is actually more kosmotropic than the DFT-simulated Na^+. In other words, the DFT hydrated electron outcompetes the cation for imposing structure on the waters in the first shells of both species, so that these shared waters more favorably solvate the e^-_{aq} at the expense of the cation. This observation does not fit well with the fact that the hydrated electron is known to have the largest possible solvation entropy of any ion,[62, 63] and as we show next, leads to a predicted spectral shift that has the opposite sign compared to experiment.

With all of the above analysis, the real arbiter of which simulated e^-_{aq} has the 'best' structure comes by comparing to experiment. Figure 5.4(a) shows experimental spectra of the e^-_{aq} in pure water (magenta curve) and that in 5 m aqueous NaCl (cyan curve), reproduced using the Gauss-Lorentz fits to the spectra given in Ref. 58. As mentioned above, the hydrated electron's spectrum shifts by only $\sim$70 meV, without changing shape, in the presence of 5 m NaCl.[58] In previous

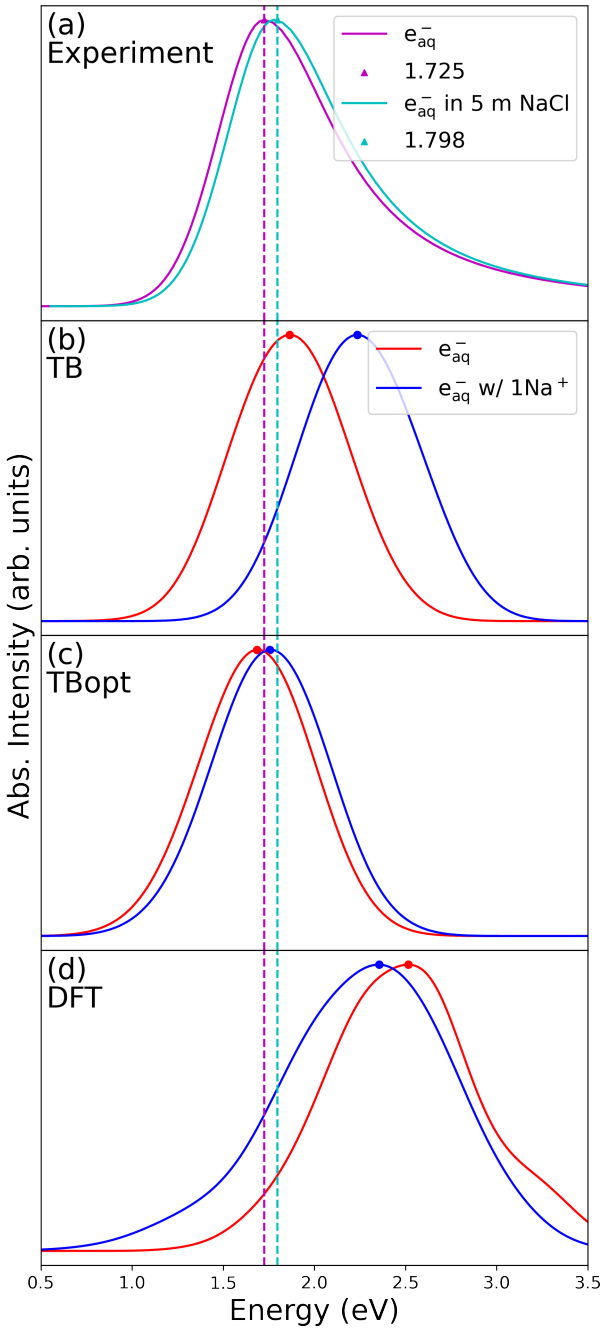

Figure 5.4: Absorption spectra of hydrated electrons in pure water and when in a contact pair with Na^+. Panel (a) shows the experimental absorption spectrum of the e^-_{aq} in pure water (magenta curve) and in 5 m NaCl solution (cyan curve), showing the ∼70 meV shift induced by the high-concentration electrolyte.[58] Panels (b), (c), and (d) show simulated absorption spectra of the TB, TBopt, and DFT e^-_{aq} models in pure water (red curves) and in the presence of a Na^+ at the equilibrium pairing distance (blue curves). The TB model overestimates the spectral blue shift because it makes a too tight e^-_{aq}–Na^+ contact pair,[64, 112] whereas the DFT model predicts that ion-pairing causes a spectral red shift, in disagreement with experiment, because the DFT e^-_{aq} is more kosmotropic than the DFT Na^+. The TBopt model, with its chaotropic hydration structure that leads to relatively weak e^-_{aq}–Na^+ contact pairing, predicts the correct magnitude of the spectral blue shift.

simulation work, we found that the TB e^-_{aq} pairs with multiple cations simultaneously at high salt concentrations, explaining why the spectral blue shift is concentration dependent. Due to the computational expense of DFT simulations, however, we have only a single Na^+ in the trajectories studied in this work, so our effective electrolyte concentration is smaller than 5 m. This means that our simulations should predict a smaller spectral blue shift, so that the ∼70 meV shift seen in Fig. 5.4(a) should be an upper limit.

Figure 5.4(b)-(d) shows the calculated spectroscopy of the three different hydrated electron models (red curves), along with the predicted spectroscopy of the different e^-_{aq}'s at their equilibrium distance in contact pairs with a Na^+ (blue curves). The details of how the absorption spectra are calculated are the same as in our previous work[56, 64, 65, 112] and are described in more detail in the SI. Figure 5.4(b) shows the calculated spectra for the TB e^-_{aq} model, which as we have discussed previously predicts a spectral blue shift that is an order of magnitude larger than that seen experimentally.[64, 112] The overly-large predicted spectral blue shift is a direct consequence of the fact that the cation and TB e^-_{aq} pair too tightly, and that the cation forces a significant reorientation of the water molecules in the hydrated electron's first solvation shell. The predicted spectrum in the presence of Na^+ is also slightly broader than that in pure water, a shape change that is also not seen experimentally.

Figure 5.4(d) shows the predicted spectroscopy of the e^-_{aq} in the presence of Na^+ from DFT-based ab initio simulations. The red curve shows that the spectrum of the DFT e^-_{aq} in pure water is blue-shifted from experiment by over 0.5 eV and has an incorrect spectral shape, as we have documented previously.[56] When the DFT hydrated electron is paired with Na^+, the calculated spectrum red-shifts by ∼160 meV, a shift that is not only too large but also which goes in the wrong direction compared to experiment; the calculated spectrum is also predicted to change shape, which again does not match what is seen experimentally.[58] As mentioned above, this spectral red-shift is a direct consequence of the fact that the DFT e^-_{aq} is more kosmotropic than the DFT Na^+, a result that is not consistent with the solvation entropy of the hydrated electron,[62, 63] as we will explore further below. Overall, the results indicate that the DFT e^-_{aq} simply has an incorrect hydration structure: neither the spectrum nor the VDE is correctly predicted,[56] and the ion-pairing behavior is opposite to what is seen experimentally.

On the other hand, Fig. 5.4(c) shows that for the TBopt model, the relative shift of the calculated

Table 5.1: Radius of gyration, direct overlap (Eq. 1) with water and Na^+, and VDE for the TB, TBopt, and DFT e^-_{aq} models both with and without an adjacent Na^+. In the absence of salt, the experimental radius of gyration is 2.45 Å,[44] and the experimental VDE is ∼3.5 eV.[16–19]

	Radius of Gyration (Å)	Water Direct Overlap (%)	Na^+ Direct Overlap (%)	VDE (eV)
TB	2.43 ± 0.11	3.3 ± 0.9	N/A	2.95 ± 0.33
TB + $1Na^+$	2.21 ± 0.07	2.1 ± 0.6	32.1 ± 7.2	3.61 ± 0.34
TBopt	2.56 ± 0.18	8.8 ± 1.5	N/A	3.84 ± 0.38
TBopt + $1Na^+$	2.50 ± 0.16	8.2 ± 1.7	15.3 ± 10.2	4.04 ± 0.39
DFT	2.35 ± 0.09	21.8 ± 2.2	N/A	2.14 ± 0.36
DFT + $1Na^+$	2.50 ± 0.18	15.5 ± 1.9	15.9 ± 6.3	3.85 ± 0.32

spectrum in the presence of Na^+ is almost identical with what is seen in experiment (both predicted spectra are slightly red-shifted from experiment, but the relative shift and lack of shape change match experiment within the simulation error). This is a direct consequence of the fact that the TBopt e^-_{aq} model has little change in either the water orientation or coordination number when paired with Na^+, as would be expected when a kosmotropic cation is weakly complexed with a highly chaotropic anion. Of course, the TBopt model is not perfect (as mentioned above, this model underestimates the red-shift of the e^-_{aq}'s spectrum with increasing temperature[97]), but the excellent agreement of its predicted ion-pairing with experiment suggests that the highly chaotropic hydration structure that this model yields is much more likely to be closer to 'correct' than either the TB or DFT e^-_{aq} models.

Clearly, even though all three models predict that the hydrated electron occupies a cavity in liquid water, not all cavity models are equivalent: the hydration structure of the electron is important to determining its interactions with other species in aqueous solution, such as pairing with Na^+. To understand why the different hydrated electron models yield different predicted spectral blue shifts when paired with Na^+, an in particular why the DFT e^-_{aq} solvation structure leads to a predicted ion-induced spectral shift that is too large and goes in the wrong direction, we have analyzed the electronic properties of the different hydrated electron models in Table 5.1. The first column summarizes the electron's radius of gyration. The second and third columns list the fraction of the electron's charge density (square of the SOMO in the DFT simulations) that lies on

top of either the surrounding water molecules or the paired Na^+ cation, Θ, calculated via:

$$\Theta = \Big\langle \sum_{i=1}^{n_{\text{molcs}}} 4\pi \int_0^{r_c} r_i^2 |\Psi(r_i)|^2 dr_i \Big\rangle, \tag{5.1}$$

where the angled brackets represent an ensemble average, Ψ is the normalized wavefunction or SOMO of the e^-_{aq}, the sum runs over all of the water molecules or the single cation, r_i is the distance between the electron's center of mass and either a water oxygen atom or the Na^+ cation, and r_c is a constant that roughly represents the size of either a water molecule or the Na^+ cation, here chosen to be 1.0 Å and 2.0 Å, respectively.[40] The final column shows the calculated vertical detachment energies (VDEs) extracted directly from the simulations, with no attempt to account for finite-size effects.[35, 56, 112]

Since the e^-_{aq} behaves roughly as a particle in a spherical box, the square of its radius of gyration should be inversely proportional to the peak of its absorption spectrum.[44] Experimentally, it is known from spectral moment analysis that the e^-_{aq}'s radius of gyration should be 2.45 Å,[44] and indeed, all three hydrated electron models predict radii of gyration in this general range. For the TB electron, the presence of Na^+ causes the radius of gyration to shrink by ∼10%. This occurs because the TB e^-_{aq} has a significant amount of overlap with the paired sodium cation, so that the system behaves as much like a solvated Na atom as a cation-perturbed hydrated electron (indeed, the TB e^-_{aq}/Na^+ overlap of 32% is almost as large as the ∼50% overlap that would be experienced by an electron on a neutral gas-phase Na atom, a process driven by the electron's hydration structure being strongly disrupted by the nearby cation).[64, 112] This is why the predicted ion-pairing spectral blue-shift is an order of magnitude too large, indicative of an incorrect hydration structure for the TB: the TB e^-_{aq} is slightly too kosmotropic.

In contrast, the TBopt model only shows a modest ∼2% decrease in radius of gyration, as the hydration structure of this e^-_{aq} model is not strongly affected by the presence of the nearby cation. The direct interaction of the TBopt hydrated electron with Na^+ is modest at only ∼15%, which when combined with the fact that the cation's and the electron's hydration structured are largely unchanged upon pairing, helps to leave the spectrum of the e^-_{aq} relatively unperturbed. All of this is because the first-shell waters can effectively solvate both the TBopt e^-_{aq} and the Na^+ at the same time, a result of the TBopt hydrated electron's structure being highly chaotropic and thus

fluxional.

In even further contrast, the radius of gyration of the DFT e^-_{aq} actually increases upon the addition of Na^+, commensurate with the (incorrectly) predicted spectral red-shift. The DFT hydrated electron has a ∼22% overlap with the surrounding water molecules,[99, 151] a value much higher than that seen with either of the two MQC e^-_{aq} models. When placed in contact with a sodium cation, the DFT electron's overlap with the first-shell waters decreases, largely because there are fewer waters in the first solvation shell. The DFT e^-_{aq} does pick up modest overlap with the Na^+, but unlike with the TBopt electron, the kosmotropic DFT electron perturbs the hydration structure of the cation. This perturbed solvation structure allows the spatial extent of the e^-_{aq}'s wavefunction to extend further beyond its original solvation cavity, increasing the radius of gyration. In other words, since the highly kosmotropic DFT e^-_{aq} has a strong preference for interacting with water, when Na^+ is nearby, the DFT hydrated electron reorients water molecules in the cation's hydration sphere by diffusing out and increasing its size, as also seen in the increase in the second solvation shell peak in Fig. 5.1(c).

Finally, Table 5.1 shows that the predicted VDE's of the TB[11] and TBopt[97] models are both within a few hundred meV of the experimental value of ∼3.5 eV;[16–19] the DFT model is off by well over an eV, as we have discussed previously.[56] When paired with Na^+, the TB model shows a significant increase in VDE of around 650 meV, a number that reflects a competition between the increased stabilization provided by overlap with the cation and the decreased stabilization caused by disruption of the e^-_{aq}'s hydration sphere. The DFT-based e^-_{aq} shows a much larger predicted increase in VDE of over 1700 meV, suggesting that it is stabilized by overlap with Na^+ without any compensating loss of hydration, as the kosmotropic structure of this hydrated electron model does not change upon ion-pairing. The TBopt model shows a very modest predicted change in VDE of only ∼200 meV, reflective of the little change in solvation structure around both species when paired. The VDE of hydrated electrons in the presence of electrolytes should be readily measurable experimentally, so these numbers serve as an additional prediction that will allow the solvation structures of the different e^-_{aq} models to be experimentally distinguished.

5.3 Conclusions

In summary, we have examined how different e^-_{aq} models with different hydration structures undergo ion pairing with Na^+. Since ion-pairing is directly controlled by the hydration structures of both ions,[61, 129, 146–150] we can use ion pairing to distinguish which model of the hydrated electron, if any, is consistent with the known experimental behavior of e^-_{aq}'s in aqueous electrolytes. The cavity-forming TB model shows strong pairing with Na^+, as evidenced by the deep PMF and the overly large predicted spectral blue shift, indicating that this model is somewhat too kosmotropic. The TBopt e^-_{aq}, which is the most chaotropic of the three models examined here, has a more weakly defined cavity and hydration structure that causes e^-_{aq}–Na^+ contact pair formation to be weak; this model predicts a spectral shift that is in reasonable agreement with experiment. But perhaps most importantly, the DFT hydrated electron model shows a strikingly strong kosmotropic hydration structure that does not fit with our expectations of hydrated electrons as champion chaotropes.[62, 63] The DFT e^-_{aq} is able to alter the hydration structure of the paired Na^+, leading to an erroneously predicted spectral red shift, a result of the fact that the DFT electron is actually more kosmotropic than DFT Na^+.

It is worth emphasizing that none of the three models that we have examined are able to reproduce all of the known experimental properties of the hydrated electron (e.g., the temperature dependence,[15, 43, 47, 56, 144] resonance Raman spectrum,[4, 15, 41] time-resolved photoelectron spectroscopy,[21, 42, 152], molar solvation volume,[45, 46], etc.). MQC models have the drawbacks that not only are they extraordinarily sensitive to the pseudopotential employed (including models that produce entirely non-cavity e^-_{aq} structures[13] as well as the TB and TBopt models explored here), but also that they cannot allow for mixing of the e^-_{aq}'s wave function into the molecular orbitals of the nearby water molecules, which is undoubtedly important to understanding their solvation and reactivity.[151] Our results show, however, that blindly moving towards ab initio simulations, at least those based on DFT, is not necessarily making any improvement. We note that several groups have developed machine learning potentials based on ab initio simulations,[144, 153] but since these potentials are based on DFT, these machine learning models still yield an incorrect hydration structure (in one case, a nonphysical 'double cavity'[153] structure) as well as incorrect VDEs and absorption spectra because the e^-_{aq} system they were trained on has an

incorrect hydration structure that is too kosmotropic.

Given that the DFT should constitute a higher-level theory compared than MQC, why does it fail so spectacularly for describing the hydration structure of the hydrated electron? We know that it is difficult to use DFT to generate the correct structure and dynamics of liquid water because DFT does a poor job accounting for dispersion and H-bonding interactions.[113, 154] Moreover, typical GGA functionals are prone to charge delocalization error, which can be particularly acute when trying to describe the properties of an excess electron that resides primarily between the water molecules. We believe that it is just too much to ask a single exchange-correlation functional to correctly describe the water intramolecular bonds, H-bonds, dispersion interactions and the properties of an excess electron that does not primarily reside in the water molecular orbitals.

Overall, we believe that it is certainly possible that a well-tweaked pseudopotential can produce an MQC-simulated e^-_{aq} with a hydration structure that is 'better' than DFT, although no MQC simulation will likely be able to fully describe the hydrated electron. Thus, until ab initio simulations based on levels of theory higher than DFT become within computational reach, we are left in a situation where we do not know the true hydration structure of the hydrated electron. Hopefully, experiments measuring the VDE of the e^-_{aq} in the presence of high salt concentrations can shed some light on this, as discussed above. The key point is that simulation models need to be tested in situations where small changes in the predicted hydration structure make large changes in the predicted observables, which is exactly the situation we have here. At the moment, based on ion-pairing, which is a highly sensitive measure of hydration structure, we conclude that the hydrated electron likely has a chaotropic structure that is more like the TBopt model and not at all like the kosmotropic structure that is seen with DFT.

5.4 Methods

Our methodology closely follows those in our previously-published DFT[56] and MQC-based[64, 65, 112, 145] simulations of the e^-_{aq}. For the DFT calculations, we used the CP2K software package[101] with the PBE0 functional[155] to run the molecular dynamics with 64 waters and one Na^+ for 15 ps after equilibration. To generate the absorption spectrum via TD-DFT calculations, we used the LRC-ωPBE functional, a range-separated version of the PBE0 functional, with an optimally

tuned range-separation parameter.[56, 112] This procedure mitigates the spurious charge-transfer excited states which are typically observed when using a hybrid functional,[35] and has been documented to produce the best absorption spectrum for the e^-_{aq} in previous work.[100] Since full TD-DFT calculations are not supported with periodic boundary conditions in CP2K, we converted the periodic configurations to non-periodic configurations by surrounding the simulation box with 26 mirror images containing water point charges and performed the TD-DFT calculations with the QChem package.[106] The procedures for MQC calculations are identical to our previous work, other than using the TBopt potential in place of the TB potential for some calculations.[64, 65, 112, 145] All the dynamics were run for at least 20 ps at room temperature in the canonical ensemble (N, V, T) using the Nose-Hoover chain thermostat to hold the temperature constant.[83] Additional simulation details are described in the Supporting Information (SI).

We note that it is tricky to generate e^-_{aq}–Na^+ PMFs, as it is not straightforward to restrain the e^-_{aq}–Na^+ distance since the hydrated electron is a quantum mechanical object represented by a wavefunction. Thus, we used a quantum umbrella sampling algorithm that we presented previously[124] and also used in our previous MQC simulations of ion-pairing with the TB potential.[64, 65, 112]. To generate the PMFs in this work, we ran a total of 17 simulation windows separated by 0.25 Å, and two more at longer distances separated by 0.5 Å, where each window was run for at least 20 ps. The force constant of the harmonic umbrella potential was set to be 1.5 eV/Å^2, and the data from each simulation window was connected into a PMF by the multi-state Bennet acceptance ratio method;[131] details are included in the SI. For the DFT-based hydrated electron model, quantum umbrella sampling was not possible due to the computational expense, so we estimated the PMF by binning the observed e^-_{aq}–Na^+ distances over our 15-ps trajectory then taking the negative natural logarithm.

Appendix

All the codes and data can be found in both the blue Toshiba external hard drive in the office and in the group NAS.

- Chapter 2 materials include minimalist model trajectories with 4 and 16 waters and data analysis code. This can be found in the directory named 'PCM_hydrated_electron'. Please refer to the README file for detailed instruction on how to run the code.

  The 4 water trajectory is in 'trj/pcm_4' directory

  The 16 water trajectory is in 'trj/pcm_16' directory

  Data analysis codes are in 'pcm_data_codes' directory

- Chapter 3 materials include AIMD trajectories with 47, 64, and 128 waters at 298 K, 350K, and 375K, TD-DFT calculations, and data analysis code. This can be found in the directory named 'AIMD_hydrated_electron'. Please refer to the README file for detailed instruction on how to run the code.

  The 47 water 298 K trajectory is in 'trj/47_298K_trj_4' directory

  The 64 water 298 K trajectory is in 'trj/64_298K_trj_4' directory

  The 64 water 350 K trajectory is in 'trj/64_350K_trj_4' directory

  The 64 water 375 K trajectory is in 'trj/64_375K_trj_4' directory

  The 128 water 298 K trajectory is in 'trj/128_298K_trj_4' directory

  The TD-DFT data is in 'abs' directory

  Data analysis codes are in 'abs/analysis' directory

- Chapter 4 materials include umbrella sampling trajectories for the TB model with and without Na^+ using three different LJ potentials and data analysis code. This can be found in the directory named 'LJ_hydrated_electron_Na'. Please refer to the README file for detailed instruction on how to run the code.

  The umbrella run using the Dang parameter is in 'Dang' directory

  The umbrella run using the Koneshan parameter is in 'Koneshan' directory

  The umbrella run using the Aqvist parameter is in 'Aqvist' directory

  Data analysis codes are in 'analysis' directory

- Chapter 5 materials include AIMD trajectories with 64 waters and a single Na^+, TD-DFT calculations, and data analysis code. This can be found in the directory named 'AIMD_Na'. Please refer to the README file for detailed instruction on how to run the code.

  The 64 water + 1 Na^+ hydrated electron trajectory is in '64_1Na_298K' directory

  The TD-DFT data is in 'abs' directory

  Data analysis codes are in 'abs/analysis' directory

Bibliography

(1) Yost, D. M.; Russell, H., et al. Systematic inorganic chemistry of the fifth-and-sixth-group nonmetallic elements. **1944**.

(2) Douthit, R. C.; Dye, J. L. Absorption Spectra of Sodium and Potassium in Liquid Ammonia1a. *Journal of the American Chemical Society* **1960**, *82*, 4472–4478.

(3) Hart, E. J.; Boag, J. Absorption spectrum of the hydrated electron in water and in aqueous solutions. *Journal of the American Chemical Society* **1962**, *84*, 4090–4095.

(4) Tauber, M. J.; Mathies, R. A. Resonance Raman spectra and vibronic analysis of the aqueous solvated electron. *Chemical Physics Letters* **2002**, *354*, 518–526.

(5) Garrett, B. C.; Dixon, D. A.; Camaioni, D. M.; Chipman, D. M.; Johnson, M. A.; Jonah, C. D.; Kimmel, G. A.; Miller, J. H.; Rescigno, T. N.; Rossky, P. J. Role of water in electron-initiated processes and radical chemistry: Issues and scientific advances. *Chemical Reviews* **2005**, *105*, 355–390.

(6) Barbara, P. F.; Meyer, T. J.; Ratner, M. A. Contemporary issues in electron transfer research. *The Journal of Physical Chemistry* **1996**, *100*, 13148–13168.

(7) Davies, M. J.; Truscott, R. J. Photo-oxidation of proteins and its role in cataractogenesis. *Journal of Photochemistry and Photobiology B: Biology* **2001**, *63*, 114–125.

(8) Gu, J.; Leszczynski, J.; Schaefer III, H. F. Interactions of electrons with bare and hydrated biomolecules: From nucleic acid bases to DNA segments. *Chemical Reviews* **2012**, *112*, 5603–5640.

(9) Kerzig, C.; Guo, X.; Wenger, O. S. Unexpected hydrated electron source for preparative visible-light driven photoredox catalysis. *Journal of the American Chemical Society* **2019**, *141*, 2122–2127.

(10) Jou, F.-Y.; Freeman, G. R. Temperature and isotope effects on the shape of the optical absorption spectrum of solvated electrons in water. *Journal of Physical Chemistry* **1979**, *83*, 2383–2387.

(11) Turi, L.; Borgis, D. Analytical investigations of an electron–water molecule pseudopotential. II. Development of a new pair potential and molecular dynamics simulations. *The Journal of Chemical Physics* **2002**, *117*, 6186–6195.

(12) Jacobson, L. D.; Herbert, J. M. A one-electron model for the aqueous electron that includes many-body electron-water polarization: Bulk equilibrium structure, vertical electron binding energy, and optical absorption spectrum. *The Journal of Chemical Physics* **2010**, *133*, 154506.

(13) Larsen, R. E.; Glover, W. J.; Schwartz, B. J. Does the hydrated electron occupy a cavity? *Science* **2010**, *329*, 65–69.

(14) Jacobson, L. D.; Herbert, J. M. Polarization-bound quasi-continuum states are responsible for the "blue tail" in the optical absorption spectrum of the aqueous electron. *Journal of the American Chemical Society* **2010**, *132*, 10000–10002.

(15) Casey, J. R.; Larsen, R. E.; Schwartz, B. J. Resonance Raman and temperature-dependent electronic absorption spectra of cavity and noncavity models of the hydrated electron. *Proceedings of the National Academy of Sciences* **2013**, *110*, 2712–2717.

(16) Shreve, A. T.; Yen, T. A.; Neumark, D. M. Photoelectron spectroscopy of hydrated electrons. *Chemical Physics Letters* **2010**, *493*, 216–219.

(17) Siefermann, K. R.; Liu, Y.; Lugovoy, E.; Link, O.; Faubel, M.; Buck, U.; Winter, B.; Abel, B. Binding energies, lifetimes and implications of bulk and interface solvated electrons in water. *Nature Chemistry* **2010**, *2*, 274.

(18) Horio, T.; Shen, H.; Adachi, S.; Suzuki, T. Photoelectron spectra of solvated electrons in bulk water, methanol, and ethanol. *Chemical Physics Letters* **2012**, *535*, 12–16.

(19) Luckhaus, D.; Yamamoto, Y.; Suzuki, T.; Signorell, R. Genuine binding energy of the hydrated electron. *Science Advances* **2017**, *3*, e1603224.

(20) Lübcke, A.; Buchner, F.; Heine, N.; Hertel, I. V.; Schultz, T. Time-resolved photoelectron spectroscopy of solvated electrons in aqueous NaI solution. *Physical Chemistry Chemical Physics* **2010**, *12*, 14629–14634.

(21) Elkins, M. H.; Williams, H. L.; Shreve, A. T.; Neumark, D. M. Relaxation mechanism of the hydrated electron. *Science* **2013**, *342*, 1496–1499.

(22) Elkins, M. H.; Williams, H. L.; Neumark, D. M. Isotope effect on hydrated electron relaxation dynamics studied with time-resolved liquid jet photoelectron spectroscopy. *The Journal of Chemical Physics* **2016**, *144*, 184503.

(23) Baltuška, A.; Emde, M. F.; Pshenichnikov, M. S.; Wiersma, D. A. Early-time dynamics of the photoexcited hydrated electron. *The Journal of Physical Chemistry A* **1999**, *103*, 10065–10082.

(24) Assel, M.; Laenen, R.; Laubereau, A. Femtosecond solvation dynamics of solvated electrons in neat water. *Chemical Physics Letters* **2000**, *317*, 13–22.

(25) Karashima, S.; Yamamoto, Y.-i.; Suzuki, T. Resolving nonadiabatic dynamics of hydrated electrons using ultrafast photoemission anisotropy. *Physical Review Letters* **2016**, *116*, 137601.

(26) Farr, E. P.; Zho, C.-C.; Challa, J. R.; Schwartz, B. J. Temperature dependence of the hydrated electron's excited-state relaxation. II. Elucidating the relaxation mechanism through ultrafast transient absorption and stimulated emission spectroscopy. *The Journal of Chemical Physics* **2017**, *147*, 074504.

(27) Neupane, P.; Katiyar, A.; Bartels, D. M.; Thompson, W. H. Investigation of the Failure of Marcus Theory for Hydrated Electron Reactions. *The Journal of Physical Chemistry Letters* **2022**, *13*, 8971–8977.

(28) Marcus, R. Theory of electron-transfer reaction rates of solvated electrons. *The Journal of Chemical Physics* **1965**, *43*, 3477–3489.

(29) Cline, J.; Takahashi, K.; Marin, T. W.; Jonah, C. D.; Bartels, D. M. Pulse radiolysis of supercritical water. 1. Reactions between hydrophobic and anionic species. *The Journal of Physical Chemistry A* **2002**, *106*, 12260–12269.

(30) Marin, T. W.; Cline, J. A.; Takahashi, K.; Bartels, D. M.; Jonah, C. D. Pulse radiolysis of supercritical water. 2. Reaction of nitrobenzene with hydrated electrons and hydroxyl radicals. *The Journal of Physical Chemistry A* **2002**, *106*, 12270–12279.

(31) Lisovskaya, A.; Bartels, D. M. Reduction of CO2 by hydrated electrons in high temperature water. *Radiation Physics and Chemistry* **2019**, *158*, 61–63.

(32) Schnitker, J.; Rossky, P. J. Quantum simulation study of the hydrated electron. *The Journal of Chemical Physics* **1987**, *86*, 3471–3485.

(33) Larsen, R. E.; Glover, W. J.; Schwartz, B. J. Does the hydrated electron occupy a cavity? *Science* **2010**, *329*, 65–69.

(34) Uhlig, F.; Marsalek, O.; Jungwirth, P. Unraveling the complex nature of the hydrated electron. *The Journal of Physical Chemistry Letters* **2012**, *3*, 3071–3075.

(35) Ambrosio, F.; Miceli, G.; Pasquarello, A. Electronic levels of excess electrons in liquid water. *The Journal of Physical Chemistry Letters* **2017**, *8*, 2055–2059.

(36) Wilhelm, J.; VandeVondele, J.; Rybkin, V. V. Dynamics of the Bulk Hydrated Electron from Many-Body Wave-Function Theory. *Angewandte Chemie International Edition* **2019**, *58*, 3890–3893.

(37) Toukan, K.; Rahman, A. Molecular-dynamics study of atomic motions in water. *Physical Review B* **1985**, *31*, 2643.

(38) Smallwood, C. J.; Larsen, R. E.; Glover, W. J.; Schwartz, B. J. A computationally efficient exact pseudopotential method. I. Analytic reformulation of the Phillips-Kleinman theory. *The Journal of Chemical Physics* **2006**, *125*, 074102.

(39) Larsen, R. E.; Glover, W. J.; Schwartz, B. J. Comment on "An electron-water pseudopotential for condensed phase simulation"[J. Chem. Phys. 86, 3462 (1987)]. *The Journal of chemical physics* **2009**, *131*, 037101.

(40) Casey, J. R.; Kahros, A.; Schwartz, B. J. To be or not to be in a cavity: the hydrated electron dilemma. *The Journal of Physical Chemistry B* **2013**, *117*, 14173–14182.

(41) Dasgupta, S.; Rana, B.; Herbert, J. M. Ab initio investigation of the resonance Raman spectrum of the hydrated electron. *The Journal of Physical Chemistry B* **2019**, *123*, 8074–8085.

(42) Zho, C.-C.; Schwartz, B. J. Time-resolved photoelectron spectroscopy of the hydrated electron: Comparing cavity and noncavity models to experiment. *The Journal of Physical Chemistry B* **2016**, *120*, 12604–12614.

(43) Zho, C.-C.; Farr, E. P.; Glover, W. J.; Schwartz, B. J. Temperature dependence of the hydrated electron's excited-state relaxation. I. Simulation predictions of resonance Raman and pump-probe transient absorption spectra of cavity and non-cavity models. *The Journal of Chemical Physics* **2017**, *147*, 074503.

(44) Bartels, D. M. Moment analysis of hydrated electron cluster spectra: Surface or internal states? *The Journal of Chemical Physics* **2001**, *115*, 4404–4405.

(45) Casey, J. R.; Schwartz, B. J.; Glover, W. J. Free energies of cavity and noncavity hydrated electrons near the instantaneous air/water interface. *The Journal of Physical Chemistry Letters* **2016**, *7*, 3192–3198.

(46) Janik, I.; Lisovskaya, A.; Bartels, D. M. Partial Molar Volume of the Hydrated Electron. *The Journal of Physical Chemistry Letters* **2019**, *10*, 2220–2226.

(47) Bartels, D. M.; Takahashi, K.; Cline, J. A.; Marin, T. W.; Jonah, C. D. Pulse radiolysis of supercritical water. 3. Spectrum and thermodynamics of the hydrated electron. *The Journal of Physical Chemistry A* **2005**, *109*, 1299–1307.

(48) Du, Y.; Price, E.; Bartels, D. M. Solvated electron spectrum in supercooled water and ice. *Chemical Physics Letters* **2007**, *438*, 234–237.

(49) Sobolewski, A. L.; Domcke, W. Hydrated hydronium: a cluster model of the solvated electron? *Physical Chemistry Chemical Physics* **2002**, *4*, 4–10.

(50) Shkrob, I. A. The structure of the hydrated electron. Part 1. Magnetic resonance of internally trapping water anions: a density functional theory study. *The Journal of Physical Chemistry A* **2007**, *111*, 5223–5231.

(51) Shkrob, I. A.; Glover, W. J.; Larsen, R. E.; Schwartz, B. J. The structure of the hydrated electron. Part 2. A mixed quantum/classical molecular dynamics embedded cluster density functional theory: single- excitation configuration interaction study. *The Journal of Physical Chemistry A* **2007**, *111*, 5232–5243.

(52) Kumar, A.; Walker, J. A.; Bartels, D. M.; Sevilla, M. D. A simple ab initio model for the hydrated electron that matches experiment. *The Journal of Physical Chemistry A* **2015**, *119*, 9148–9159.

(53) Kumar, A.; Walker, J. A.; Bartels, D. M.; Sevilla, M. D. A simple ab initio model for the hydrated electron that matches experiment. *The Journal of Physical Chemistry A* **2015**, *119*, 9148–9159.

(54) Uhlig, F.; Marsalek, O.; Jungwirth, P. Unraveling the complex nature of the hydrated electron. *The Journal of Physical Chemistry Letters* **2012**, *3*, 3071–3075.

(55) Wilhelm, J.; VandeVondele, J.; Rybkin, V. V. Dynamics of the Bulk Hydrated Electron from Many-Body Wave-Function Theory. `https://archive.materialscloud.org/record/2019.0022/v1`.

(56) Park, S. J.; Schwartz, B. J. Understanding the Temperature Dependence and Finite Size Effects in Ab Initio MD Simulations of the Hydrated Electron. *The Journal of Chemical Theory and Computation* **2022**, *18*, 4973–4982.

(57) Asaad, A.; Chandrasekhar, N.; Nashed, A.; Krebs, P. Is there any effect of solution microstructure on the solvated electron absorption spectrum in LiCl/H2O solutions? *The Journal of Physical Chemistry A* **1999**, *103*, 6339–6343.

(58) Bonin, J.; Lampre, I.; Mostafavi, M. Absorption spectrum of the hydrated electron paired with nonreactive metal cations. *Radiation Physics and Chemistry* **2005**, *74*, 288–296.

(59) Kumagai, Y.; Lin, M.; Lampre, I.; Mostafavi, M.; Muroya, Y.; Katsumura, Y. Temperature effect on the absorption spectrum of the hydrated electron paired with a metallic cation in deuterated water. *Radiation Physics and Chemistry* **2008**, *77*, 1198–1202.

(60) Coudert, F.-X.; Archirel, P.; Boutin, A. Molecular Dynamics Simulations of Electron- Alkali Cation Pairs in Bulk Water. *The Journal of Physical Chemistry B* **2006**, *110*, 607–615.

(61) Hofmeister, F. Zur Lehre von der Wirkung der Salze. *Arch. für Exp. Pathol. und Pharmakologie* **1888**, *25*, 1–30.

(62) Han, P.; Bartels, D. M. Reevaluation of Arrhenius parameters for hydrogen atom + hydroxide → (e-)aq + water and the enthalpy and entropy of hydrated electrons. *Journal of Physical Chemistry* **1990**, *94*, 7294–7299.

(63) Han, P.; Bartels, D. On the hydrated electron as a structure-breaking ion. *The Journal of Physical Chemistry* **1991**, *95*, 5367–5370.

(64) Narvaez, W. A.; Park, S. J.; Schwartz, B. J. Hydrated Electrons in High-Concentration Electrolytes Interact with Multiple Cations: A Simulation Study. *The Journal of Physical Chemistry B* **2022**, *126*, 3748–3757.

(65) Narvaez, W. A.; Park, S. J.; Schwartz, B. J. Competitive Ion Pairing and the Role of Anions in the Behavior of Hydrated Electrons in Electrolytes. *The Journal of Physical Chemistry B* **2022**.

(66) Casey, J. R.; Kahros, A.; Schwartz, B. J. To be or not to be in a cavity: the hydrated electron dilemma. *The Journal of Physical Chemistry B* **2013**, *117*, 14173–14182.

(67) Herbert, J. M. Structure of the aqueous electron. *Physical Chemistry Chemical Physics* **2019**, *21*, 20538–20565.

(68) Rossky, P. J.; Schnitker, J. The hydrated electron: Quantum simulation of structure, spectroscopy, and dynamics. *The Journal of Physical Chemistry* **1988**, *92*, 4277–4285.

(69) Turi, L.; Gaigeot, M.-P.; Levy, N.; Borgis, D. Analytical investigations of an electron–water molecule pseudopotential. I. Exact calculations on a model system. *The Journal of Chemical Physics* **2001**, *114*, 7805–7815.

(70) Pizzochero, M.; Ambrosio, F.; Pasquarello, A. Picture of the wet electron: a localized transient state in liquid water. *Chemical Science* **2019**, *10*, 7442–7448.

(71) Schlick, S.; Narayana, P.; Kevan, L. ESR line shape studies of trapped electrons in γ-irradiated 17O enriched 10 M NaOH alkaline ice glass: Model for the geometrical structure of the trapped electron. *The Journal of Chemical Physics* **1976**, *64*, 3153–3160.

(72) Herbert, J. M.; Jacobson, L. D. Structure of the aqueous electron: Assessment of one-electron pseudopotential models in comparison to experimental data and time-dependent density functional theory. *The Journal of Physical Chemistry A* **2011**, *115*, 14470–14483.

(73) Cavanagh, M. C.; Martini, I. B.; Schwartz, B. J. Revisiting the pump–probe polarized transient hole-burning of the hydrated electron: Is its absorption spectrum inhomogeneously broadened? *Chemical Physics Letters* **2004**, *396*, 359–366.

(74) Kevan, L. Solvated electron structure in glassy matrixes. *Accounts of Chemical Research* **1981**, *14*, 138–145.

(75) Kumar, A.; Adhikary, A.; Shamoun, L.; Sevilla, M. D. Do solvated electrons (eaq–) reduce DNA bases? A Gaussian 4 and density functional theory-Molecular dynamics study. *The Journal of Physical Chemistry B* **2016**, *120*, 2115–2123.

(76) Zho, C.-C.; Vlček, V.; Neuhauser, D.; Schwartz, B. J. Thermal Equilibration Controls H-Bonding and the Vertical Detachment Energy of Water Cluster Anions. *The Journal of Physical Chemistry Letters* **2018**, *9*, 5173–5178.

(77) Smith, D. M.; Smets, J.; Elkadi, Y.; Adamowicz, L. Ab initio theoretical study of dipole–bound anions of molecular complexes: Water tetramer anions. *The Journal of Chemical Physics* **1998**, *109*, 1238–1244.

(78) Verlet, J.; Bragg, A.; Kammrath, A.; Cheshnovsky, O.; Neumark, D. Observation of large water-cluster anions with surface-bound excess electrons. *Science* **2005**, *307*, 93–96.

(79) Young, R. M.; Neumark, D. M. Dynamics of solvated electrons in clusters. *Chemical Reviews* **2012**, *112*, 5553–5577.

(80) Kong, J.; White, C. A.; Krylov, A. I.; Sherrill, D.; Adamson, R. D.; Furlani, T. R.; Lee, M. S.; Lee, A. M.; Gwaltney, S. R.; Adams, T. R.; et al. Q-Chem 2.0: a high-performance ab initio electronic structure program package. *The Journal of Computational Chemistry* **2000**, *21*, 1532–1548.

(81) Cances, E.; Mennucci, B.; Tomasi, J. A new integral equation formalism for the polarizable continuum model: Theoretical background and applications to isotropic and anisotropic dielectrics. *The Journal of Chemical Physics* **1997**, *107*, 3032–3041.

(82) You, Z.-Q.; Mewes, J.-M.; Dreuw, A.; Herbert, J. M. Comparison of the Marcus and Pekar partitions in the context of non-equilibrium, polarizable-continuum solvation models. *The Journal of Chemical Physics* **2015**, *143*, 204104.

(83) Martyna, G. J.; Klein, M. L.; Tuckerman, M. Nosé–Hoover chains: The canonical ensemble via continuous dynamics. *The Journal of Chemical Physics* **1992**, *97*, 2635–2643.

(84) Humphrey, W.; Dalke, A.; Schulten, K. VMD: visual molecular dynamics. *Journal of Molecular Graphics* **1996**, *14*, 33–38.

(85) Baer, R.; Neuhauser, D. Density functional theory with correct long-range asymptotic behavior. *Physical Review Letters* **2005**, *94*, 043002.

(86) Baer, R.; Livshits, E.; Salzner, U. Tuned range-separated hybrids in density functional theory. *Annual Review of Physical Chemistry* **2010**, *61*, 85–109.

(87) Janak, J. F. Proof that ∂ e / ∂ ni = ε in density-functional theory. *Physical Review B* **1978**, *18*, 7165.

(88) Glover, W. J.; Schwartz, B. J. The fluxional nature of the hydrated electron: Energy and entropy contributions to aqueous electron free energies. *Journal of Chemical Theory and Computation* **2020**, *16*, 1263–1270.

(89) Liu, K.; Cruzan, J.; Saykally, R. Water clusters. *Science* **1996**, *271*, 929–933.

(90) Rudnick, J.; Gaspari, G. The asphericity of random walks. *Journal of Physics A: Mathematical and General* **1986**, *19*, L191.

(91) Corcelli, S.; Lawrence, C.; Skinner, J. Combined electronic structure/molecular dynamics approach for ultrafast infrared spectroscopy of dilute HOD in liquid H2O and D2O. *The Journal of Chemical Physics* **2004**, *120*, 8107–8117.

(92) Corcelli, S.; Skinner, J. Infrared and Raman line shapes of dilute HOD in liquid H2O and D2O from 10 to 90 C. *The Journal of Physical Chemistry A* **2005**, *109*, 6154–6165.

(93) Auer, B.; Kumar, R.; Schmidt, J.; Skinner, J. Hydrogen bonding and Raman, IR, and 2D-IR spectroscopy of dilute HOD in liquid D2O. *Proceedings of the National Academy of Sciences* **2007**, *104*, 14215–14220.

(94) Woodcock, H. L.; Zheng, W.; Ghysels, A.; Shao, Y.; Kong, J.; Brooks, B. R. Vibrational subsystem analysis: A method for probing free energies and correlations in the harmonic limit. *The Journal of Chemical Physics* **2008**, *129*, 12B603.

(95) Cossi, M.; Rega, N.; Scalmani, G.; Barone, V. Energies, structures, and electronic properties of molecules in solution with the C-PCM solvation model. *Journal of Computational Chemistry* **2003**, *24*, 669–681.

(96) Ma, L.; Majer, K.; Chirot, F.; von Issendorff, B. Low temperature photoelectron spectra of water cluster anions. *The Journal of Chemical Physics* **2009**, *131*, 144303.

(97) Glover, W. J.; Schwartz, B. J. Short-range electron correlation stabilizes noncavity solvation of the hydrated electron. *The Journal of Chemical Theory and Computation* **2016**, *12*, 5117–5131.

(98) Borsarelli, C. D.; Bertolotti, S. G.; Previtali, C. M. Thermodynamic changes associated with the formation of the hydrated electron after photoionization of inorganic anions: a time-resolved photoacoustic study. *Photochemical & Photobiological Sciences* **2003**, *2*, 791–795.

(99) Shen, Z.; Peng, S.; Glover, W. J. Flexible boundary layer using exchange for embedding theories. II. QM/MM dynamics of the hydrated electron. *The Journal of Chemical Physics* **2021**, *155*, 224113.

(100) Uhlig, F.; Herbert, J. M.; Coons, M. P.; Jungwirth, P. Optical spectroscopy of the bulk and interfacial hydrated electron from ab initio calculations. *The Journal of Physical Chemistry A* **2014**, *118*, 7507–7515.

(101) Hutter, J.; Iannuzzi, M.; Schiffmann, F.; VandeVondele, J. cp2k: atomistic simulations of condensed matter systems. *Wiley Interdisciplinary Reviews: Computational Molecular Science* **2014**, *4*, 15–25.

(102) Grimme, S.; Antony, J.; Ehrlich, S.; Krieg, H. A consistent and accurate ab initio parametrization of density functional dispersion correction (DFT-D) for the 94 elements H-Pu. *The Journal of Chemical Physics* **2010**, *132*, 154104.

(103) Goedecker, S.; Teter, M.; Hutter, J. Separable dual-space Gaussian pseudopotentials. *Physical Review B* **1996**, *54*, 1703.

(104) Guidon, M.; Hutter, J.; VandeVondele, J. Auxiliary density matrix methods for Hartree-Fock exchange calculations. *The Journal of Chemical Theory and Computation* **2010**, *6*, 2348–2364.

(105) Nicolas, C.; Boutin, A.; Lévy, B.; Borgis, D. Molecular simulation of a hydrated electron at different thermodynamic state points. *The Journal of Chemical Physics* **2003**, *118*, 9689–9696.

(106) Shao, Y.; Gan, Z.; Epifanovsky, E.; Gilbert, A. T.; Wormit, M.; Kussmann, J.; Lange, A. W.; Behn, A.; Deng, J.; Feng, X., et al. Advances in molecular quantum chemistry contained in the Q-Chem 4 program package. *Molecular Physics* **2015**, *113*, 184–215.

(107) Marsalek, O.; Uhlig, F.; Frigato, T.; Schmidt, B.; Jungwirth, P. Dynamics of electron localization in warm versus cold water clusters. *Physical Review Letters* **2010**, *105*, 043002.

(108) Frigato, T.; VandeVondele, J.; Schmidt, B.; Schütte, C.; Jungwirth, P. Ab initio molecular dynamics simulation of a medium-sized water cluster anion: From an interior to a surface-located excess electron via a delocalized state. *The Journal of Physical Chemistry A* **2008**, *112*, 6125–6133.

(109) Park, S. J.; Schwartz, B. J. Evaluating Simple Ab Initio Models of the Hydrated Electron: The Role of Dynamical Fluctuations. *The Journal of Physical Chemistry B* **2020**, *124*, 9592–9603.

(110) Ambrosio, F.; Miceli, G.; Pasquarello, A. Redox levels in aqueous solution: Effect of van der Waals interactions and hybrid functionals. *The Journal of Chemical Physics* **2015**, *143*, 244508.

(111) Hart, E. J.; Boag, J. W. Absorption spectrum of the hydrated electron in water and in aqueous solutions. *Journal of the American Chemical Society* **1962**, *84*, 4090–4095.

(112) Park, S. J.; Narvaez, W. A.; Schwartz, B. J. How Water–Ion Interactions Control the Formation of Hydrated Electron: Sodium Cation Contact Pairs. *The Journal of Physical Chemistry B* **2021**, *125*, 13027–13040.

(113) Gillan, M. J.; Alfè, D.; Michaelides, A. Perspective: How good is DFT for water? *The Journal of Chemical Physics* **2016**, *144*, 130901.

(114) Willow, S. Y.; Zeng, X. C.; Xantheas, S. S.; Kim, K. S.; Hirata, S. Why is MP2-water "cooler" and "denser" than DFT-water? *The Journal of Physical Chemistry Letters* **2016**, *7*, 680–684.

(115) Fessenden, R. W.; Verma, N. Time resolved electron spin resonance spectroscopy. III. Electron spin resonance emission from the hydrated electron. Possible evidence for reaction to the triplet state. *Journal of the American Chemical Society* **1976**, *98*, 243–244.

(116) Shiraishi, H.; Ishigure, K.; Morokuma, K. An ESR study on solvated electrons in water and alcohols: difference in the g factor and related analysis of the electronic state by MO calculation. *The Journal of Chemical Physics* **1988**, *88*, 4637–4649.

(117) Hare, P. M.; Price, E. A.; Stanisky, C. M.; Janik, I.; Bartels, D. M. Solvated electron extinction coefficient and oscillator strength in high temperature water. *The Journal of Physical Chemistry A* **2010**, *114*, 1766–1775.

(118) Spezia, R.; Nicolas, C.; Archirel, P.; Boutin, A. Molecular dynamics simulations of the Ag+ or Na+ cation with an excess electron in bulk water. *The Journal of Chemical Physics* **2004**, *120*, 5261–5268.

(119) Johnson, E. R.; Otero-De-La-Roza, A.; Dale, S. G. Extreme density-driven delocalization error for a model solvated-electron system. *The Journal of Chemical Physics* **2013**, *139*, 184116.

(120) Tay, K. A.; Coudert, F.-X.; Boutin, A. Mechanism and kinetics of hydrated electron diffusion. *The Journal of Chemical Physics* **2008**, *129*, 054505.

(121) Borgis, D.; Staib, A. Quantum adiabatic umbrella sampling: The excited state free energy surface of an electron-atom pair in solution. *The Journal of Chemical Physics* **1996**, *104*, 4776–4783.

(122) Glover, W. J.; Larsen, R. E.; Schwartz, B. J. The roles of electronic exchange and correlation in charge-transfer-to-solvent dynamics: Many-electron nonadiabatic mixed quantum/classical simulations of photoexcited sodium anions in the condensed phase. *The Journal of Chemical Physics* **2008**, *129*, 164505.

(123) Durand, P.; Barthelat, J.-C. A theoretical method to determine atomic pseudopotentials for electronic structure calculations of molecules and solids. *Theoretica Chimica Acta* **1975**, *38*, 283–302.

(124) Glover, W. J.; Casey, J. R.; Schwartz, B. J. Free energies of quantum particles: The coupled-perturbed quantum umbrella sampling method. *Journal of Chemical Theory and Computation* **2014**, *10*, 4661–4671.

(125) Verlet, L. Computer "experiments" on classical fluids. I. Thermodynamical properties of Lennard-Jones molecules. *Physical Review* **1967**, *159*, 98.

(126) Feynman, R. P. Forces in molecules. *Physical Review* **1939**, *56*, 340.

(127) Dang, L. X.; Smith, D. E. Molecular dynamics simulations of aqueous ionic clusters using polarizable water. *The Journal of Chemical Physics* **1993**, *99*, 6950–6956.

(128) Koneshan, S.; Rasaiah, J. C. Computer simulation studies of aqueous sodium chloride solutions at 298 K and 683 K. *The Journal of Chemical Physics* **2000**, *113*, 8125–8137.

(129) Pettitt, B. M.; Rossky, P. J. Alkali halides in water: Ion–solvent correlations and ion–ion potentials of mean force at infinite dilution. *The Journal of Chemical Physics* **1986**, *84*, 5836–5844.

(130) Aqvist, J. Ion-water interaction potentials derived from free energy perturbation simulations. *The Journal of Physical Chemistry* **1990**, *94*, 8021–8024.

(131) Shirts, M. R.; Chodera, J. D. Statistically optimal analysis of samples from multiple equilibrium states. *The Journal of Chemical Physics* **2008**, *129*, 124105.

(132) Sauer, M. C.; Shkrob, I. A.; Lian, R.; Crowell, R. A.; Bartels, D. M.; Chen, X.; Suffern, D.; Bradforth, S. E. Electron photodetachment from aqueous anions. 2. Ionic strength effect on geminate recombination dynamics and quantum yield for hydrated electron. *The Journal of Physical Chemistry A* **2004**, *108*, 10414–10425.

(133) Renou, F.; Mostafavi, M.; Archirel, P.; Bonazzola, L.; Pernot, P. Solvated electron pairing with earth alkaline metals in THF. 1. Formation and structure of the pair with divalent Magnesium. *The Journal of Physical Chemistry A* **2003**, *107*, 1506–1516.

(134) Rutherford, A.; Duffy, D. The effect of electron–ion interactions on radiation damage simulations. *Journal of Physics: Condensed Matter* **2007**, *19*, 496201.

(135) Savéant, J.-M. Effect of ion pairing on the mechanism and rate of electron transfer. Electrochemical aspects. *The Journal of Physical Chemistry B* **2001**, *105*, 8995–9001.

(136) Cavanagh, M. C.; Larsen, R. E.; Schwartz, B. J. Watching Na Atoms Solvate into (Na+, e-) Contact Pairs: Untangling the Ultrafast Charge-Transfer-to-Solvent Dynamics of Na-in Tetrahydrofuran (THF). *The Journal of Physical Chemistry A* **2007**, *111*, 5144–5157.

(137) Glover, W. J.; Larsen, R. E.; Schwartz, B. J. First principles multielectron mixed quantum/classical simulations in the condensed phase. II. The charge-transfer-to-solvent states of sodium anions in liquid tetrahydrofuran. *The Journal of Chemical Physics* **2010**, *132*, 144102.

(138) Widmer, D. R.; Schwartz, B. J. The role of the solvent in the condensed-phase dynamics and identity of chemical bonds: The case of the sodium dimer cation in THF. *The Journal of Physical Chemistry B* **2020**, *124*, 6603–6616.

(139) Vong, A.; Widmer, D. R.; Schwartz, B. J. Nonequilibrium Solvent Effects during Photodissociation in Liquids: Dynamical Energy Surfaces, Caging, and Chemical Identity. *The Journal of Physical Chemistry Letters* **2020**, *11*, 9230–9238.

(140) Garrett, B. C.; Dixon, D. A.; Camaioni, D. M.; Chipman, D. M.; Johnson, M. A.; Jonah, C. D.; Kimmel, G. A.; Miller, J. H.; Rescigno, T. N.; Rossky, P. J., et al. Role of water in electron-initiated processes and radical chemistry: Issues and scientific advances. *Chemical Reviews* **2004**, *105*, 355–390.

(141) Andrieux, C. P.; Saveant, J. M. The origin of leaving-group effects in radical reactions triggered by solvated electron reduction. *Journal of the American Chemical Society* **1993**, *115*, 8044–8049.

(142) Barbara, P. F.; Meyer, T. J.; Ratner, M. A. Contemporary issues in electron transfer research. *The Journal of Physical Chemistry* **1996**, *100*, 13148–13168.

(143) Kloepfer, J. A.; Vilchiz, V. H.; Lenchenkov, V. A.; Bradforth, S. E. Electron photodetachment in solution. **2002**.

(144) Lan, J.; Rybkin, V. V.; Pasquarello, A. Temperature dependent properties of the aqueous electron. *Angewandte Chemie International Edition* **2022**, e202209398.

(145) Narvaez, W. A.; Wu, E. C.; Park, S. J.; Gomez, M.; Schwartz, B. J. Trap-Seeking or Trap-Digging? Photoinjection of Hydrated Electrons into Aqueous NaCl Solutions. *The Journal of Physical Chemistry Letters* **2022**, *13*, 8653–8659.

(146) Smith, D. E.; Dang, L. X. Computer simulations of NaCl association in polarizable water. *The Journal of Chemical Physics* **1994**, *100*, 3757–3766.

(147) Fennell, C. J.; Bizjak, A.; Vlachy, V.; Dill, K. A. Ion pairing in molecular simulations of aqueous alkali halide solutions. *The Journal of Physical Chemistry B* **2009**, *113*, 6782–6791.

(148) Zhang, Y.; Cremer, P. S. Chemistry of Hofmeister Anions and Osmolytes. *Annual Review of Physical Chemistry* **2010**, *61*, 63–83.

(149) Ganguly, P.; Schravendijk, P.; Hess, B.; van der Vegt, N. F. Ion pairing in aqueous electrolyte solutions with biologically relevant anions. *The Journal of Physical Chemistry B* **2011**, *115*, 3734–3739.

(150) Van Der Vegt, N. F.; Haldrup, K.; Roke, S.; Zheng, J.; Lund, M.; Bakker, H. J. Water-mediated ion pairing: Occurrence and relevance. *Chemical Reviews* **2016**, *116*, 7626–7641.

(151) Li, X.; Jia, X.; Paz, A. S.; Cao, Y.; Glover, W. J. Evidence for water antibonding orbital mixing in the hydrated electron from its oxygen 1s X-ray absorption spectrum. *Journal of the American Chemical Society* **2022**.

(152) Tang, Y.; Shen, H.; Sekiguchi, K.; Kurahashi, N.; Mizuno, T.; Suzuki, Y.-I.; Suzuki, T. Direct measurement of vertical binding energy of a hydrated electron. *Physical Chemistry Chemical Physics* **2010**, *12*, 3653–3655.

(153) Lan, J.; Kapil, V.; Gasparotto, P.; Ceriotti, M.; Iannuzzi, M.; Rybkin, V. V. Simulating the ghost: quantum dynamics of the solvated electron. *Nature Communications* **2021**, *12*, 1–6.

(154) VandeVondele, J.; Mohamed, F.; Krack, M.; Hutter, J.; Sprik, M.; Parrinello, M. The influence of temperature and density functional models in ab initio molecular dynamics simulation of liquid water. *The Journal of Chemical Physics* **2005**, *122*, 014515.

(155) Perdew, J. P.; Burke, K.; Ernzerhof, M. Generalized gradient approximation made simple. *Physical Review Letters* **1996**, *77*, 3865.